MECHANISMS OF ELEVATED TEMPERATURE FATIGUE DAMAGE IN 2 1/4 Cr - Mo STEEL

Pierre G. Vining

NAVAL POSTGRADUATE SCHOOL
Monterey, California

THESIS

MECHANISMS OF ELEVATED TEMPERATURE FATIGUE
DAMAGE IN 2 1/4 Cr - 1 Mo Steel

by

Pierre G. Vining

June 1981

Thesis Advisor   K. D. Challenger

Approved for public release; distribution unlimited

REPORT DOCUMENTATION PAGE	READ INSTRUCTIONS BEFORE COMPLETING FORM

1. REPORT NUMBER	2. GOVT ACCESSION NO.	3. RECIPIENT'S CATALOG NUMBER

4. TITLE (and Subtitle)	5. TYPE OF REPORT & PERIOD COVERED
Mechanisms of Elevated Temperature Fatigue Damage in 2 1/4 Cr - 1 Mo Steel	Master's/Engeeners Thesis, June 1981
	6. PERFORMING ORG. REPORT NUMBER

7. AUTHOR(s)	8. CONTRACT OR GRANT NUMBER(s)
Pierre G. Vinig	

9. PERFORMING ORGANIZATION NAME AND ADDRESS	10. PROGRAM ELEMENT, PROJECT, TASK AREA & WORK UNIT NUMBERS
Naval Postgraduate School Monterey, California 93940	

11. CONTROLLING OFFICE NAME AND ADDRESS	12. REPORT DATE
Naval Postgraduate School Monterey, California 93940	June 1981
	13. NUMBER OF PAGES
	137

14. MONITORING AGENCY NAME & ADDRESS(If different from Controlling Office)	15. SECURITY CLASS. (of this report)
	Unclassified
	15a. DECLASSIFICATION/DOWNGRADING SCHEDULE

16. DISTRIBUTION STATEMENT (of this Report)

Approved for public release; distribution unlimited

17. DISTRIBUTION STATEMENT (of the abstract entered in Block 20, if different from Report)

18. SUPPLEMENTARY NOTES

19. KEY WORDS (Continue on reverse side if necessary and identify by block number)

Steel
2 1/ Cr - 1 Mo steel
Fatigue
Creep-fatigue

Elevated temperature fatigue
Interaction solid solution hardening

20. ABSTRACT (Continue on reverse side if necessary and identify by block number)

The microstructural changes and fatigue crack growth rates induced by elevated temperature push-pull fatigue and creep fatigue tests in 2 1/4 Cr - 1 Mo steel have been examined using optical and electron microscopy techniques. The only microstructural change noted was the development of dislocation substructures in the proeutectoid ferrite. Creep fatigue tests with a single maximum strain hold period per cycle created a cellular substructure whose size was solely dependent on the carbide interparticle

DD FORM 1473 EDITION OF I NOV 65 IS OBSOLETE
1 JAN 73
(Page 1)   S/N 0102-014-6601 |

Item #20 continued:

spacing. Temperature and strain range effects were noted on the
dislocation densities in the matrix which were generally consis-
tent with work reported in the literature. As there were no
resolvable changes in the carbides in the ferrite, it was concluded
that there must be some change in the microstructure on a finer
scale, such as the early stages of M0-C-Mo cluster formation,
which might explain the cyclic hardening/cyclic softening response
of the alloy. The fatigue crack growth rate of the alloy was
strongly dominated by the hold periods imposed during the loading
cycle. A single 0.1 hr. hold period doubled the fatigue crack
growth rate obtained for a continuously cycled test and two hold
periods per loading cycle gave a four fold increase over the
continuously cycled crack growth rate. Although some temperature
and strain range effects were noted in the continuously cycled
tests, they were totally absent in the hold period tests.

Mechanisms of Elevated Temperature Fatigue
Damage in 2 1/4 Cr - 1 Mo Steel

by

Pierre G. Vining
Lieutenant Commander, United States Navy
B.S., United States Naval Academy, 1973

Submitted in partial fulfillment of the
requirements for the degree of

MASTER OF SCIENCE IN MECHANICAL ENGINEERING

and the degree of

MECHANICAL ENGINEER

from the

NAVAL POSTGRADUATE SCHOOL
June 1981

ABSTRACT

The microstructural changes and fatigue crack growth rates induced by elevated temperature push-pull fatigue and creep fatigue tests in a 2 1/4 Cr - 1 Mo steel have been examined using optical and electron microscopy techniques. The only microstructural change noted was the development of dislocation substructures in the proeutectoid ferrite. Creep fatigue tests with a single maximum strain hold period per cycle created a cellular substructure whose size was solely dependent on the carbide interparticle spacing. Temperature and strain range effects were noted on the dislocation densities in the matrix which were generally consistent with work reported in the literature. As there were no resolvable changes in the carbides in the ferrite, it was concluded that there must be some change in the microstructure on a finer scale, such as the early stages of Mo-C-Mo cluster formation, which might explain the cyclic hardening/cyclic softening response of the alloy. The fatigue crack growth rate of the alloy was strongly dominated by the hold periods imposed during the loading cycle. A single 0.1 hr. hold period doubled the fatigue crack growth rate obtained for a continuously cycled test and two hold periods per loading cycle gave a four fold increase over the continuously cycled crack growth rate. Although some temperature and strain range effects were noted in the continuously cycled tests, they were totally absent in the hold period tests.

4

TABLE OF CONTENTS

LIST OF TABLES

LIST OF FIGURES

I. INTRODUCTION

2 1/4 Cr - 1 Mo steels have been used extensively in power generation equipment for over twenty-five years. The alloy system recently has received new attention due to its selection as the structural material for steam generators in the Clinch River Liquid Metal Cooled Fast Breeder Reactor (CRLMFBR). Because the ASME Pressure Vessel Code requires that accurate predictions be made for the high temperature fatigue life of materials used in nuclear applications, Oak Ridge National Laboratories (ORNL) organized and coordinated a series of creep and high temperature fatigue tests on several different heats of this alloy.

This thesis research has examined selected samples from the ORNL test series using optical, scanning electron and transmission electron microscopy. The effects of various testing parameters on the microstructure and fatigue crack growth behavior of the alloy have been examined and an attempt has been made to quantify the changes observed. The purpose of this work has been to better characterize the high temperature behavior of this steel.

The balance of this paper will present the background of past work on this alloy system, a brief outline of the laboratory techniques employed both during this investigation and by ORNL, a discussion of the results obtained and conclusions

11

and recommendations. Appendix A provides a detailed, step-by-
step description of some of the more complicated specimen pre-
paration techniques developed during the course of this research.

II.   BACKGROUND

A.   GENERAL

The selection of 2 1/4 Cr - 1 Mo steel for application in the CRLMFBR was based on three primary criteria [Ref. 1]:

1.   Resistance to stress corrosion cracking

2.   Fabricability

3.   Acceptance by ASME Pressure Vessel and Boiler Code

Additional considerations included carbon transport (through the liquid sodium to the stainless steel components in the system), mechanical properties, wastage resistance, general corrosion resistance and a successful history of applications in conventional power generation equipment.

The research reported here has considered two separate facets of the material's behavior under cyclic loading at elevated temperatures:

1.   Microstructural changes induced by the testing conditions,

2.   Environmental effects on fatigue crack propagation rates.

Previous investigations of these two areas have progressed more or less independently, and so the background for each will be outlined separately.

B. MICROSTRUCTURAL EFFECTS

The long popularity of 2 1/4 Cr - 1 Mo steel for high temperature applications stems primarily from its extremely good creep resistance. However, there was a singular lack of any firm understanding of the physical basis for this behavior when the alloy was first used.

Two early researchers who investigated this aspect were Baker and Nutting [Ref. 2]. In 1959, they reported a study of the changes in microstructure, carbide morphology and carbide chemical composition resulting from tempering both quenched and normalized 2 1/4 Cr - 1 Mo steel. Tempering was performed for up to 1000 hours in the range 400-750°C. Their work, which employed transmission electron microscopy, x-ray diffraction and x-ray flourescence techniques, revealed that the sequence of carbide formation in the alloy was quite complex, and involved several intermediate compositions. They also observed different sequences depending on whether (in the case of the normalized material) the bainite or proeutectoid ferrite was examined. In the case of bainite, the carbides present before tempering were ε-carbide, cementite and M_7C_3. The ε-carbide transformed to cementite which then, along with the original cementite, transformed partly to Mo_2C. These two carbides eventually converted to $M_{23}C_6$ and then to the stable M_6C. The M_7C_3 apparently transformed directly to M_6C. The process observed in the proeutectoid ferrite was much more straightforward, but proceeded at a slower rate, the initial Mo_2C changing to $M_{23}C_6$ and then to M_6C.

Baker and Nutting postulated that the Mo_2C carbides pre-cipitated in the ferrite independently (i.e. without any inter-action with the pearlite) and that they might initially appear as coherent needles which would then coarsen and lose coherency. They suggested that the smaller, more finely dispersed carbides might be highly effective at pinning dislocations at elevated temperatures even though the hardness is essentially unchanged by their presence.

In concluding their report on the aging response of the material, Baker and Nutting made three other interesting observations. First, the Mo_2C carbides in the proeutectoid ferrite, although only metastable, were very resistant to change. Second, fringes of Mo_2C carbides formed (in the ferrite) at the edges of the bainite colonies. This was explained as being the result of carbon diffusing from the bainite into the proeutectoid ferrite which then became super-saturated with molybdenum during cooling, especially near the prior austenite-ferrite grain boundaries. Finally, they determined that the alloy possessed the primary requirement for extended creep life: a stable microstructure.

The next important work related to the alloy system was reported in 1966 by Baird and Jamieson [Ref. 3]. This paper was one of a series by them which discussed the effects of alloying elements in solid solution on the behavior of steel at elevated temperatures, primarily above the blue brittleness range. The strength of Fe-N, Fe-Mn and Fe-Mn-N synthesized

(as opposed to commercially available) alloys was evaluated at temperatures in the range 20-600°C, and significant strengthening was noted only in the Fe-Mn-N alloys above 400°C, which is beyond the normal blue brittleness range of 200-300°C.

Blue brittleness is generally attributed to dynamic strain aging. At elevated temperatures the diffusivity and thus the mobility of solute atoms is increased. When the material is deformed, dislocations move through the structure at some average velocity. If the temperature and strain rate conditions are such that the solute atoms can impede the motion of the dislocations, dynamic strain aging occurs. At temperatures below the blue brittleness range the solute atoms are too immobile to interact dynamically with the dislocation. At temperatures above the blue brittleness range the solute atoms move easily with the dislocations. In either case the solute atoms cannot as effectively impede the dislocation motion. A more complete description of this phenomenon is given by Reed-Hill [Ref. 4].

Baird and Jamieson ascribed this strengthening effect to the interaction of Mn-N pairs and clusters with dislocations in the microstructure and termed the process interaction solid solution hardening (ISSH). They postulated that the high temperature strengthening might be explained by one or more of three mechanisms:

1. A temperature-insensitive solid solution hardening,

16

2. An extension of the blue-brittleness strengthening range if the substitutional solute atoms slowed the movement of interstitials,

3. A separate high temperature strain aging effect supplied by Mn and N.

Their data suggested that two mechanisms were involved. First, Mn-N pairs and clusters formed, extending solid solution hardening to higher temperatures. This would result from a reduction in the mobility of the Mn atoms by combination with the N atoms, slowing diffusion and therefore also the precipitation rate of semicoherent nitrides in the proeutectoid ferrite. Second, the Mn atoms raised the blue-brittleness temperature range by slowing the migration of nitrogen atmosphere around moving dislocations.

In summary, it was noted that the strengthening of the binary alloys (Fe-Mn and Fe-N) was negligible compared with the ternary alloy.

In 1972 Baird and Jamieson reported similar work on synthesized alloys containing Mo and Cr [Ref. 5]. They noted the same kind of strengthening mechanism observed earlier in the Fe-Mn-N alloys. The effects were more pronounced in the Fe-Mo-C and Fe-Mo-C-N alloys, which was thought to be a result of the stronger mutual afinity of molybdenum for either carbon or nitrogen relative to that between manganese and nigrogen. The results of this work can be summarized as follows:

1. Fe-Mo-C alloys showed the highest rate of strain hardening in the dynamic strain aging temperature range.

2. Fe-Mo-C alloys showed a distinct rise in yield stress above 400°C.

3. The binary alloys examined showed no serrated yield behavior.

4. Cr did not produce as pronounced in ISSH effect as Mo. Cr is a more aggressive carbide former and may be a slight more mobile sustitutional atom than Mo.

In a companion work to reference [5], Baird and Jamieson investigated the creep strengths of their synthesized alloys [Ref. 6] and again compared the response of pure iron with binary, ternary and quarternary alloys. Creep rate was plotted against time on log-log coordinates to simplify determining the durations of primary, secondary and tertiary stages of creep. An advantage of this technique is that the exponential relation between creep rate and time can be easily evaluated for the primary stage. During primary creep, log (strain rate) dedreases linearly with log (time at load and temperature) for constant-load creep tests on many materials. The slope strain hardening in the alloy under study.

It was found that the binary alloys exhibited more or less classical primary and secondary creep stages with some solid solution strengthening observed although it was generally minor. The behavior of the ternary alloys was much more complex. The Fe-Mn-N alloys had significantly higher initial creep resistance.

18

Comparing two Fe-1% Mn Alloys, one nitrogen free and one with 0.008% N, the binary alloy reached secondary creep after about 400 hours while the ternary alloy tested at twice the load had not reached secondary (steady-state) creep after 800 hours. Additionally, the strain rate fell more rapidly in the ternary alloy than in the binary alloy during the primary creep stage. The log (strain rate) - log (time) plots were also significantly different, the ternary alloy curves having up to three straight line portions. Baird and Jamieson theorized that changes in active strengthening mechanisms might be one explanation of this anomalous creep behavior. The Fe-Mo-C alloys seemed to strain harder even faster in the primary stage, approximating logarithmic creep behavior.

One other experiment carried out was a creep test on a Fe-1 Mo-.01 C-.001 N pre-aged for 250 hours at 550°C. The noticeably lower creep resistance relative to the unaged alloy was suggested to be due to the depletion of carbon and nitrogen in solution prior to the creep test. The authors stated that such an effect would probably take much longer in a commercial alloy since the carbon content would be an order of magnitude higher. The commercial alloy would have both cementite colonies which could dissolve to provide additional carbon and a higher level of carbon supersaturation in the proeutectoid ferrite. Their primary conclusions were that, for the ternary and quarternary alloys:

1. Initial creep strengths were due to ISSH.

2. Solute atoms remained in solution far longer than originally expected.

3. Pre-aging the synthesized alloys removed solute atoms from solution and lowered strength.

4. The long term creep resistance for the synthesized alloys resulted from a fine dispersion of second phase particles in the ferrite.

Several studies have been performed on the elevated temperature behavior of commercial 2 1/4 Cr- 1 Mo steels since 1972. Bynum, et. al. [Ref. 7] found that primary stage creep behavior was very nearly logarithmic, a result consistent with Baird and Jamieson's work. Jaske, et. al. [Ref. 8] examined tensile properties at elevated temperatures. Booker et. al. [Ref. 9] compared creep ductility data for several high temperature structrual materials including 2 1/4 Cr 1 Mo steel.

One of the more active researchers has been R. L. Klueh. In 1975 he and Leitnaker [Ref. 10] conducted experiments on the alloy's thermal aging and decarburization response. Samples were aged in an inert atmosphere at 566°C for 26,500 hours and the carbide morphologies, distributions, and chemical compositions were evaluated at various points in the aging process. Their results were consistent with those reported by Baker and Nutting concerning the sequence of carbides formed.

Subsequent work by Klueh [Ref. 11] noted a strong dependence of the material properties on whether the alloy was fully

annealed or normalized. The normalized material exhibited higher dynamic strain aging peaks and ISSH behavior over a wider temperature range. Based on this research, Klueh made several conclusions which supported the earlier work of Baker and Nutting and Baird and Jamieson:

1. The Mo_2C carbides, while not absolutely stable in the proeutectoid ferrite, resist dissolution during thermal aging.

2. ISSH becomes an active mechanism prior to completion of the precipitation process for Mo_2C carbides. In fact, the microstructural features associated with ISSH may be analogous to GP I zone formation in Al-Cu alloys.

3. The temperature range over which ISSH is active is governed by diffusional nucleation and growth principles. The region of the microstructure near the pearlite (or bainite) - proeutectoid ferrite interface has a relative greater concentration of both carbon and moybdenum. Thus, the precipitation of Mo_2C carbides can proceed at a faster rate in these areas and ISSH effects would therefore be present at lower temperatures and would persist for shorter periods. This enhanced precipitation was noted by Baker and Nutting [Ref. 2].

4. The starting microstructure in both the annealed and normalized conditions is about 80 percent proeutectoid ferrite and since the formation of Mo_2C carbides proceeds at a slower rate in the proeutectoid ferrite, it can be asserted that the favorable high temperature properties of 2 1/4 Cr - 1 Mo steel are controlled by the ferrite. This is consistent with similar

observations made by Baker and Nutting [Ref. 2] in their com-
parisons of the creep strength of quenched and tempered vs.
normalized and tempered 2 1/4 Cr - 1 Mo steels.

In a companion work to reference [11] Klueh examined the
creep behavior of annealed 2 1/4 Cr - 1 Mo steel [Ref. 12].
Using the same heats of material subjected to the same heat
treatments, he noted anomalous (non-classical) creep behavior
with two steady state creep stages.

Classical creep behavior is described as having three
phenomenologically distinct phases. In primary creep, the
creep rate decreases with time due in large measure to the
development of a higher dislocation density in the material
and a reduction in dislocation mobility. During secondary
or steady state creep, these strain-hardening mechanisms are
balanced by various softening mechanisms in the material. As
this balance is lost and the material progressively softens,
tertiary creep is reached and rupture ultimately occurs. The
softening during secondary and tertiary creep stages of the
material can be the result of precipitation, corrosion,
microvoid coalescence and/or localized necking. A more de-
tailed description of creep can be found in Hertzberg [Ref.
13].

Figure 1 compares a classical creep curve to one repre-
senting the non-classical behavior observed by Klueh for
annealed 2 1/4 Cr - 1 Mo steel. As noted previously, an alloy's
creep behavior is directly related to its microstructural

stability, and annealed 2 1/4 Cr - 1 Mo steel is in a meta-
stable state. Klueh postulated that his non-classical creep
was related to that observed by Baird and Jamieson [Ref. 6]
and explained it as follows:

1. Initially the Mo-C clusters interact with dislocations
to form resistive atmospheres and produce an approximately
steady state creep phase.

2. This continues until they form larger clusters which
coarsen and begin to evolve as rather larger and more immobile
second phase particle. The Mo-C clusters are thus removed
from the dislocations, which in turn gain mobility. This is
reflected as a pseudotertiary creep stage.

3. Finally, the semicoherent Mo_2C carbides lose coherency,
greatly reducing their surrounding strain fields. These car-
bides are fairly stable and the now precipitation hardened
steel exhibits a second steady state creep phase, albeit at a
higher strain rate.

Unfortunately, Klueh did not report any transmission
electron microscopy that might have verified his conclusions
and his proposed explanation has been questioned in a recent
paper summarized below. It should be emphasized, however,
that while his proposed physical mechanism may not be accurate,
the observed non-classical behavior is generally consistent
with the work of Baird and Jamieson [Ref. 6] and is quite
possibly representative of the material's creep response under
the given test conditions.

Klueh's description of the phenomena contributing to the non-classical behavior was challenged by Jones and Van Den Avyle [Ref. 14]. They examined the structure of aged, creep tested and fatigued specimens taken from the same heats of steel studied in this thesis research.

The work they performed showed that the rod-like or acicular M_2C carbides in the proeutectoid ferrite were representative of only one morphology found for the precipitates in 2 1/4 Cr - 1 Mo steel. Specifically, Jones and Van Den Avyle noted the presence of more or less spherical Mo_2C carbides decorating the dislocations in the steel, which appeared after very short periods (2.5 hrs.) of fatigue testing at 593°C. These Mo_2C carbides were not seen in other thermally aged or creep tested materials even after 804 hrs. at 593°C. These observations led them to conclude that Klueh's assumtions concerning Mo_2C precipitation during creep were not valid. Based on their study, Jones and Van Den Avyle concluded that even if Mo-C clustering had occurred, no critical sized Mo_2C nuclei would have formed during the creep tests.

Thus, dispersion hardening could not be the mechanism involved in the second steady state creep stage. Instead they proposed that a form of solute drag mechanism involving Mo-C was responsible for the first steady state creep stage and that ISSH was the controlling mechanism for the second.

It was reasoned that Mo-C pairs are the first agglomerations to form in the ferrite matrix. Using an average mobile

dislocation density, they were then able to calculate a range of strain rates for a given temperature within which the drag effect could be expected. For lower strain rates, the Mo-C pairs diffuse without causing dislocation drag. For higher strain rates the dislocations break away from the Mo-C pairs easily and again no drag is induced.

Plotting the minimum creep rates observed by Klueh for his non-classical creep results, Jones and Van Den Avyle found that they fell within the ranges where the drag effect would be active. It was concluded that this mechanism was a more appropriate explanation of Klueh's first steady state creep stage.

Toward the end of their paper a discussion of the extreme stability of the proeutectoid ferrite microstructure was presented. Molybdenum and carbon atoms interact strongly with dislocations and with each other. It is likely therefore that Mo-C pairs form preferentially on dislocations. These atom pairs are highly effective at pinning dislocations. As dislocations move through the lattice, Mo atoms are pulled along and can combine with Mo-C pairs to form clusters. These clusters are highly immobile, stable enough to inhibit Mo diffusion, and at the same time are too small to serve as critical nuclei for Mo_2C carbides.

This mechanism also helps to explain another facet of the high temperature behavior of 2 1/4 Cr - 1 Mo steel. After thermal aging at 600°C for several thousand hours, Klueh and

Leitnaker [Ref. 19] reported the formation of M_2C carbides in the ferrite. These particles were found to contain significant quantities of Fe and Cr in addition to Mo, consistent with Baker and Nutting's findings [Ref. 2]. The M_2C carbides formed during fatigue tests however are alomst entirely Mo_2C. Molybdenum's diffusivity in iron is fairly low; thus, it is apparent that the shuttling of dislocations through the lattice during fatigue may be a dominant transport mechanism in the formation of Mo_2C in this steel.

Finally, Jones and Van Den Avyle characterized the fatigue and creep fatigue behavior of the alloy. Their results were similar to those of other researchers [Ref. 15, 16] however, they provided the most detailed description of the microstructural changes involved, which can now be summarized.

1. The initial softening in fatigue is due to the loss of free Mo-C pairs as larger clusters form. This is most likely the result of a Mo-C solute drag type interaction with mobile dislocations and the sweeping of molybdenum atoms through the matrix by these dislocations.

2. These persistent, metastable Mo-C-Mo clusters in the ferrite decorate dislocation lines and attain a critical size for Mo_2C nuclei much sooner under cyclic loading. Spherical Mo_2C carbides, distinct from the acicular M_2C carbides present in the proeutectoid ferrite in the as heat treated material, while resolvable after very limited cyclic loading, were not encountered after nearly 1000 hrs. of thermal aging or

creep testing. This reinforced the concept that the shuttling of dislocations during fatigue testing provided the necessary transport mechanism for the formation of these particles.

The most recent work on this alloy was reported by Challenger, et. al. [Ref. 17]. They investigated more of the samples from the series run by Mar Test, Battelle (Columbus), and Oak Ridge and addressed the question of whether creep fatigue interaction or environment fatigue interaction was responsible for the greatly reduced fatigue life (in cycles to failure) for specimens tested with hold periods at maximum strains when compared with the fatigue life for a continuously cycled specimen at the same temperature.

One effect of the hold times reported is an acceleration of the precipitation of Mo_2C carbides in the ferrite. This infers that the effects of ISSH are largely eliminated, an assertion based on comparisons of specimens from three heats of 2 1/4 Cr - 1 Mo steel, two standard commercial heats and the other a low carbon heat. It was found that with very short (.01 hr.) hold times the number of cycles to failure in the standard heats was very similar to that of the low carbon heat. One other general trend noted was that at temperatures above about 538°C ISSH was not an active mechanism due to the more rapid formation of Mo_2C. This again was based on the negligible differences in fatigue life between the standard and low carbon heats above that temperature.

C. ENVIRONMENTAL EFFECTS ON FATIGUE CRACK GROWTH RATE

Previous work on corrosion enhanced fatigue crack propagation has generally examined aqueous and aggressive gaseous (e.g. flue gases) effects qualitatively and discussed the results from an empirical correlation approach. The effects of high temperature oxidation on crack growth rates for low alloy carbon steels and development of plausible physical mechanisms for the phenomenon have received much less attention however, so this portion of the background review will necessarily be more general than the previous discussion on microstructural effects.

Studies of environmental effects on fatigue crack growth are multivariable exercises. Base line behavior in inert atmospheres must be determined; environmental conditions (temperature, pressure, pH, active elements) must be evaluated; microstructural aspects (grain size, alloy composition, morphology) can affect the response; and loading parameters (wave-form, frequency, strain range) are also factors. While it is generally agreed that even mildly aggressive environments can modify fatigue crack growth rates, the exact physical mechanisms are largely unknown. There are some observations which do appear to be germane to the process however.

Evaluating fatigue crack growth rates is often accomplished using precracked fracture toughness specimens which are fatigue tested in an axial fashion, the so called mode I with loading applied perpendicular to crack opening. A more complete

28

description of the procedures can be found in Hertzberg [Ref. 18].

One common analytical method for analyzing the data is to plot the log of the crack advance rate per cycle (da/dN) vs. the log of the stress intensity factor range imposed on the specimen. In his work, Marcus [Ref. 19] employed a slight modification of this by plotting log da/dN against the log of the maximum stress intensity for a pull-pull type test with a zero load ratio (0 to tension loading) conducted in an aggresive environment. He then performed constant load tests in the same environment and plotted log crack growth rate (da/dt) vs. log K_I, the mode I stress intensity. These plots are reproduced here as Figure 2. His intention was to show the relation between stress corrosion cracking (SCC) and corrosion fatigue crack growth rate.

Figure 2.a. reveals three regions for constant load tests. Region I corresponds to the onset of SCC, with $K_{I_{SCC}}$ the threshold stress intensity value. Region II shows a relatively K insensitive behavior suggesting that some transport mechanism for the reactive constituent of the gas is controlling growth. Region III is dominated by fracture toughness considerations. K_{IC} is the plane strain fracture toughness.

The curves in Figure 2.b. can also be treated as having three separate regions. Region I is again a threshold region, Region II conforms to the Paris Law for fatigue crack propagation, and Region III is governed by fracture toughness as before.

The significant point here is that an envrionmental effect can be observed below $K_{I_{SCC}}$, which implies that superposition of SCC effects on the nonenvironmental fatigue behavior will not accurately model material behavior under both conditions.

Marcus next examined some specifics concerning gaseous effects, and although his discussion most directly applied to room temperature corrosion enhanced fatigue, some interesting points were made concerning physical mechanisms involved in the process which may be relevent to the situation studied here.

In order for gaseous environments to influence fatigue crack growth, the gas molecules first must be physically ad-sorbed onto the surface. This has to be followed by chemical adsorption and molecular dissolution to permit atomic chemical adsorption. The active element atoms can then find their way to the interior of the material through one of several mechanisms.

The most obvious (and slowest) transport mechanism is normal diffusion. Other work by Morris [Ref. 20] and Marcus in concert with others [Refs. 21, 22] has suggested that the diffusion distances involved are significantly greater than normal diffusion lengths. These assertions were based on comparisons of plastic deformation behavior of the material near the crack for tests conducted in inert and aggressive environments. This enhanced transport is thought to be the result of an interaction of the impurities and dislocations

30

at the crack tip in one of two ways. First, diffusion could be enhanced by the existence of preferential paths. This so-called dislocation pipe diffusion could occur along grain boundaries or dislocation tangles in the cell substructure at the crack tip. These tangles have been observed in iron by Awatani, et. al [Ref. 23]. Second, the impurities could be swept into the interior of the plastic zone ahead of the crack tip by mobile dislocations. In the papers referenced above this second mechanism is postulated to be the most likely one involved, although the transport may be dependent on both [Refs. 22, 24].

The exact mechanisms of the effect of these impurities on the fatigue crack growth are not understood. However, it has been theorized that the gas atoms strengthen the plastic zone by some sort of dislocation pinning process. This would tend to reduce the plastic deformation at the tip resulting in an increase in fatigue crack growth per cycle.

In summary this particular approach to the issue can be outlined as follows:

1. Gas atoms must be adsorbed onto the surface for en-vironmental effects to occur. The primary effect is to provide the crack tip with a fresh supply of active elements.

2. The gas atoms diffuse to the interior of the plastic zone at the crack tip, probably by some interaction with the dislocation structure.

3. The impurity atoms reduce the plastic deformation at the crack tip and this lower ductility is seen as an increase in fatigue crack growth.

The deleterious effects of oxygen on high temperature fatigue crack growth has been studied by a number of researchers for stainless steels [Refs. 25-28] and low alloy carbon steels [Refs. 29, 30, 31]. There is general agreement that the diffusion of oxygen into the crack tip plastic zone reduces plastic deformation and thus increases fatigue crack growth rate. All of these studies noted a strong dependence of fatigue crack growth on the potential of oxygen in the test environment. For example, tests run on low alloy steels in inert atmospheres at temperatures in the range 500-600°C with and without hold times showed essentially the same fatigue life as tests run in air at room temperature [Refs. 30, 31]. These results lend credence to the general theories of environmentally assisted fatigue crack growth in low alloy steels presented, however extensive research is needed to verify the exact physical mechanisms involved.

III. EXPERIMENTAL

The specimens examined in this work were taken from a
series of high temperature fatigue tests cooperatively under-
taken by Mar Test Inc., Batelle (Columbus) Laboratory, and
Oak Ridge National Laboratories on 2 1/4 Cr - 1 Mo steel.
Although three different heats were used in the original series
only a portion of those specimens machined from Babcock and
Wilcox heat 3P5601 were studied here. The hour-glass shaped
specimens were machined from one inch plate which had received
an isothermal anneal as follows: austenitized at 927 ± 14°C
for 1 hr., cooled to 704 ± 14°C at a maximum rate of 83°C/hr.,
held at 704 ± 14°C for 2 hrs., and cooled to room temperature
at a maximum rate of 6°C/min. Table I lists the composition
of the subject heat. Additional information on the specimen
geometry and testing conditions has been reported by Brinkman,
et. al. [Ref. 16].

The specimens were all subjected to fully reversed, axial
push-pull, strain controlled cyclic loading performed on
closed loop electrohydraulic fatigue testing machines. The
hourglass gage lengths were maintained at the desired tempera-
tures by induction heaters. Each test was instrumented for
stress, temperature, diametral strain, time and number of
cycles to failure. Triangular strain vs. time wave forms
were employed both for continuously cycled and creep fatigue

33

tests. Hold times for the creep fatigue tests were imposed at the maximum strains in tension, compression or both. Figure 3 shows typical strain vs. time plots and stress/strain hysteresis loops for each of the four types of tests made. Table II lists each specimen examined during the course of this research, the pertinent test data for each, and the types of observations performed for this study.

The as heat treated material was characterized using optical metallography and transmission electron microscopy of carbon extraction replicas and thin foils. This was done to provide a basis for determining the microstructural changes effected by the various testing conditions. The as heat treated material was considered to be accurately represented by samples taken from the large end of one of the continuously cycled specimens; this region was neither heated nor loaded during the test.

The fracture surfaces were cut from the specimen halves as near to the lowest point of the fracture as practical. Some of the fractures were mounted for fractographic examination using a Cambridge Stereoscan scanning electron microscope. Prior to mounting, the majority of the surfaces were cleaned with an inhibited HCl solution to remove the heavy oxidation in order to reveal more fracture surface detail.

Fine striations were first observed by Zapple and Worden [Ref. 32] in 1951 as a characteristic of some fatigue fracture surfaces, but it was almost ten years before a correlation between striation spacing and fatigue crack growth rate was

obtained. This link was reported by Forsyth and Ryder in 1960 [Ref. 33] and further substantiated by them in 1961 [Ref. 34]. They noted a one to one correspondence between the number of loading cycles experienced by the material and the number of fatigue striations observed in a precracked specimen. They also stated that larger strain ranges gave wider spacing in the same material.

The striation spacing was measured for several elevated temperature fatigue tests on the material. The procedure for these measurements was as follows: Several photographs were taken using the scanning electron microscope of each fracture surface at about 500X to 1000X and at various radial locations from the apparent final fracture region, generally located near the center of the specimen. Measurements were then made using a line intercept technique of the striation spacing for each region of each specimen and the average maximum and minimum values for each region of of each specimen were tabulated. Approximately 1000 separate readings were made during this phase of the research.

Comparisons of spacing data between specimens were made using the minimum spacings obtained. Most of the fracture surfaces exhibited highly featured topographies indicating multiple, non-coplanar fatigue crack initiation sites. The crack geometries for each specimen and thus the stress inten- sities at the crack tips would more probably be similar from sample to sample early in the fatigue crack growth stage.

Accordingly, comparisons between specimens to evaluate the effects of the testing parameters were made using the minimum spacing values obtained, that is, the measurements made near the specimen surface.

After calculating a standard deviation for each mean spacing, 95% confidence intervals were determined for each test pieces minimum average value using the Student's t distribution. Details of this calculation are outlined by Spiegel [Ref. 35]. Statistically, there is a 95% probability that the actual mean lies within the interval which is based on the observed mean and the sample standard deviation.

The material adjacent to the fracture surface for each specimen was mounted, polished and then etched for 8 seconds in 2% nital for optical metallography. This phase of the research was performed on a Zeiss research optical microscope.

Once the optical microscopy was completed, carbon extraction replicas were obtained from the metallographic surfaces. The carbon layer was deposited in a Fullam evaporation chamber and the replicas floated off in a 20% nitric acid in ethanol solution.

Thin foils were prepared using a modified Buehler Electromet jet thinning apparatus and a Fischione specimen holder. A 5% perchloric -95% glacial acetic acid electrolyte was used at room temperature with a cell potential of 70 VDC. The specimens were mechanically ground to about .004 inch thickness using 600 grit static sanding paper prior to electrothinning. The

foils as well as the carbon replicas were examined in either a JEOL JEM-7 or a Phillips EM201 transmission electron microscope (TEM).

Detailed procedures for specimen preparation techniques for electron microscopy are contained in Appendix A.

IV. RESULTS

A. MICROSTRUCTURAL EFFECTS

The microstructure of the as heat treated material was
found to be 75-80 percent proeutectoid ferrite containing a
fine dispersion of carbide particles. The balance of the ma-
terial was pearlitic or bainitic. This correlates well with
results of studies on this particular heat reported elsewhere
[Refs. 14, 16, 17].

There were no changes in the microstructure due to the
testing observable using optical microscopy techniques. In
all cases, the as tested material possessed microstructural
features similar to those in the as heat treated condition.
No appreciable coarsening of the carbides in the proeutectoid
ferrite was noted nor was any measurable breakdown of the
pearlitic/bainitic regions. Figures 4 through 17 show typical
microstructures seen in this study.

The carbon replicas of the as heat treated material revealed
a wide variety of microstructural features. Figures 18 through
30 are representative photographs of the types of structures
observed. The pearlitic/bainitic regions ranged from dense,
overlapping tangles of carbides to fine, evenly spaced lamellae.
The ferrite regions held varying concentrations of acicular
and irregularly shaped carbides. The acicular carbides were

frequently seen in an apparently orthogonal arrangement suggesting some degree of coherency with the ferrite matrix.

The changes observed in the as tested samples were in general very subtle. There was evidence of some breakdown of the pearlitic and bainitic regions, and the degree of spheroidization seemed to be more directly related to time at temperature than any other test parameter (compare Figure 19 to Figure 29). An interesting result observed in all of the as tested specimens was the formation of colonies of very fine whiplike carbide whiskers extending from the edges of the pearlite or bainite into the proeutectoid ferrite (see for example Figures 20, 24, and 28). These carbides were also noted by Baker and Nutting [Ref. 2].

The proeutectoid ferrite regions did not show any easily discerned, consistent trends in carbide transformations. No meaningful statements can be made concerning variations in carbide particle distribution as a function of testing conditions for two reasons. First, the carbide population in the ferrite for each sample was highly nonuniform, making the validity of sample to sample comparisons tenuous at best. Second, while the carbon extraction replica specimen technique seems to be preserving the pearlite and bainite regions intact, it may not be removing all the carbides from the proeutectoid ferrite regions (see Fig. A7 and A8 in Appendix A). There is some noticeable coarsening of the rod-like carbides and the appearance of some nearly equiaxed

39

particles in the ferrite regions when comparing MIL 36 (482°C, .5% Δε) or MIL 45 (538°C, .3% Δε) (Figures 25 and 30 respectively) with the as heat treated material, Figure 18.

The thin foil transmission electron microscopy revealed many more details of the alloy's microstructure than the carbon extraction replicas. Figures 31 through 45 are representative photographs of the thin foils examined in this thesis research.

The as heat treated material is shown in Figure 31. The region of fairly coarse pearlite depicted shows little evidence of any dislocation structure between the lamella. The remaining views in Figure 31 show typical carbide morphologies and distributions found in the proeutectoid ferrite. Note the variety of particle concentrations and morphologies in the different photographs and also the very low dislocation density of the ferrite.

The continuously cycle specimens represented by Figure 32 (MIL 44, 482°C, .5% Δε), Figure 36 (MIL 18, 482°C, 1.% Δε) and Figure 39 (MIL 10, 538°C, .5% Δε) all showed a significantly higher dislocation density than the as heat treated material. There does not appear to be any development of a cellular dislocation structure however. Further, there is no significant change in either the carbide morphology or distribution in the ferrite.

The imposition of a single 0.1 hour hold period at the maximum tensile or compressive strain limit of each loading cycle leads to the development of much more sharply defined

dislocation cells in the proeutectoid ferrite. There is still
no remarkable change in the carbides, however. Comparing
Figure 33 (MIL 36, 482°C, 0.5% $\Delta\epsilon$, 0.1 hr tension hold) and
34 (MIL 27, 482°C, 0.5% $\Delta\epsilon$, 0.1 hr compression hold) with
Figure 32, an obvious increase in dislocation density can be
observed. Additionally, there is also a distinct cellular
nature to the arrangements, with the cell dimensions more or
less fixed by the carbides. It was generally found that the
dislocation density was strongly dependent on the carbide dis-
tribution as was the cell size when they formed in each sample.
There was however virtually no difference between dislocation
structures of the specimen subjected to a tension hold period
(Figure 33) and the one subjected to a compression hold period
(Figure 34) at 482°C and 0.5 percent strain range.

The hold period tests also affected the pearlite and bainite
regions. Figure 34 depicts a dislocation structure beginning
to form between the carbides in a bainitic region which is also
decomposing. The evolving dislocation structure suggests that
there has been some deformation in the bainite.

The development of cellular dislocation arrangments can
also be seen in hold period tests conducted at 482°C and 1.0
percent strain range [Figure 37 (MIL 24, 482°C, 1.0% $\Delta\epsilon$, 0.1
hr compression hold) and Figure 38 (MIL 35, 482°C, 1.0% $\Delta\epsilon$,
0.1 hr tension hold)]. As in the specimens tested at 0.5 per-
cent strain range, the hold period tests developed denser,
more distinct dislocation arrangements than the continuously

cycled test (Figure 36). Also, there is no noticeable differ-
ence between the microstructures resulting from the tension
hold (Figure 38) and the compression hold tests (Figure 37)
conducted at 482°C and 1.0 percent strain range.

Several comparisons to examine the strain range effects
on the alloy can be made; one for continuously cycled tests
(Figure 32 vs. Figure 36), one for tension hold tests (Figure
33 vs. Figure 38), and one for compression hold tests (Figure
34 vs. Figure 37). In each case, the dislocation density can
be seen to increase with increasing strain range; however,
where cellular structures evolved their size was not affected
by the strain range.

The hold period effects seem to be much more pronounced
at 482°C than at 538°C. Comparing Figure 30 with Figure 40
(MIL 34, 538°C, 1.0% Δε, 0.1 hr compression hold) and Figure
41 (MIL 20, 538°C, 1.0% Δε, 0.1 hr tension hold), the creep
fatigue specimens, while having a higher dislocation density
than the continuously cycled sample, do not exhibit the same
degree of cell formation found in similar creep fatigue tests
conducted at 482°C (Figures 37 and 38). A further remark is
germane; MIL 10 (Figure 39) was continuously cycled at 0.5
percent strain range and the hold period tests represented by
Figures 40 and 41 were conducted at 1.0 percent strain range.
This indirect comparison between a 0.5 percent strain range
continuously cycled test and 1.0 percent strain range hold
period tests suggests that the hold period effects on

dislocation arrangements are almost insignificant at 538°C. A continuously cycled specimen tested at 583°C and 1.0 percent strain range was not available for a direct comparison. Finally, in contrast to the tests conducted at 482°C, there is a stark difference in the structures resulting from compression hold and tension hold periods (Figures 40 and 41).

One noteworthy similarity between the substructures resulting from the hold period tests conducted at 482°C and those conducted at 583°C is that the size of the dislocation cells formed appears to be <u>solely</u> dependent on the carbide distribution; that is, the cell size is independent of both temperature and strain range for the conditions studied during this research.

The imposition of both a tension and a compression hold period on the sample provided some very curious results. Figure 35 (MIL 65, 482°C, 0.5% Δε, 0.1 hr. tension plus 0.1 hr. compression hold) shows nearly the same dislocation density as Figure 32, a continuously cycled test. The same result can be seen comparing Figure 42 (ITL 127, 538°C, 0.5% Δε, 0.1 hr. tension plus 0.1 hr. compression hold) and Figure 39.

B. ENVIRONMENTAL EFFECTS ON FATIGUE CRACK GROWTH

The results of the fractographic studies are recorded in Table III. It can be seen that the striation spacing for each specimen increased with proximity to the final fracture zone, as would be predicted by fracture mechanics. Figures 44 through 51 are typical of the photographs evaluated for this

analysis. As previously noted, there is a direct correspondence between striation spacing and fatigue crack growth rate.

The relevant test parameters which may affect fatigue crack growth are testing temperature, strain range and hold regime (loading waveform). Several histograms have been prepared for comparing the effects of each parameter on striation spacing and therefore fatigue crack growth.

Figure 52 shows the pronounced affect of a hold period on the crack growth rate. A 0.1 hour hold period imposed at either the maximum tension or compression strain point of the cycle doubles the crack growth rate over that seen for the continuously cycled specimen. There is no statistically meaningful difference between the spacing resulting from a compression hold or tension hold period. Imposing a 0.1 hour hold period at both strain extremes gives about a four fold increase from the continuously cycled test.

Figures 53 and 54 show an interesting aspect of the temperature effects on crack growth. In Figure 53, it is clear that for the continuously cycled case raising the test temperature has significantly increased the crack growth rate. Conversely, Figure 54 shows that the temperature effects are largely eliminated by the imposition of a 0.1 hour tension hold period. Data were not available which would show whether or not compression hold periods similarly mask the temperature effects.

44

The effects of strain range also seem to be masked by hold periods in tension. Figures 55 and 56 show strain range effects for continuously cycled and 0.1 hour tension hold tests respectively. Compression hold specimen fracture surfaces were too badly damaged to obtain any meaningful results from them.

V. DISCUSSION

A. MICROSTRUCTURAL EFFECTS

Brinkman et. al. [Ref. 16] reported conclusive data which showed that a compressive hold period had a greater effect on fatigue life of 2 1/4 Cr - 1 Mo steel at low strain ranges than a tensile hold period. In a later paper, Challenger et. al. [Ref. 17] examined the phenomenon and offered two explanations; first, that the compressive hold period effect on fatigue crack initiation is environmental and second, that the cyclic hardening/cyclic softening of the alloy could be ascribed to a loss of interaction solid solution hardening. Both optical and transmission electron microscopy were used to examine the effects of the testing parameters in this thesis research in an effort to determine whether or not there was any resolvable difference in the microstructural changes brought about by tensile versus compressive hold periods, which might further explain the alloy's response to cyclic loading.

As mentioned above, the results of the optical metallography were inconclusive. Clearly, if the testing is inducing any metallurgical changes in the material, they are occurring on a much smaller scale than can be examined by optical techniques.

The pearlitic and bainitic regions under went two significant changes resolvable in the transmission electron microscope

and neither seems to be directly attributable to an environmental effect. The breakdown of the individual carbide lamella in these areas appears to be primarily a function of the testing time and, possibly, temperature. This suggests that the process is controlled in part by diffusion. The dislocation structure forming in the lamella are fairly extensive. McGrath and Bratina [Ref. 36] reported low density dislocation structures evolving in the inter-lamellar ferrite which they ascribe to local strain resulting from the volume changes accompanying the eutectoid transformation in a normalized low carbon steel. The cellular structures seen in the pearlitic/bainitic regions in this research must be due to some deformation in these areas during the testing since they were essentially absent in the as heat treated material. Additionally, the stage of development in the cellular structures appeared to be directly related to the extent of spheroidization in the region. Since plastic deformation would become easier in the pearlite as the carbide lamella (or sheaves, in the case of bainite) break up, this supports the conclusion that these dislocation structures are a consequence of plastic deformation.

The whiplike carbides which appeared in all of the as tested specimens originated from more or less equiaxed nuclei at the pearlite/proeutectoid ferrite interfaces. Baker and Nutting [Ref. 2] identified these whiskers as primarily Mo_2C. Their extent seems to be independent of most of the testing parameters, although the individual whips may be slightly

47

longer and thicker in specimens tested for longer periods. One possible explanation for their formation involves the molybdenum and carbon gradients in the material as it is initially cooled below 723°C, the eutectoid temperature. Briefly, there exists at the prior austenite-proeutectoid ferrite interface relatively greater quantities of carbon and molybdenum than elsewhere in the matrix, so these Mo_2C whiskers form preferentially in these regions [Ref. 2]. There has been no explanation offered to date as to why the carbides assume this particular morphology. There is obviously no coherency with the ferrite matrix, as the carbide filaments are generally smoothly curved and filaments in the same colony occasionally cross each other.

The changes in the proeutectoid ferrite resolvable in the transmission electron microscope primarily involved the dislocation structures produced, and each test parameter had its own effect on the substructures, which will be discussed individually in the following paragraphs.

The development of a cellular substructure in the proeutectoid ferrite depends on the imposition of a hold period in the loading cycle. The application of a nearly constant external load at elevated temperatures may enhance the dislocation mobility in the matrix, giving rise to two effects. First, dislocations of opposite sense could combine and annihilate each other. This would result in a softening of the alloy. Second, dislocation tangles could form, eventually developing

into cell walls which would strengthen the material in the same manner as described by the Hall-Petch grain size analysis. It is thought that both of these phenomenon are occurring simultaneously in this alloy. In the case of tests with both tensile and compressive hold periods, the dislocation structures are much less pronounced and the dislocation density much lower. This suggests that an annealing out or annihilation of the dislocations may be occurring due to repeatedly reversed creep. One observation which might help to test this hypothesis would be the examination of the microstructure resulting from a 0.2 hour zero stress hold test.

Referring to Table II, it can be seen that there is at most about a 6% difference between the reported saturated stress for a continuously cycled test and that for a simple hold period test at the same temperature and strain range. Further, the recorded stress for MIL 44 (continuously cycled, 0.5% $\Delta\varepsilon$) is greater than that for either MIL 36 (tensile hold, 0.5% $\Delta\varepsilon$) or MIL 27 (compressive hold, 0.5% $\Delta\varepsilon$) while that for MIL 18 (continuously cycled, 1.0% $\Delta\varepsilon$) is in between that for MIL 35 (tensile hold, 1.0% $\Delta\varepsilon$) and MIL 24 (compressive hold, 1.0% $\Delta\varepsilon$). Thus, for the specimens examined in this research, there appears to be no conclusive statement which can be made relating the stress recorded at half the fatigue life of the test to the imposition of a hold period. Similarly, although there does appear to be a slight (5-15%) increase in the plastic strain range for hold period tests, no definitive

statements can be made concerning the relation of these two parameters. A more complete analysis of the data provided by Jaske and Leis [Ref. 37] on the entire test series the samples examined here were drawn from is required to determine the dependence, if any, of both the plastic strain range and the stress at half the fatigue life on the imposition of a hold period.

There is additional evidence that the hold periods are allowing dislocations to be annealed out of the structure obtained by comparing the dislocation density of specimens subjected to hold period tests at different temperatures, holding the other testing parameters constant. The tests performed at 482°C and 1.0% $\Delta\varepsilon$ (Figures 37 and 38) resulted in higher dislocation densities than those done at 538°C and 1.0% $\Delta\varepsilon$ (Figures 40 and 41). Further comparisons of these results with those obtained by Jones and Van Den Avyle [Ref. 14] on samples tested at 593°C confirms this trend. Two other effects of increasing the testing temperature are that the cell structures appear to be less well defined and that the striking similarity in the microstructures resulting from single hold period tests at 482°C is not present at 538°C. Both of these phenomenon may be consequences of the lower dislocation densities observed at the higher temperature.

The strain range effects observed in this research are fairly straightforward: high strains give greater dislocation densities which, in the case of hold period tests result in

more distinct cell walls being formed. This effect has also
been reported by McGrath and Bratina [Ref. 36].

One final characteristic affecting the nature of the dis-
location substructure is the carbide structure in the proeu-
tectoid ferrite matrix. In a single specimen there exists a
direct relationship between the carbide particle density and
the dislocation density. The dislocations also appear to be
tangled around the carbides, suggesting that the particles do
not shear and are thus highly effective at pinning the dislo-
cations. As mentioned earlier in this paper the dislocation
cell structure dimensions seem to be dependent only on the
carbide particle spacing and do not show an inverse relationship
with saturated stress as reported in the literature [Refs.
38-41]. This lack of a cell size-stress relationship is found
in alloys containing precipitate particles. Embury et. al.
[Ref. 42] noted that the initial cell size in a Fe-2.0Cu alloy
was fixed by the interparticle spacing, stating that the
relatively coarse (on the order of .5 μm long) particles
effectively pinned the dislocations. This particle size is
similar to the rod-like carbides observed in 2 1/4 Cr - 1 Mo
steel. Other researchers [Refs. 43-45] have observed subgrain
boundaries pinned by second phase particles. The result that
the cell size is independent of strain range for smaller plastic
strains is significant. Increasing the strain range does
increase the dislocation density in the cell walls however.
This may explain the significant increase in the recorded

stress at half the fatigue life between MIL36 (0.5% $\Delta\varepsilon$, 209 MPa) or MIL 27 (0.5% $\Delta\varepsilon$, 216 MPa) and MIL 24 (1.0% $\Delta\varepsilon$, 264 MPa) or MIL 35 (1.0% $\Delta\varepsilon$, 252 MPa).

The lack of resolvable changes in the carbide morphology and distribution in the proeutectoid ferrite was very surprising at first. There was no appreciable coarsening of the rod-like carbides reported in previous work [Ref. 10, 14, 16 and 17) and the spherical Mo_2C carbides observed by Jones and Van Den Avyle [Ref. 14] were conspicuously absent from the specimens studied in this research. Additionally, the sub-structures obtained did not seem consistent with the fatigue behavior of 2 1/4 Cr - 1 Mo steel reported in the literature [Ref. 8, 12, 16, 17 and 37]. Specifically, the hypothesis that interaction solid solution hardening is rapidly eliminated in fatigue tests with short hold periods conducted in the temperature ranges addressed here is not supported. There is no evidence of additional precipitation of the Mo_2C carbides during the testing.

One possible explanation of this result can be drawn from the description of the precipitation process under the effects of cyclic loading offered by Jones and Van Den Avyle. Briefly reviewing, they proposed that there were a series of steps involved:

1. Molybdenum atoms are shuttled through the matrix by the dislocations.

51

2. These atoms come in proximity to interstitial carbon atoms and form Mo-C pairs.

3. The diffusivity of the Mo-C pairs is very low, tending to retard dislocation motion.

4. Eventually these pairs are moved and can form multi atom Mo-C-Mo clusters with the aid of the dislocation.

5. These Mo-C-Mo clusters are quite immobile and serve as essentially stable subcritical nuclei for Mo_2C carbides.

6. Under continued cyclic loading at elevated temperature, these clusters eventually agglomerate to form critical size nuclei and precipitates form.

Clearly, there is some change occurring in the material based on the reported cyclic hardening/cyclic softening fatigue behavior of the alloy. The absence of any resolvable new precipitates suggests that these changes must be occurring on a much finer scale than was observed in this thesis research. Therefore, it is concluded that the alloy must be experiencing the early stages of the process outlined above.

If the Mo-C pairs are more effective solid solution strentheners than the Mo-C-Mo clusters, then the depletion of the pairs would cause a softening of the material as it is cycled. This implies that when the Mo-C-Mo clusters are lost and the precipitates form, there would be a second period of cyclic softening during the fatigue life of the alloy in the temperature range studied in this research. This could be observed in a creep-fatigue test at, say, 482°C, 0.5% $\Delta\varepsilon$

conducted in a vacuum. Conducting the test in a vacuum would eliminate the environmental enhancement of fatigue crack initiation and growth permitting the specimen to be cycled for a longer time before failure.

Jones and Van Den Avyle reported new precipitates after only 2.5 hrs. of fatigue at 593°C [Ref. 14]. This suggests that the entire precipitation process could occur. Recall however, that the dislocation density in the material appears to be highly temperature sensitive. Further, at 593°C the diffusivity of the Mo-C pairs and Mo-C-Mo clusters is higher, as is the dislocation mobility. Finally, there was no dislocation cell structure evident in the samples fatigued or creep-fatigued at 593°C. Considering these three aspects, an explanation of why the precipitation process does not run to completion at 482°C or 538°C can be proposed. The key point is reduced mobility and therefore reduced transport of the required atoms. This inhibited transport can be ascribed directly to the lower temperature; diffusivities are reduced, and a distinct dislocation substructure forms. The substructure reduces the dislocation mobility, further impeding the transport mechanism for creation of the precipitates.

Conducting a hold period fatigue test on the alloy in the temperature range 482-538°C with a long (0.5-1.0 hr) hold period at a small strain range might provide some evidence to support or refute this last hypothesis. The longer hold periods would permit more of the dislocation substructure developed by

the cyclic loading to be annealed out. Conducting the test in a vacuum or an inert environment would again eliminate the environmental effects on fatigue life. Unfortunately, this would be a very long, very expensive test.

In summary, the most distinct change observed in the microstructure is the development of a dislocation structure in the proeutectoid ferrite. The cellular structure resulting from the hold period tests is thought to be a consequence of the increased time at temperature. The dependence of the cell dimension on the interparticle spacing is consistent with work reported in the literature on precipitate bearing alloys [Refs. 42-45]. The dislocation structures do not adequately explain the fatigue behavior of the alloy in the temperature range examined however. The absence of resolvable carbide changes or new precipitates suggests that the alloy has only completed the first stages of the precipitation process described by Jones and Van Den Avyle [Ref. 14]. The slower precipitation at 482°C and 538°C is thought to be a result of decreased dislocation and Mo-C pair mobility at the lower temperature.

B. ENVIRONMENTAL EFFECTS ON FATIGUE CRACK GROWTH

The overriding testing parameter governing fatige crack growth rates appears to be the imposition of a hold period at the maximum strain point of the loading cycle. As noted earlier, a single (tensile or compressive) 0.1 hour hold period effectively doubles the crack growth rate observed in

the continuously cycled test conducted at the same temperature and strain range, and an additional two-fold increase results if hold periods are imposed at both strain extremes. (0.1 hr. T + 0.1 hr. C)

Referring to Figure 52 it can be seen that at 482°C and 0.5 percent strain range, there is not a significant difference between the crack growth rates for a compressive versus tensile hold period test. This last point suggests a rather simple explanation of the hold period effects, based on the assumptions that the enhancement mechanism for each case is the same and the hold period effect is fundamentally an environmental one. Several researchers [Refs. 25-31] have reported that the presence of oxygen at the crack tip will accelerate fatigue crack growth in steels. In particular, White [Ref. 30] and Corwin and Brinkman [Ref. 31] reported that the crack growth rate was highly dependent on the amount of oxygen present at the crack tip. Further, recall that one postulated mechanism of damage is a three step process:

1. Oxygen is physically and chemically adsorbed onto the surface near the crack tip.

2. The oxygen atoms diffuse either by lattice diffusion or some preferential path such as dislocation tangles to the interior of the plastic zone ahead of the crack tip.

3. The oxygen interferes with plastic flow ahead of the crack tip, enhancing the crack growth rate.

The hold period greatly increases the length of time at

temperature for each cycle and one or both of two consequences of this additional time could be used to explain the effect on crack growth rate. The longer time per cycle would allow the crack to be exposed to the oxygen for a correspondingly longer period per cycle. Assuming the physical and chemical adsorption is the rate controlling step in moving the oxygen into the plastic zone, the longer exposure per cycle would result in more oxygen atoms being adsorbed. This higher concentration of impurities would be more effective in modifying the plastic behavior of the material, which would be seen as a higher crack growth rate. On the other hand, if the diffusion is rate controlling, the longer time per cycle would allow the oxygen atoms to achieve greater penetration into the plastic zone ahead of the crack tip, regardless of the diffusion mechanism involved. This would result in a reduction in the material's plasticity to a greater depth in the crack plane which would also increase the crack tip advance per cycle. Clearly, this is a form of frequency dependence of crack growth rate. This phenomenon has been reported previously by Corwin and Brinkman [Ref. 31] for 2 1/4 Cr - 1 Mo steel and has also been reported by Wells [Ref. 24].

The assumption that the cause of the enhanced crack growth rate is the same for both tensile and compressive hold periods seems reasonable based on the limited data available. It would be highly coincidental for the crack growth rates to be so similar if a different mechanism were active for each type

of hold period. Further, because the specimen tested with <u>both</u> a tensile and compressive hold period showed approximately double the crack growth rate of either of the single hold period tests, the assertion that the growth rates in the two single hold period test are essentially the same appears well founded.

There are two tests which must be run to verify the assumption that the hold period effect on fatigue crack growth is environmental. First a test at 482°C, and 0.5 percent strain range should be run with a zero stress 0.1 hour hold period. If the crack growth rate is similar to that obtained for the tensile and compressive hold period tests that would imply that the creep crack growth effects are negligible. Second, a series of five tests should be made in a vacuum at 482°C and 0.5 percent strain range; one continuously cycled test and four with 0.1 hour hold periods at zero stress, maxium tensile strain, maximum compressive strain, and both strain range extrema, respectively.

Obviously the above hypotheses are really only directly applicable to the test conditions stated. A series of similar tests at several different strain ranges and temperatures in air and in vacuum would have to be conducted to determine their general validity.

The effects of strain range and temperature on the crack growth rate of continuously cycled specimens were consistent with previous fatigue crack propagation studies. Higher temperatures promote greater crack growth rates by reducing the

the flow stress in the vicinity of the crack tip [Ref. 24]. Larger strain ranges result in greater deformation at the crack tip, accelerating crack tip advance [Ref. 24]. It should be noted, however, that the temperature and strain range effects are nullified by the imposition of a 0.1 hour tensile hold period (see Figures 54 and 56). This substantiates the assertion that the hold period effects dominate fatigue crack growth rates.

The next step in evaluating the effects of hold periods on the fatigue crack growth rate in this alloy is to determine the threshold level, if it exists. In power generation applications, the hold periods are two orders of magnitude greater than those examined in this thesis research. Conducting a series of hold period tests with various hold periods from a very short (0.1 hr.) to a fairly long (1-10 hr.) time, all at the same strain range and temperature would provide ample data for establishing an empirical relationship between length of hold period and a reduction in fatigue life.

This crack growth condition could then be combined with the crack initiation correlation developed by Challenger et. al. [Ref. 17] to more accurately predict the materials behavior under complex loading wave forms. In the final analysis, a more accurate prediction of material behavior at elevated temperatures in oxidizing environments loaded with complex waveforms was the principle motivation for this research.

VI. CONCLUSIONS AND RECOMMENDATIONS

The development of cellular dislocation substructures in single hold period tests is the result of a recovery process. This may also explain the lower dislocation densities observed in the tension plus compression hold tests and in all of the tests conducted at higher temperatures.

The cyclic hardening/cyclic softening reported for the alloy at 482°C and 538°C [Ref.]6] is not due to microstructural changes resolvable by transmission electron microscopy techniques. It may be the result of Mo-C atoms pairs agglomenating at an atomistic level to form Mo-C-Mo clusters. This would be consistent with the model proposed by Jones and Van Den Avyle [Ref. 14] for the formation of Mo_2C carbides in this alloy during elevated temperature fatigue.

The dislocation cell size is solely a function of carbide interparticle spacing. This is not consistent with the general dependence of cell size on saturated stress reported in the literature [Ref. 36-41] but has been observed in other precipitate bearing alloys [Ref. 42-45]. Based on the hypothesized change in the material at these temperatures, longer testing times would possibly result in a second cyclic softening as the Mo-C-Mo clusters combine to form critical nuclei for Mo_2C carbides.

The fatigue crack growth rate is dominated by the time per cycle the specimen is exposed to the environment. There is evidence to support the theory that the crack growth rate is dependent on the presence (concentration and residence) of oxygen at the crack tip. The damage may be the result of oxygen atoms impeding plastic flow ahead of the crack tip. The time per cycle dependence suggests that the rate controlling step is either surface adsorption of the oxygen atoms, or diffusion of them to the material ahead of the crack tip.

It is recommended that a series of hold period fatigue tests be conducted in a vacuum or inert environment at low strain ranges in the temperature range 482°C-538°C. This would eliminate the environmental enhancement prolonging the fatigue life and permit the evaluation of microstructural changes resulting from longer lifetimes.

A series of hold period fatigue test with varying hold times should be run at elevated temperature in air to establish the relation between length of hold period and fatigue crack growth rate.
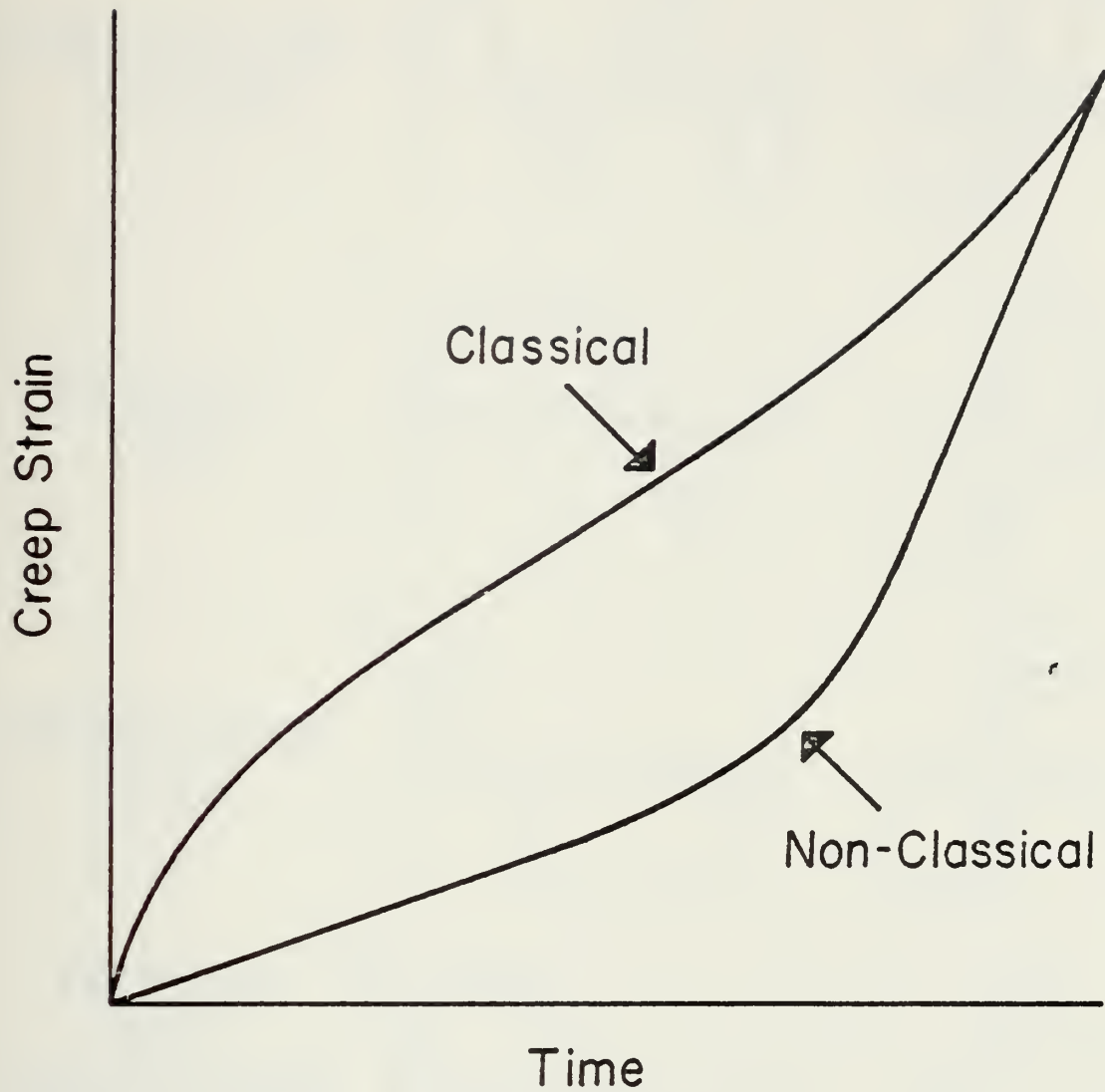
Figure 1. Classical vs. Nonclassical Creep Behavior
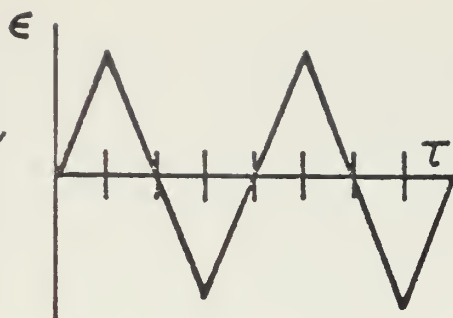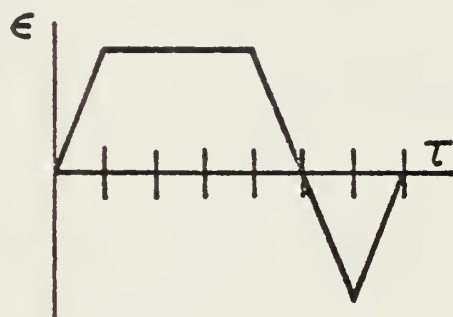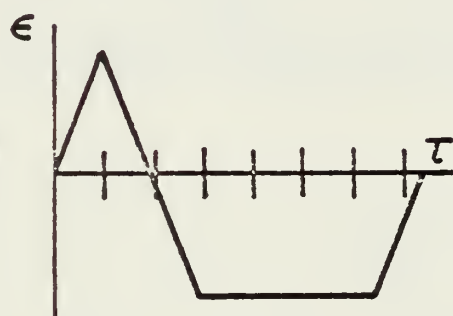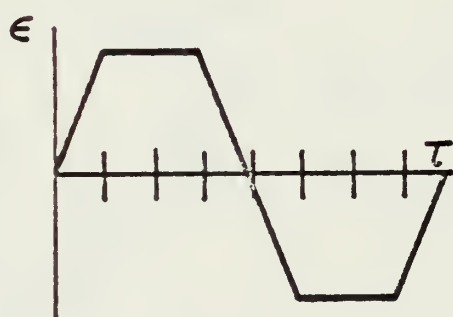
Figure 2. Loading Waveforms
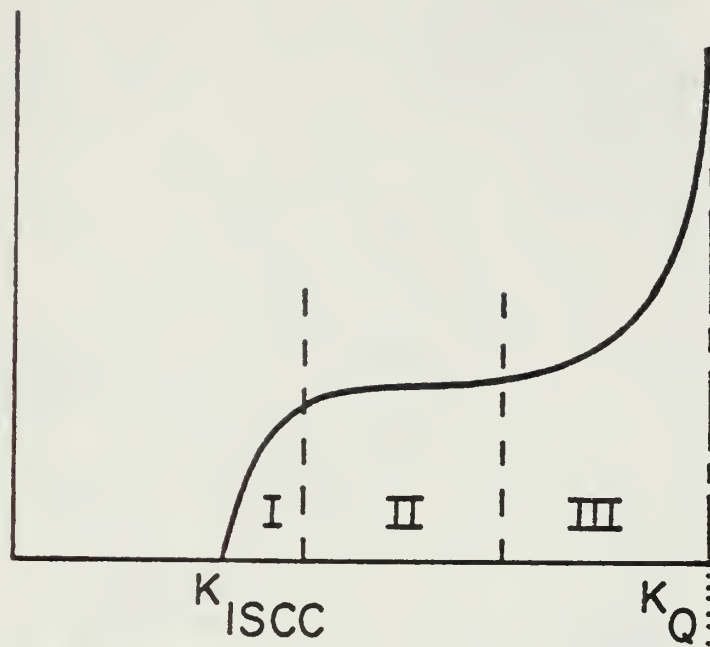
62
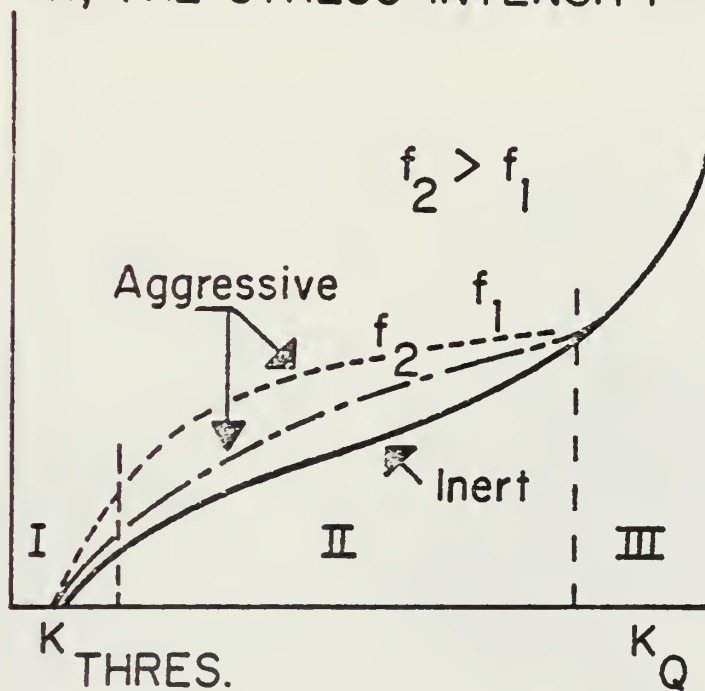
Figure 3. Stress Corrosion Cracking and Environmentally Enhanced Fatigue Behavior

63
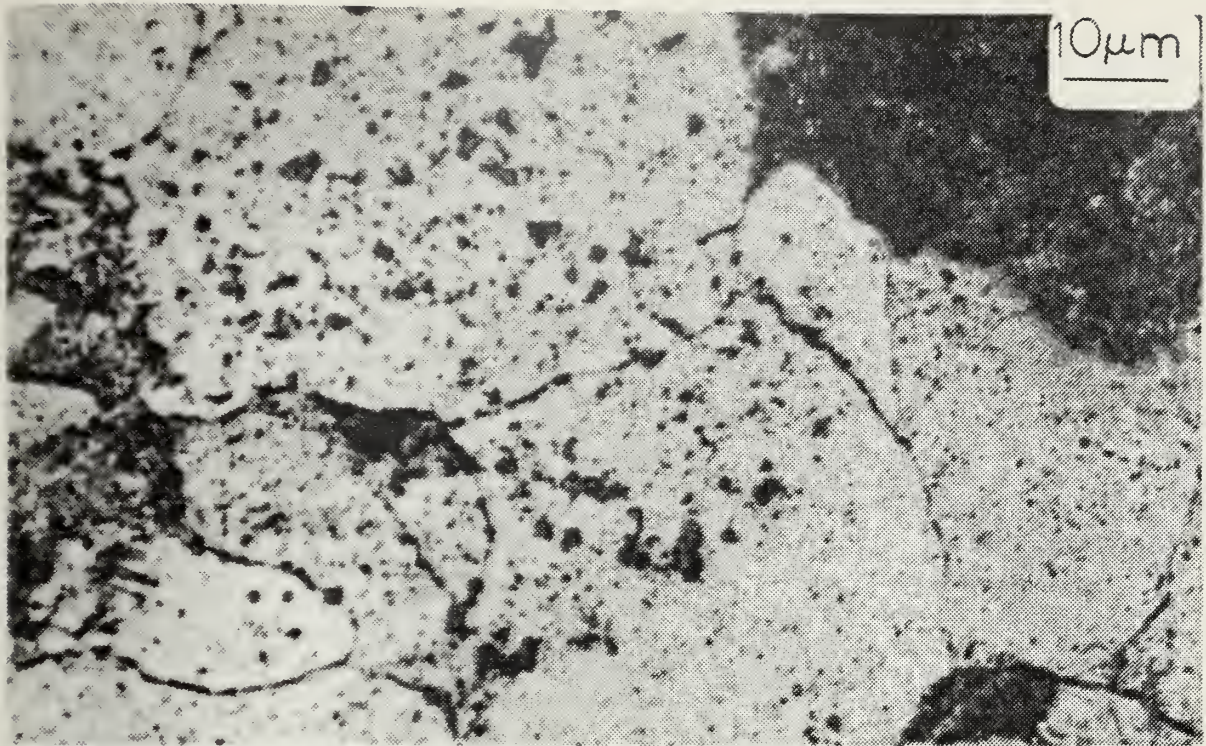
Figure 4. As Heat Treated Material - Optical Micrograph
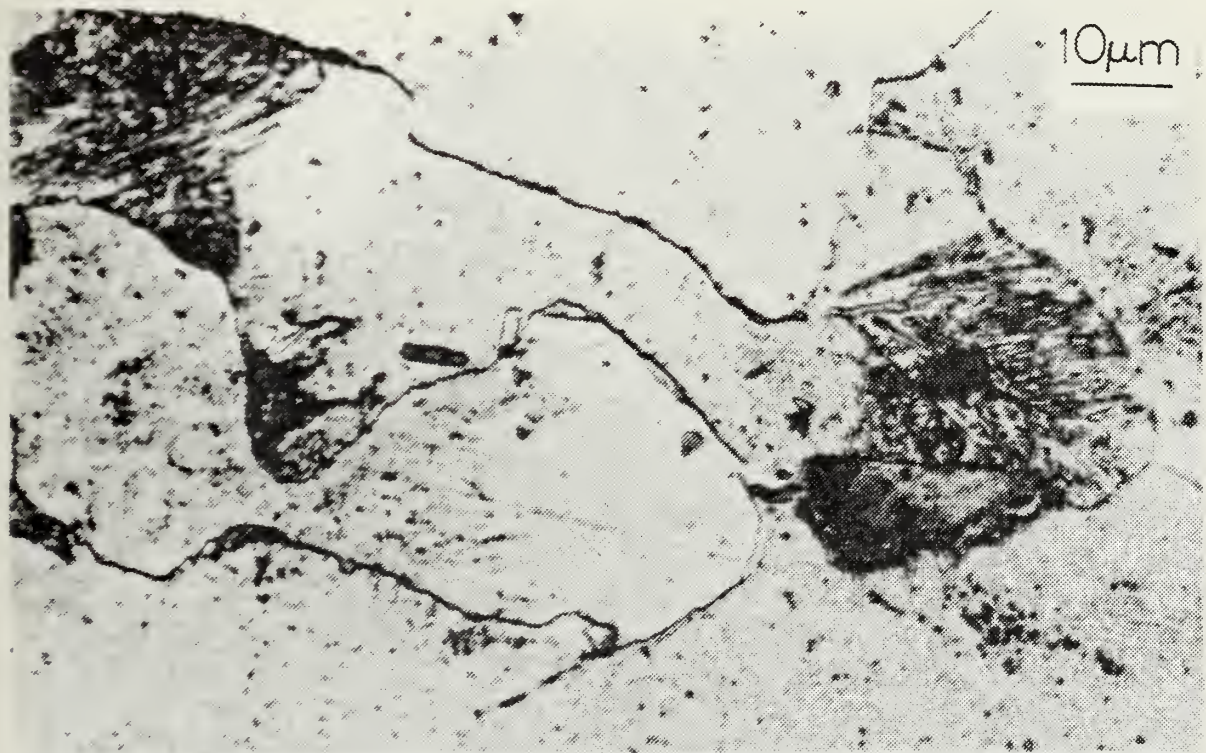
Figure 5. As Heat Treated Material - Optical Micrograph

64
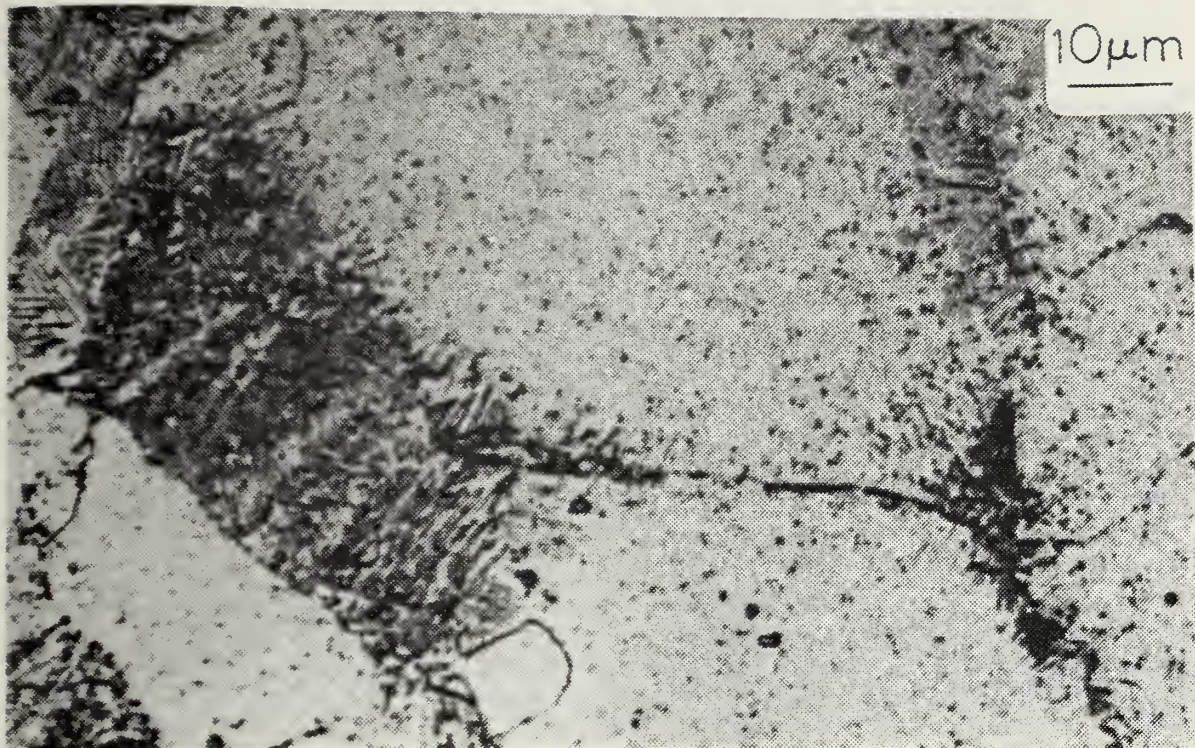
Figure 6.   As Heat Treated Material - Optical Micrograph
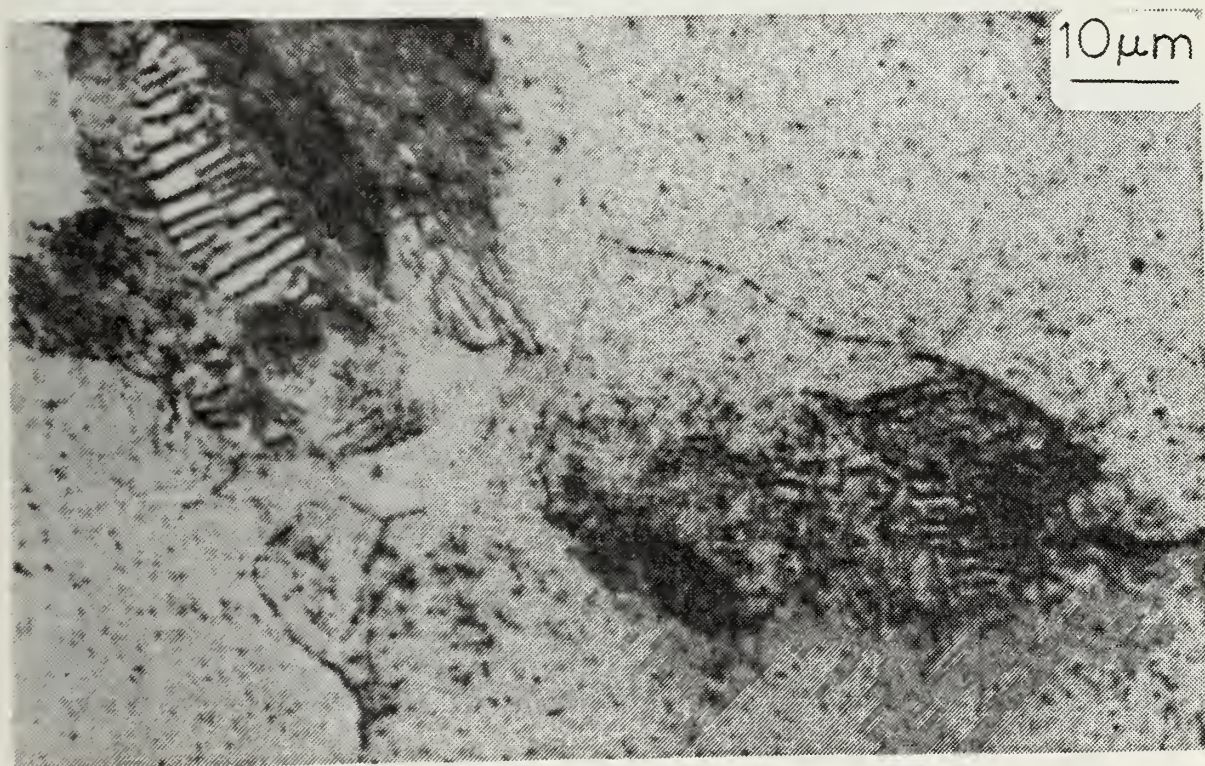
Figure 7.   MIL18 - Optical Micrograph

65
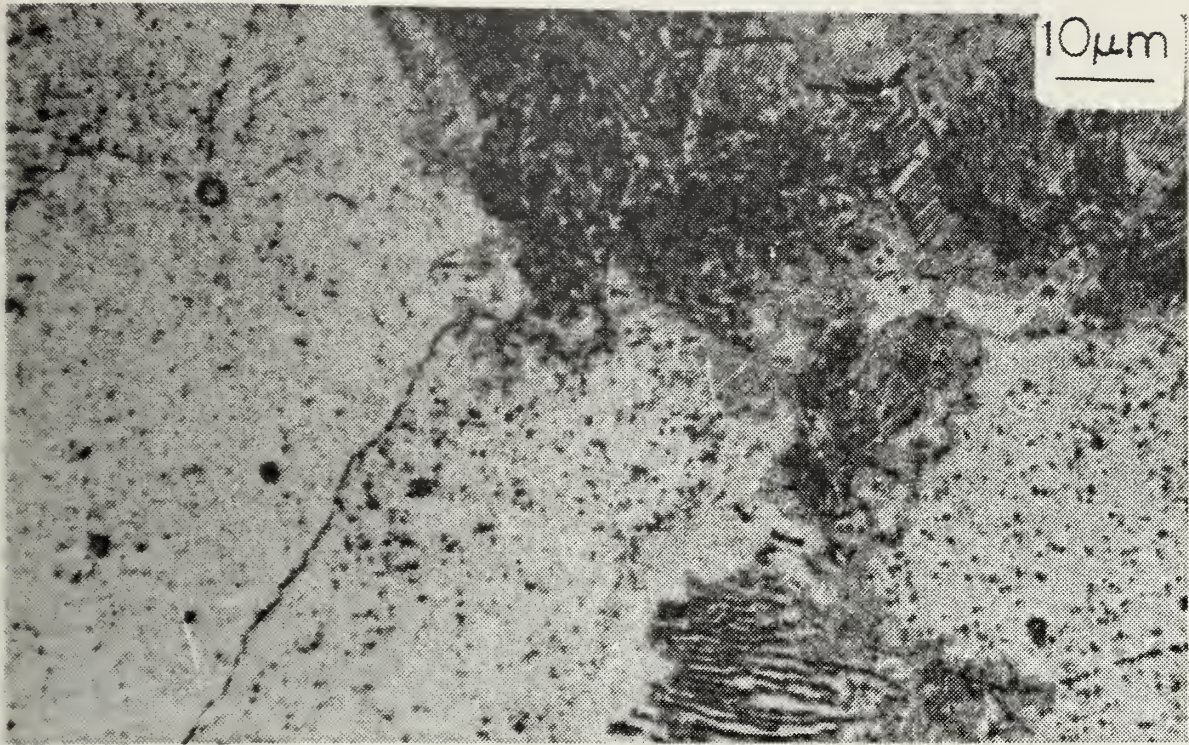
Figure 8. MIL 44 - Optical Micrograph
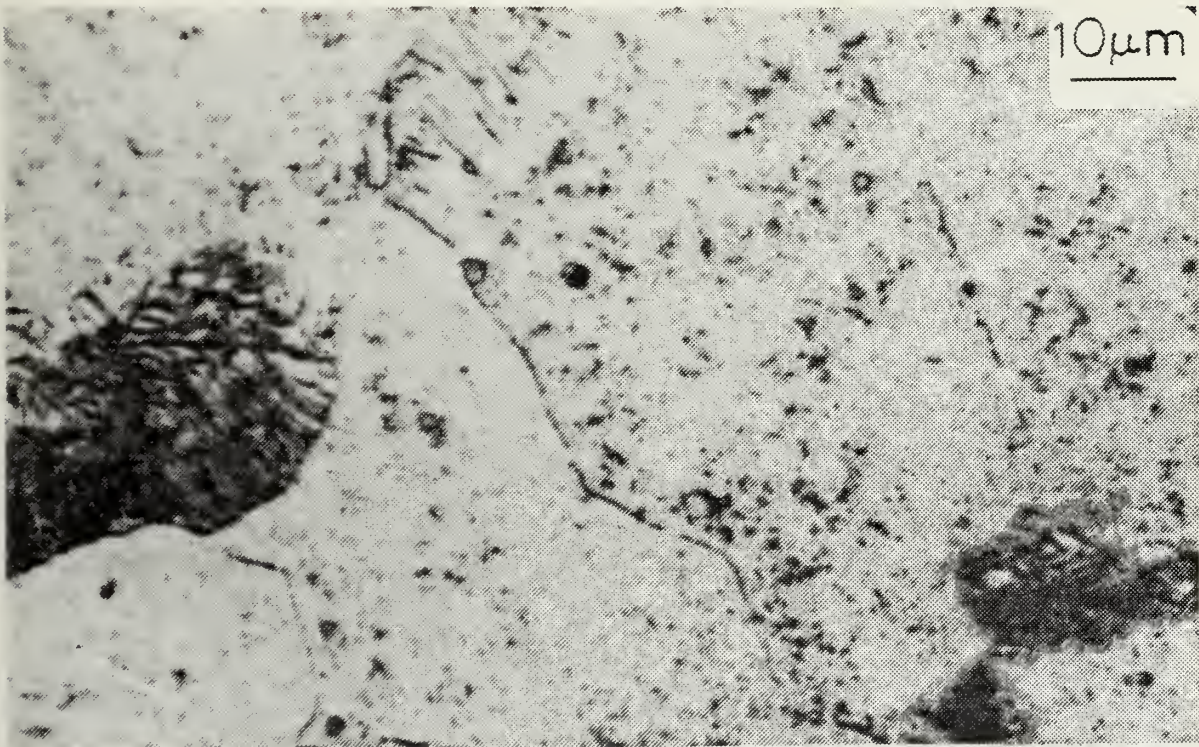
Figure 9. MIL10 - Optical Micrograph

66
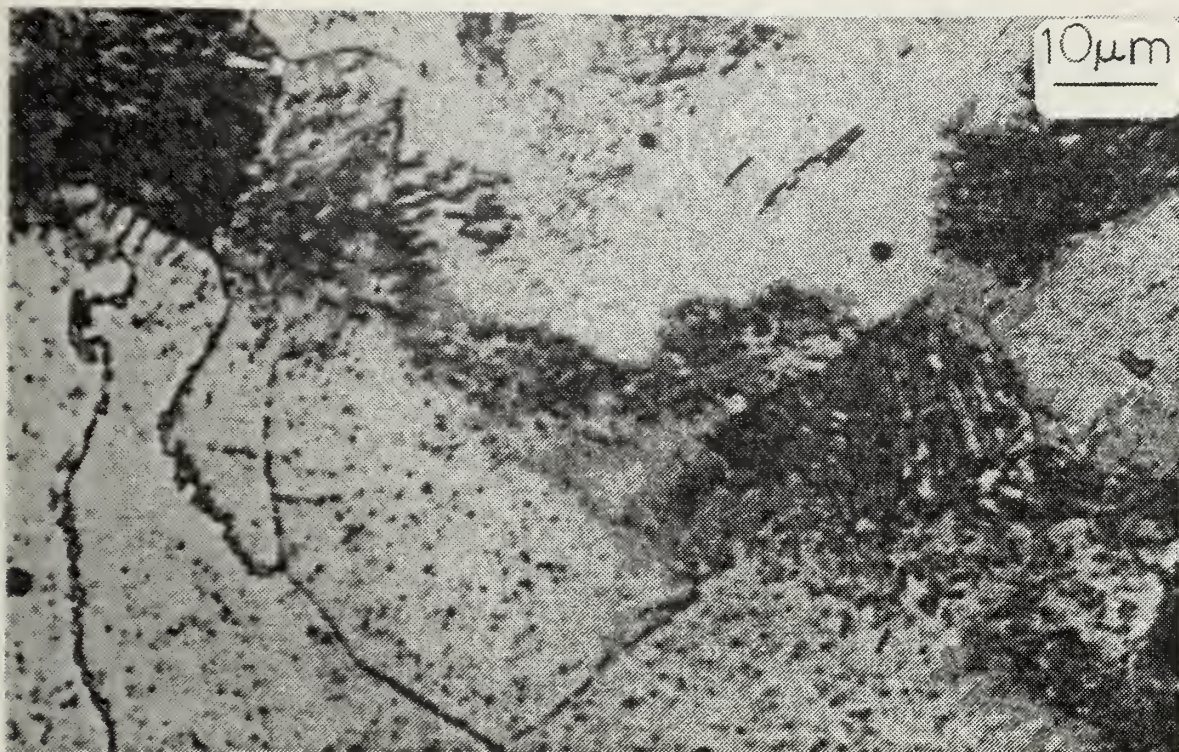
Figure 10. MIL24 - Optical Micrograph

Figure 11. MIL34 - Optical Micrograph
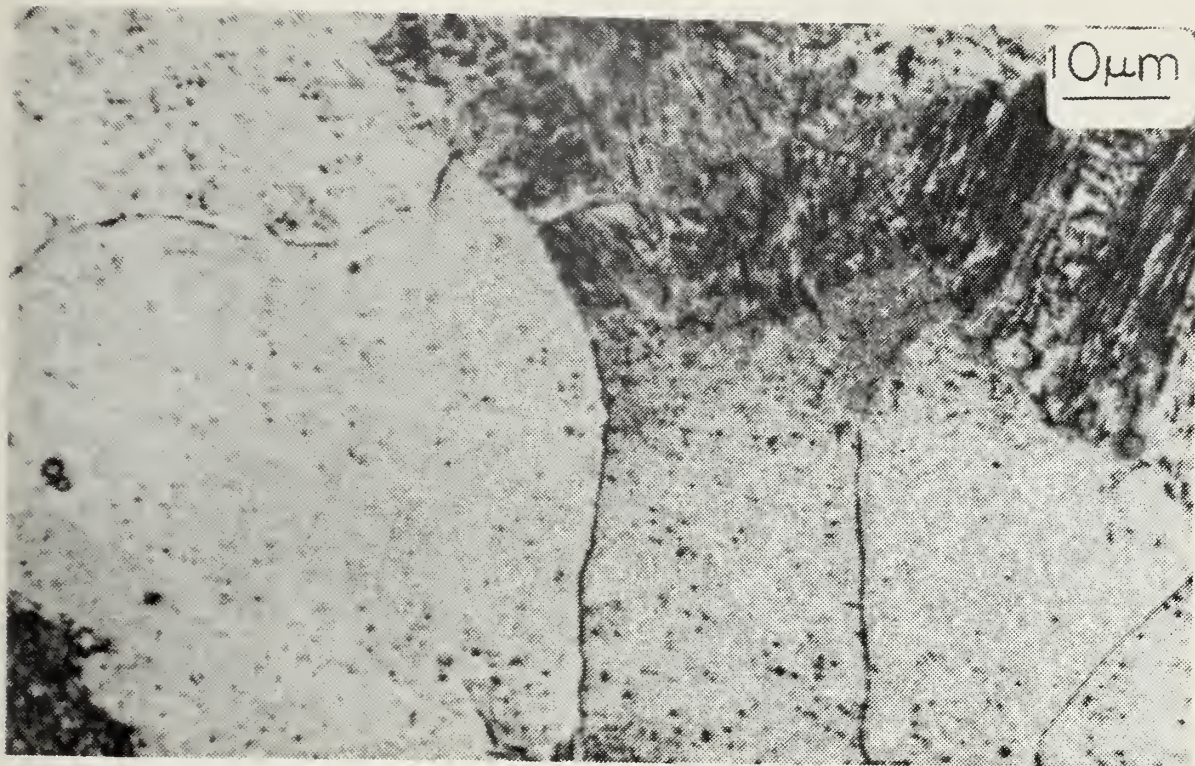
Figure 12. MIL20 - Optical Micrograph
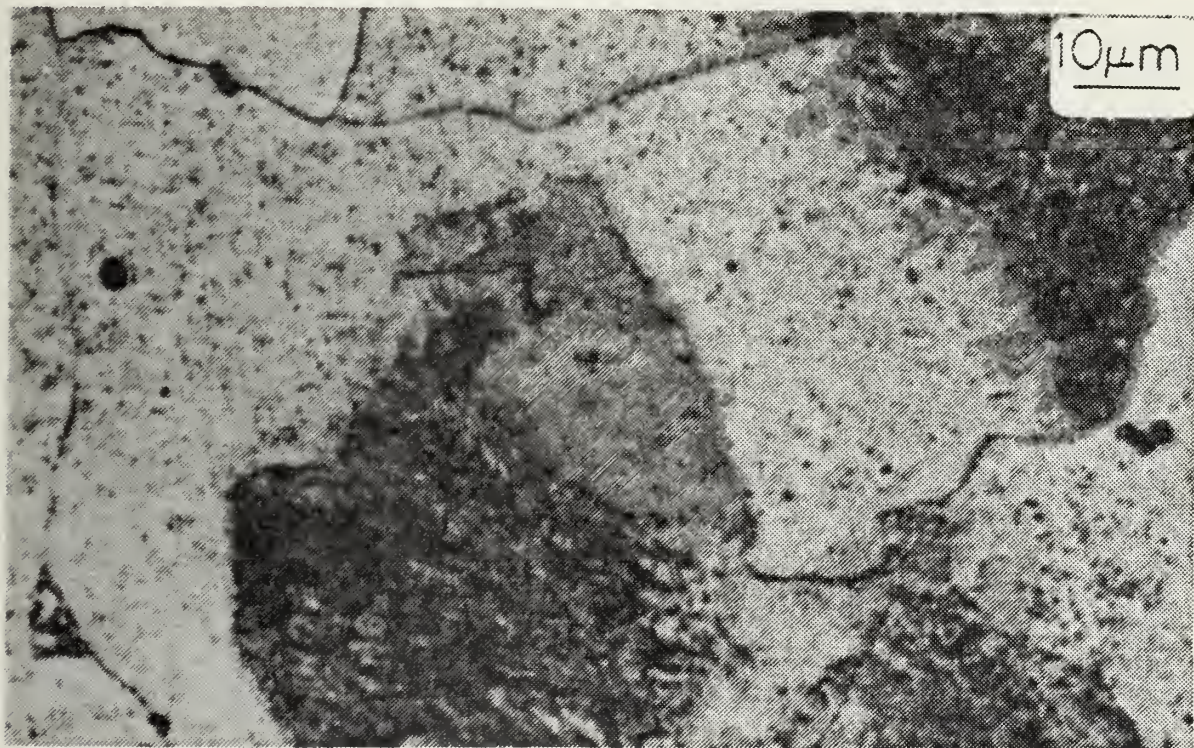
Figure 13. MIL27 - Optical Micrograph

68
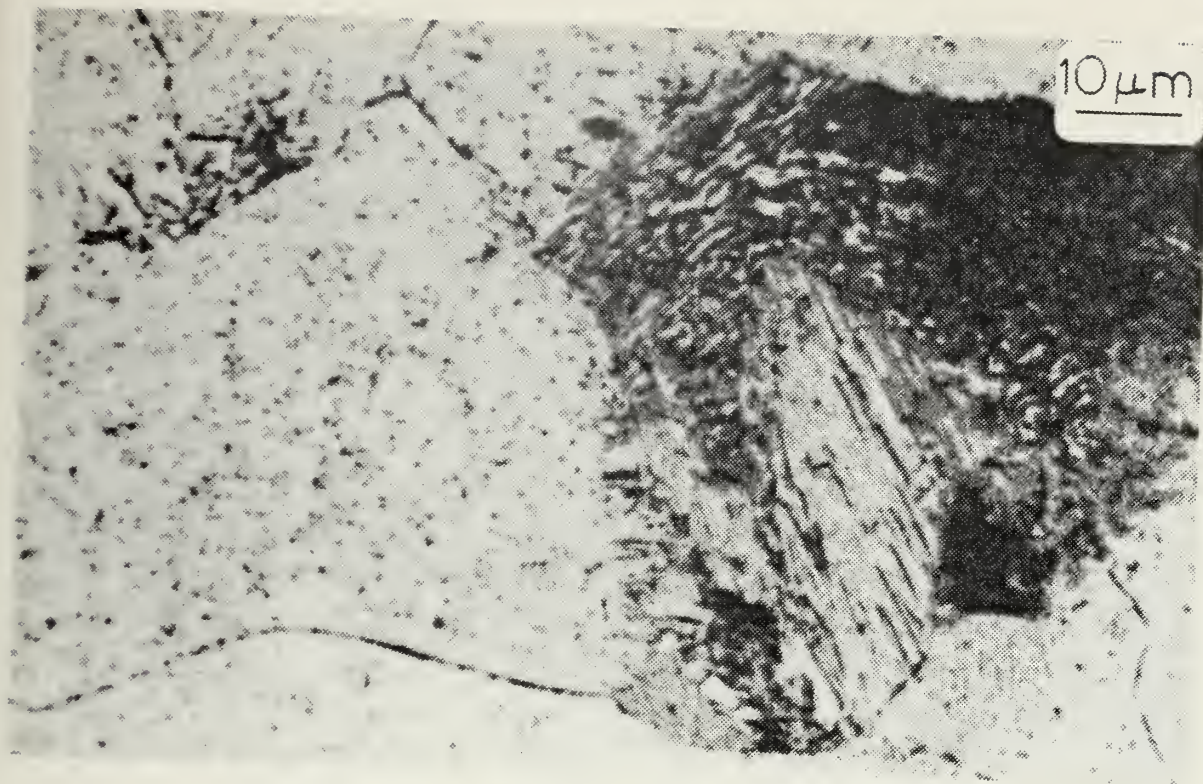
Figure 14.   MIL36 - Optical Micrograph
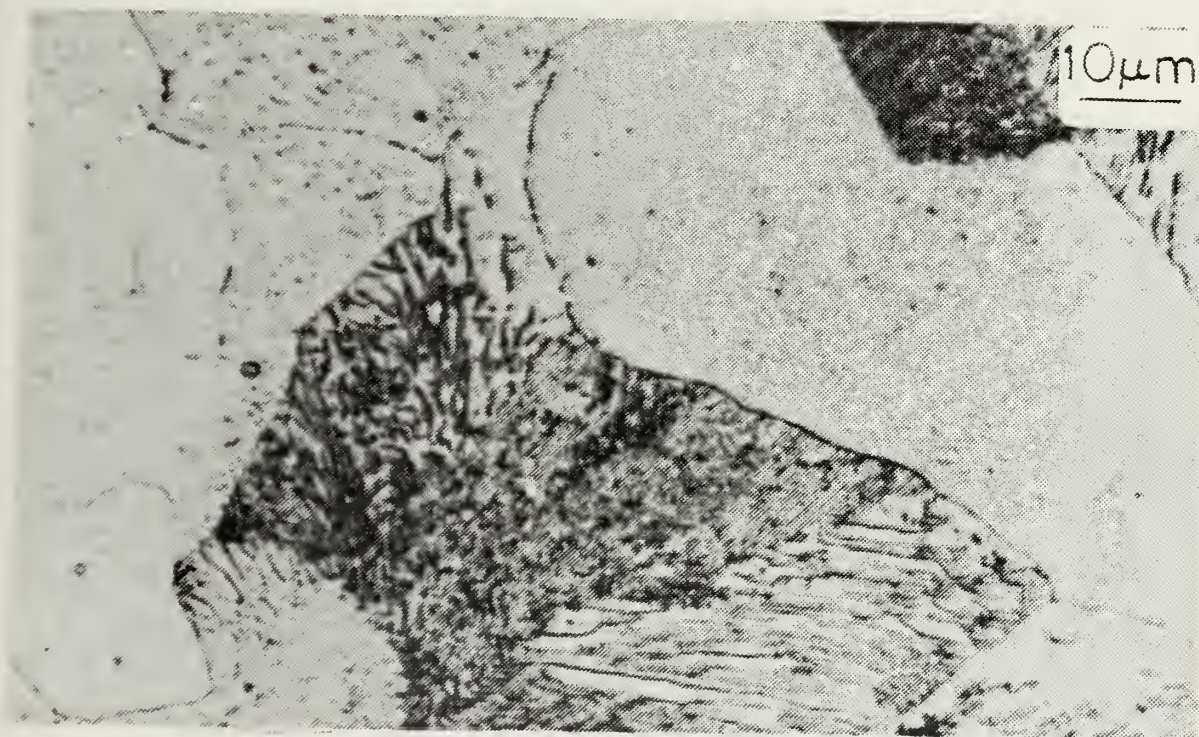
Figure 15.   MIL35 - Optical Micrograph

69
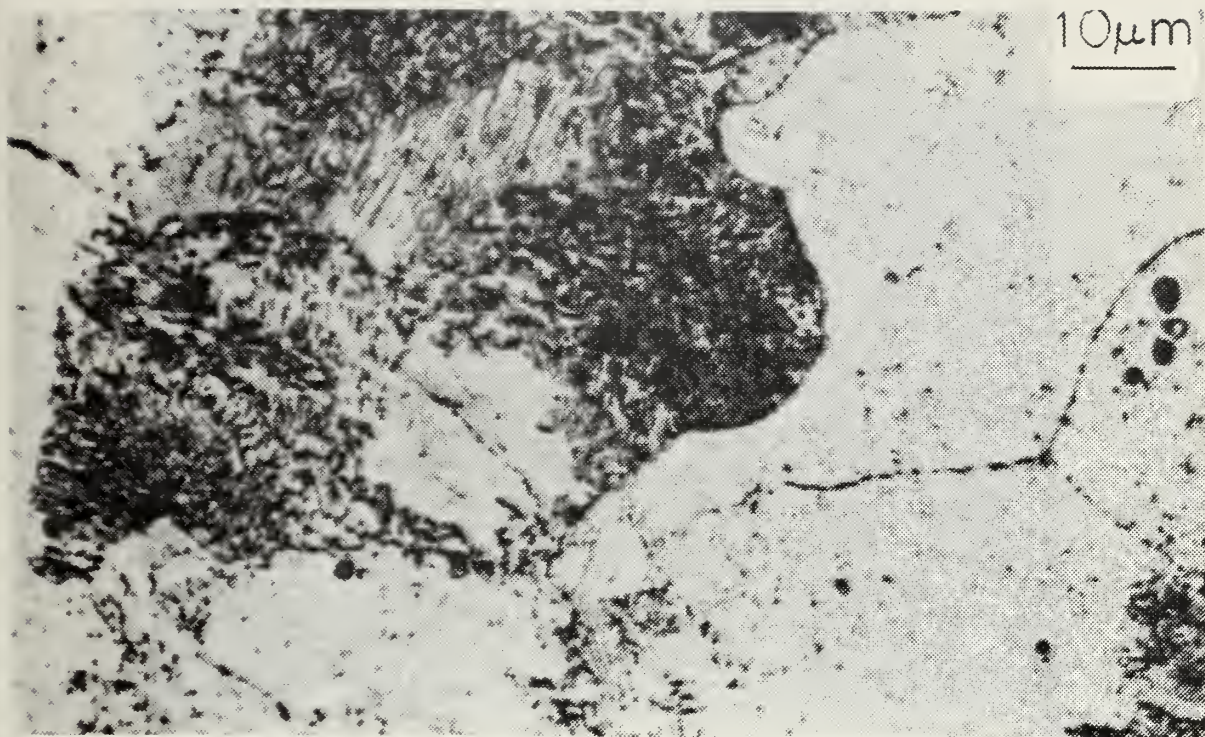
Figure 16.   MIL65 - Optical Micrograph
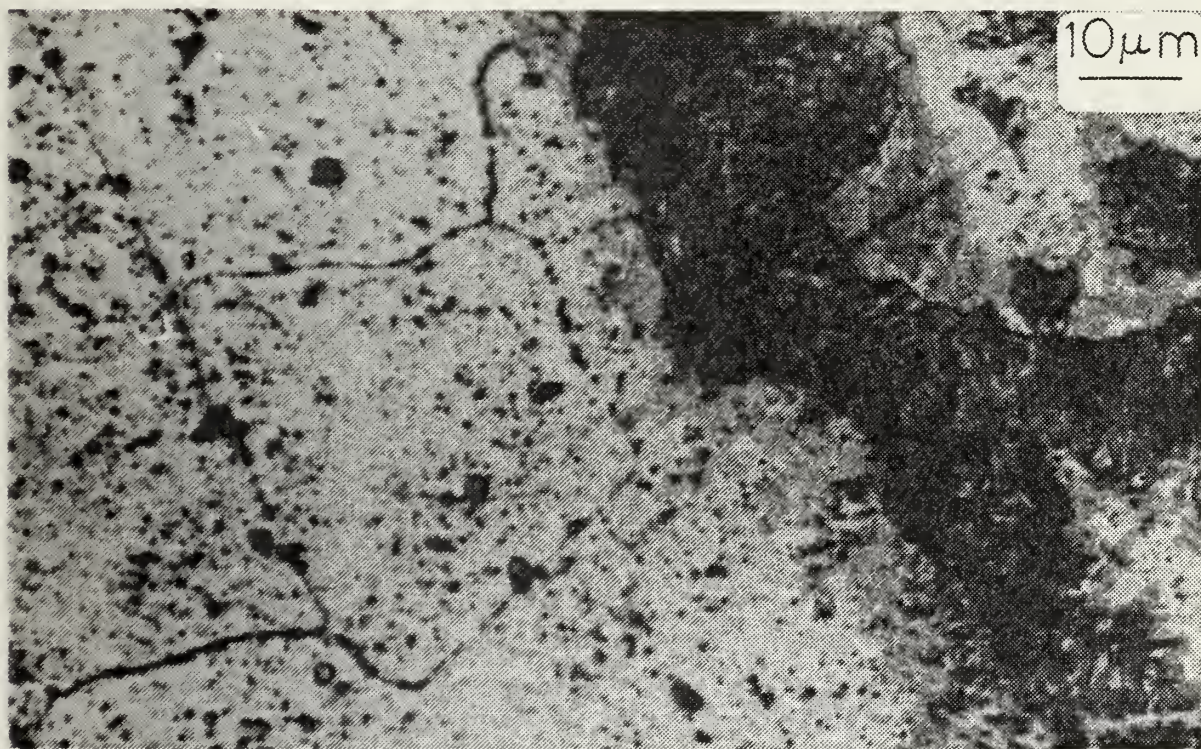
Figure 17.   ITL127 - Optical Micrograph

70
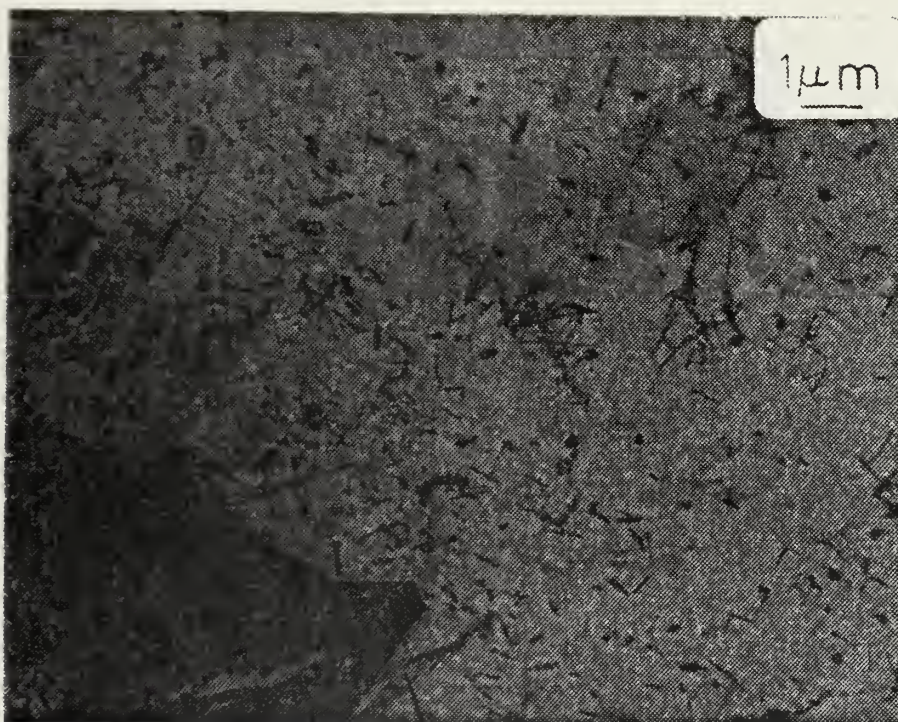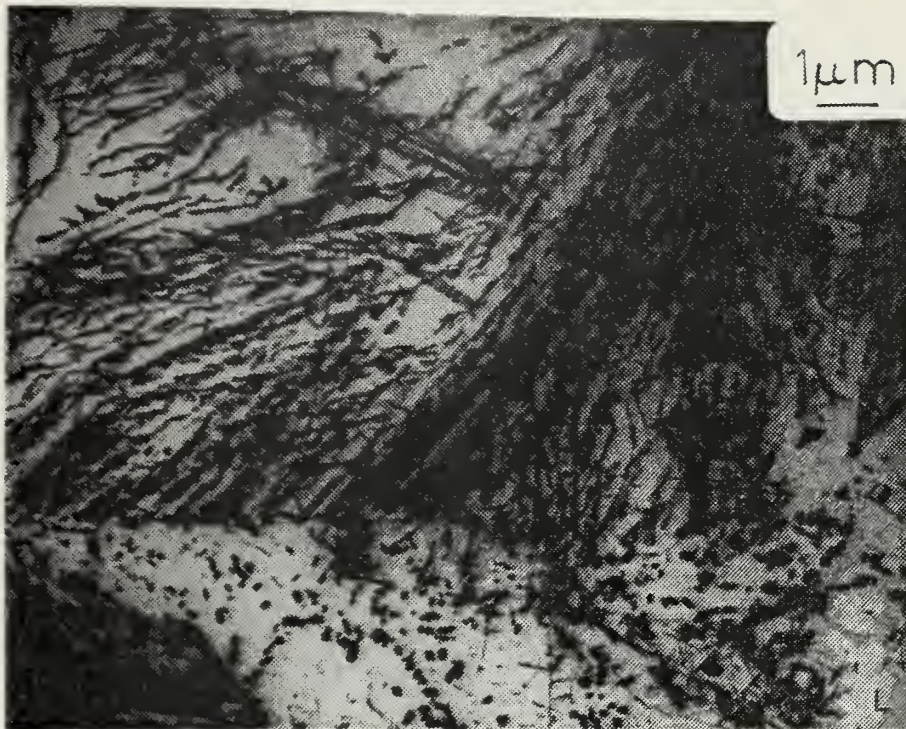
Figure 18. As Heat Treated Material - TEM Photo of Carbon
            Extraction Replica

71

Figure 18 (continued)

72

Figure 18 (continued)

73
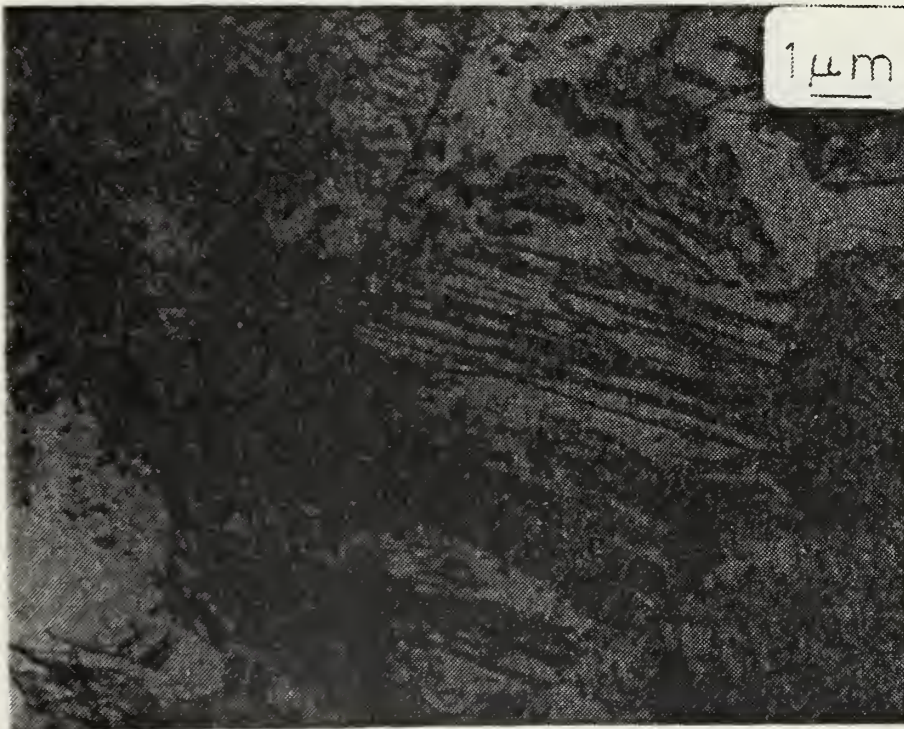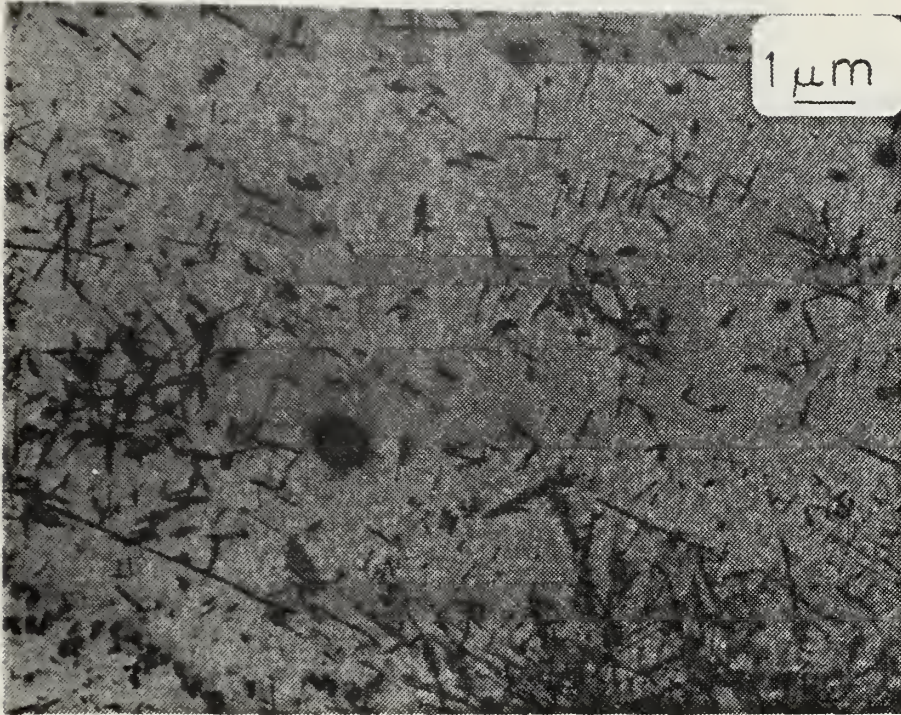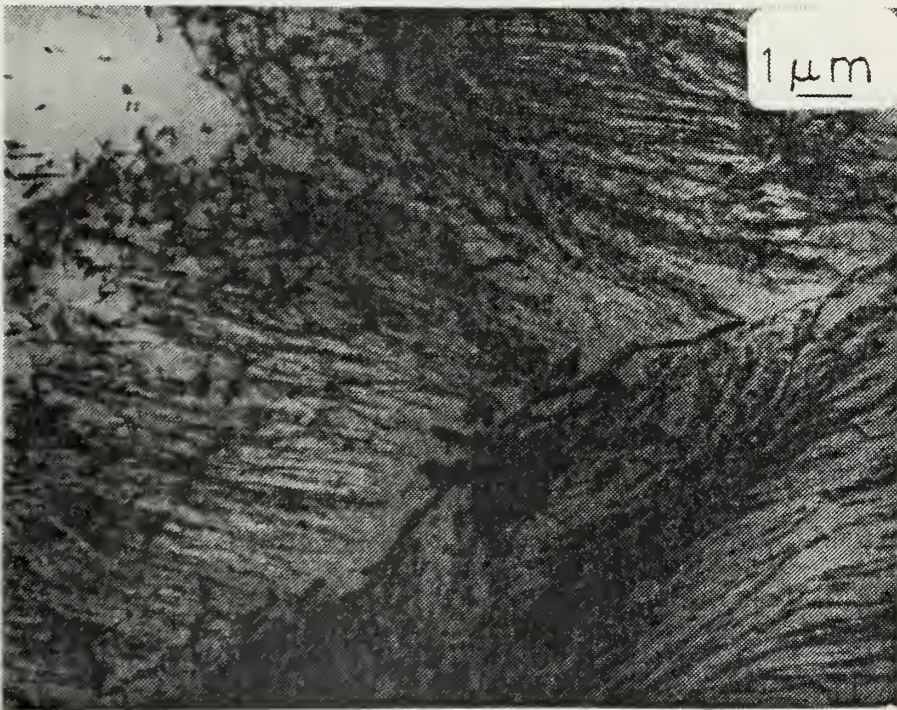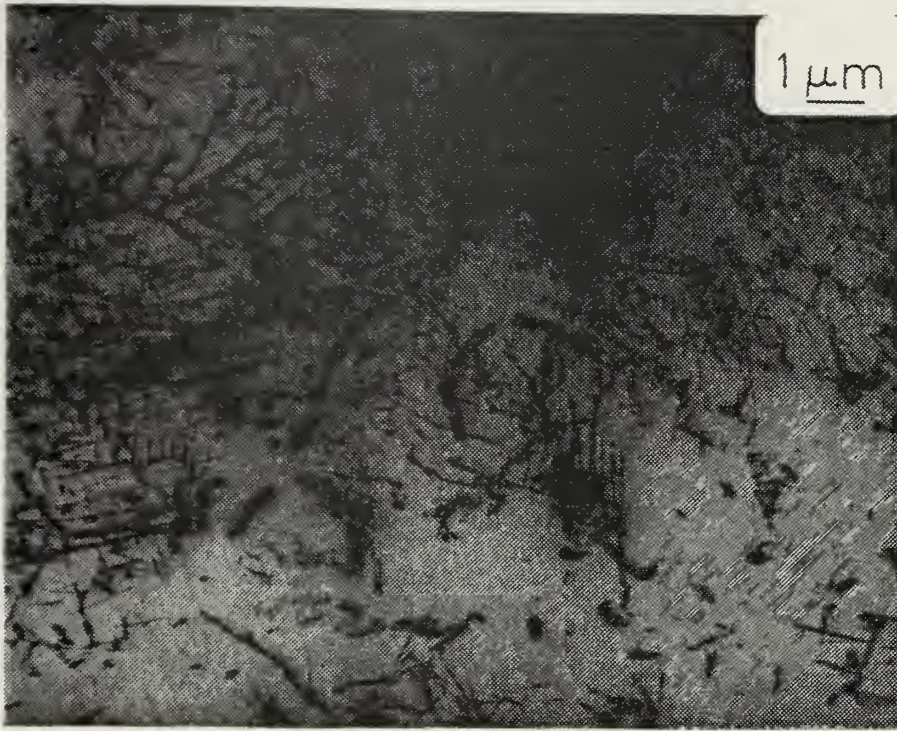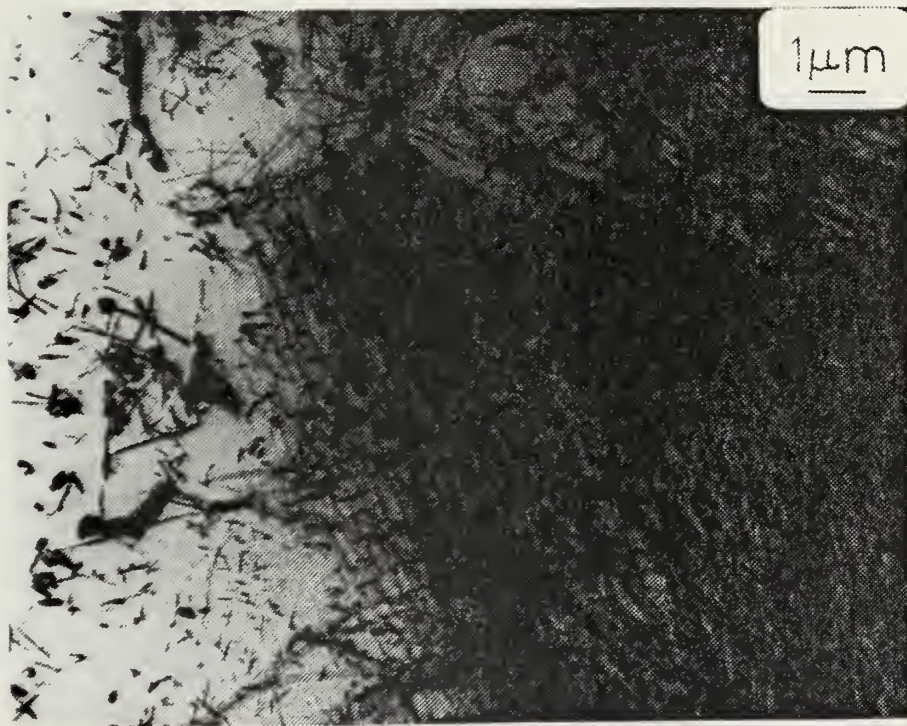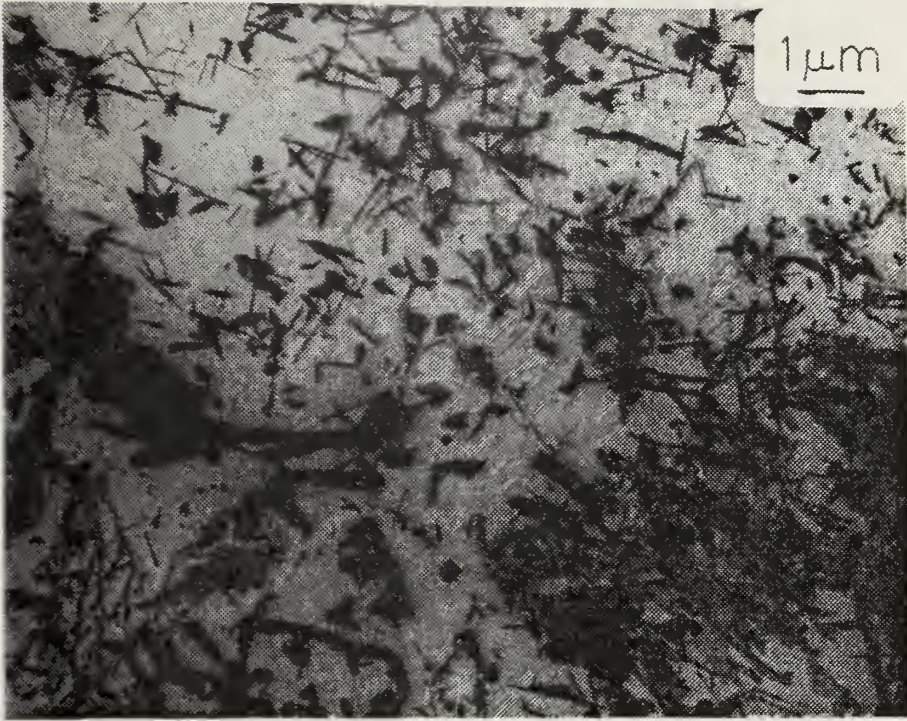
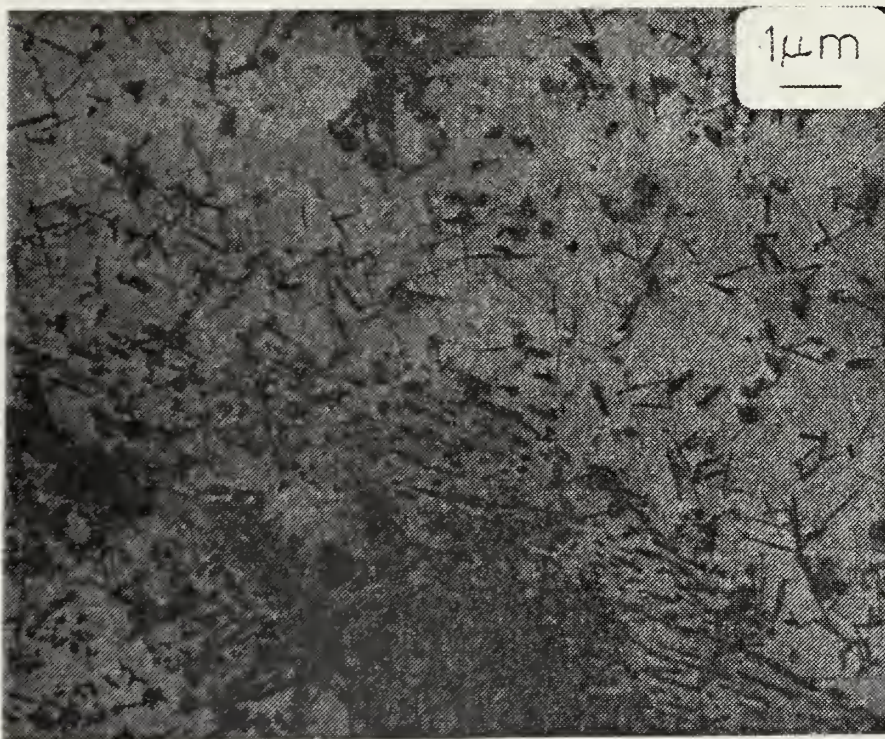Figure 19.   MIL18 - TEM Photo
of Carbon Extraction
Replica

74
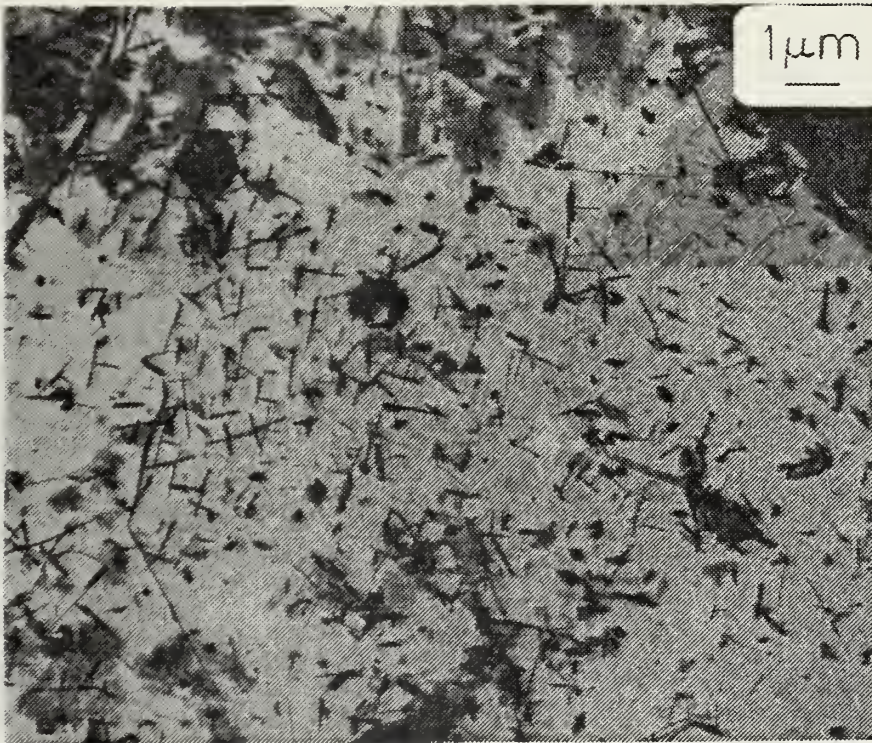
Figure 20. MIL44 - TEM Photo of Carbon Extraction Replica
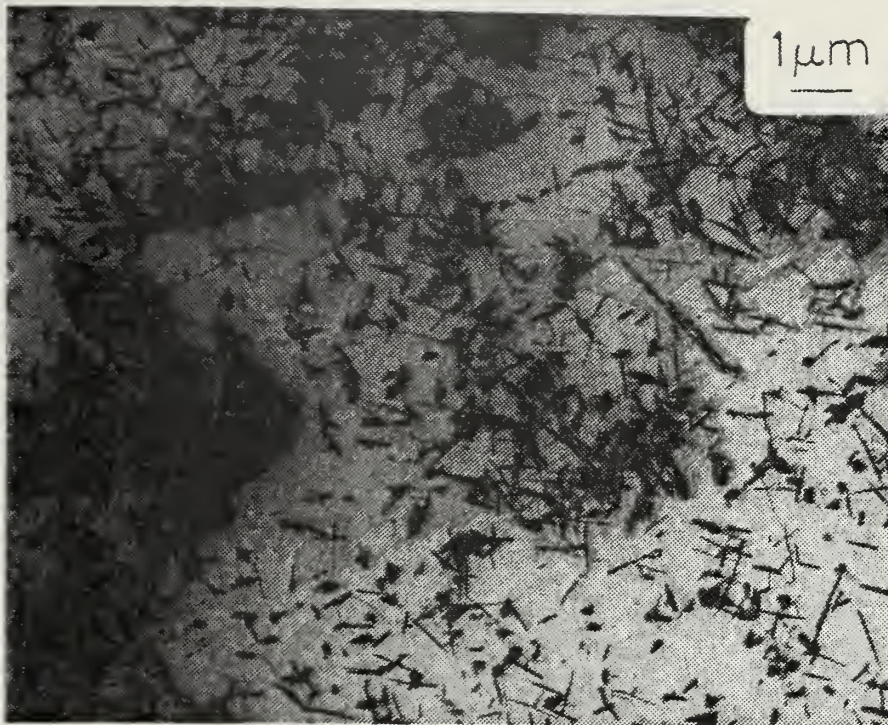
Figure 21.   MIL24 - TEM Photo of Carbon Extraction Replica

76
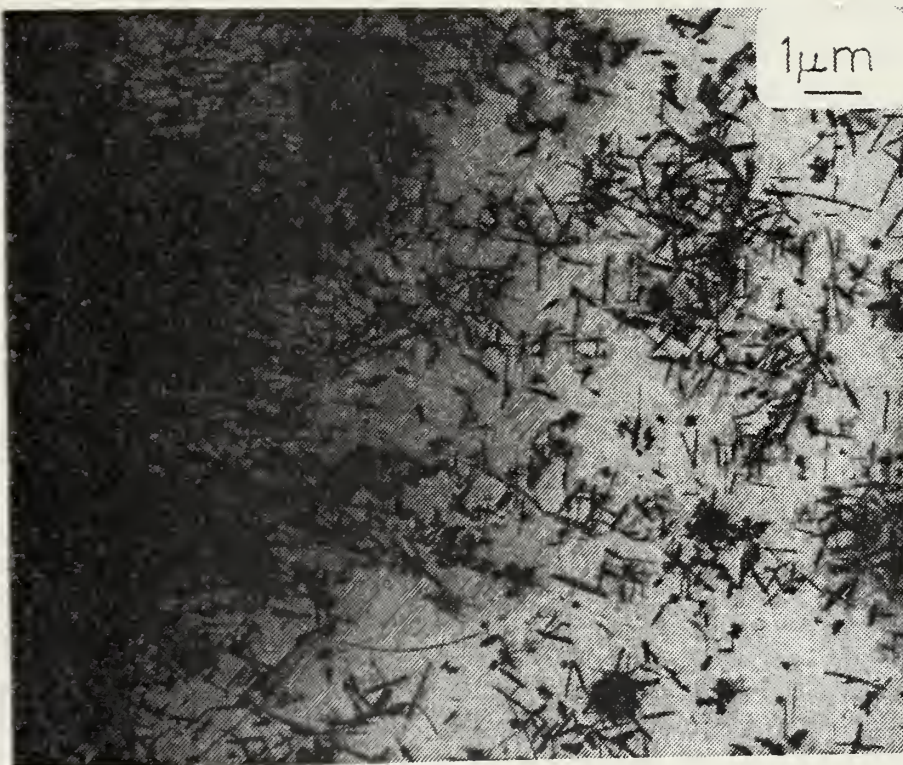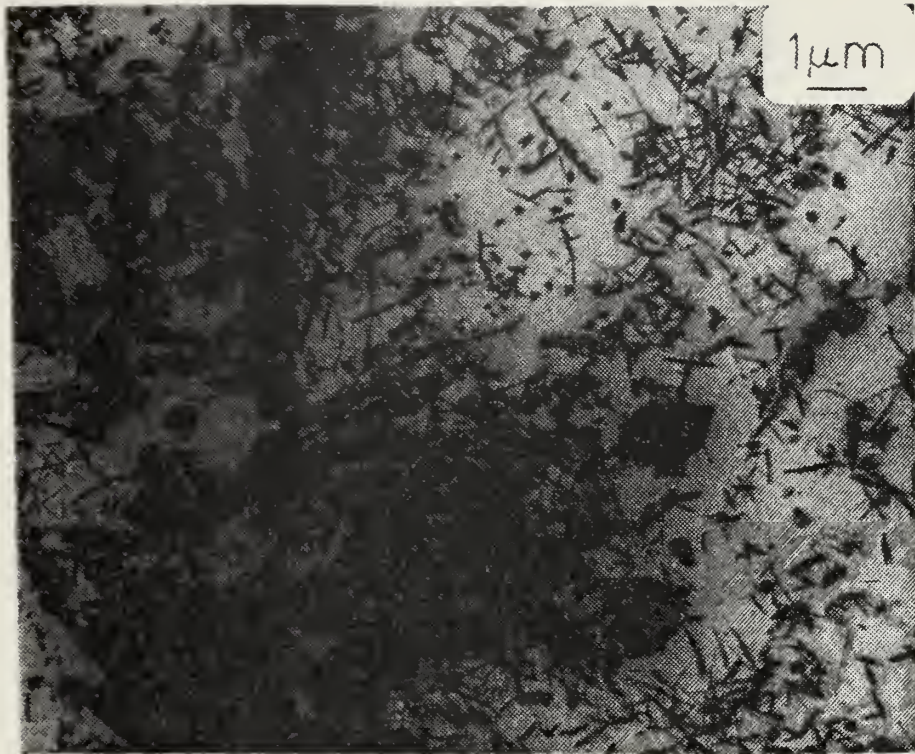
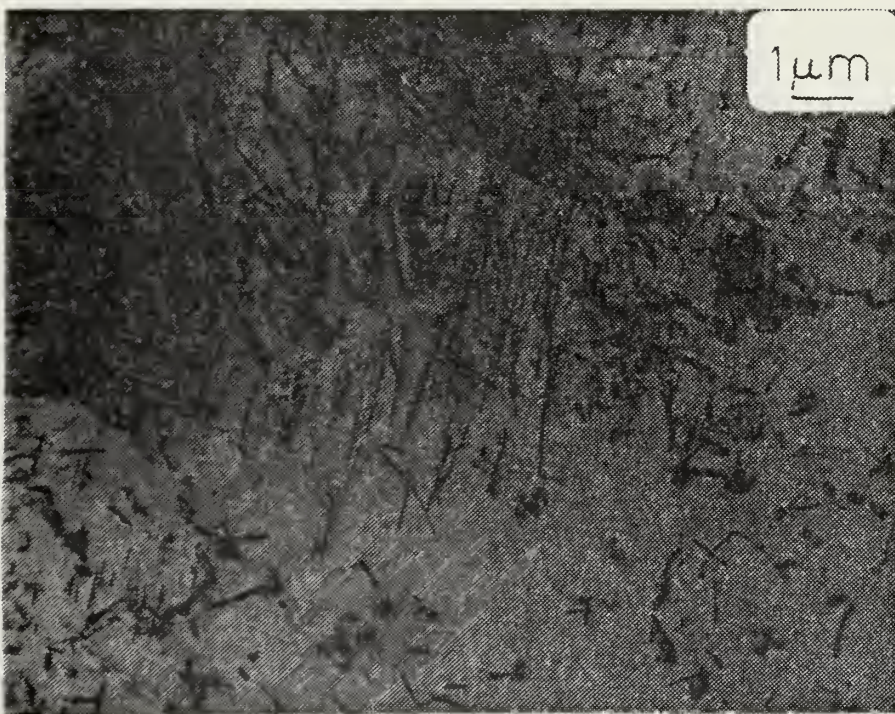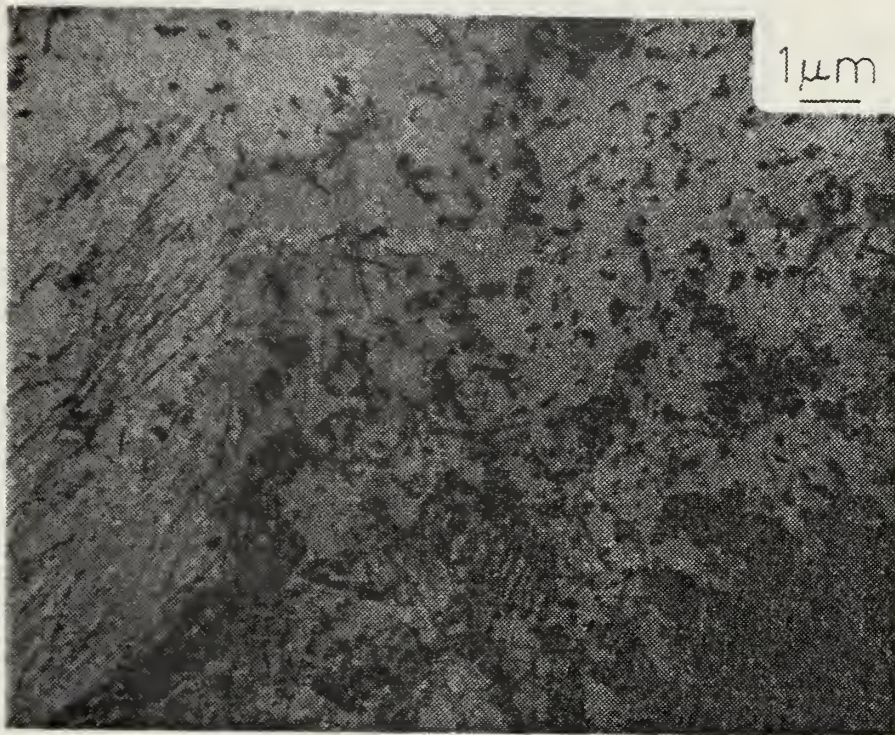Figure 22.   MIL35 - TEM Photo of Carbon Extraction Replica
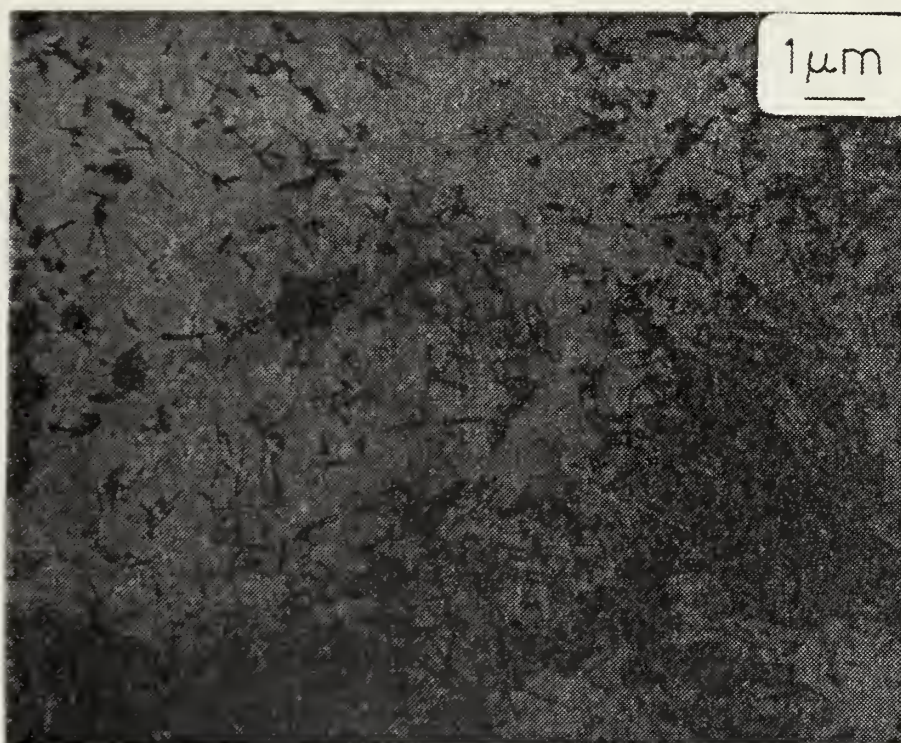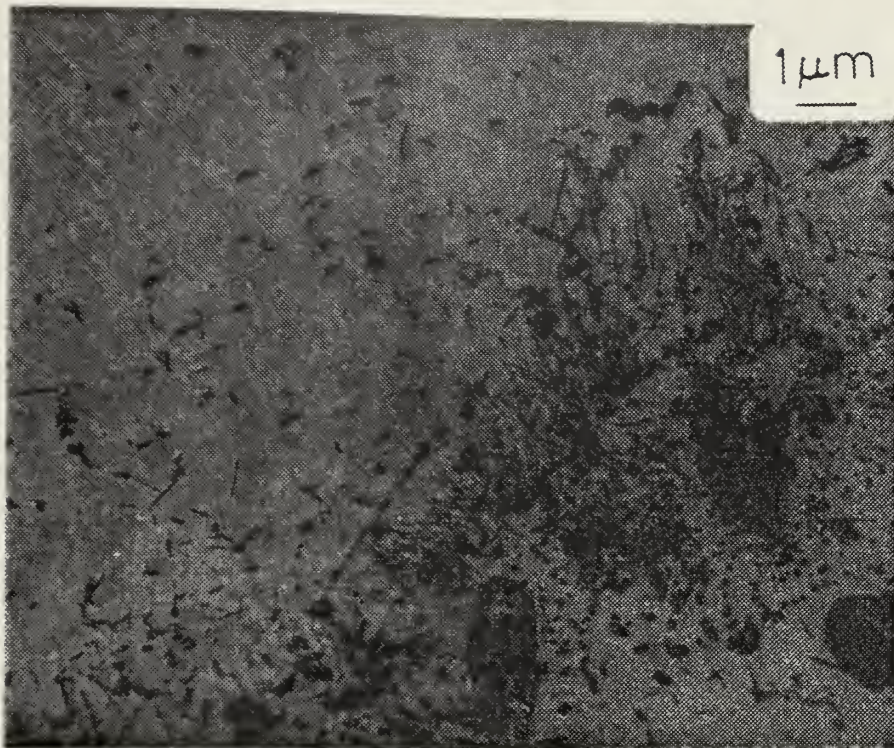
Figure 23. MIL27 - TEM Photo of Carbon Extraction Replica

78
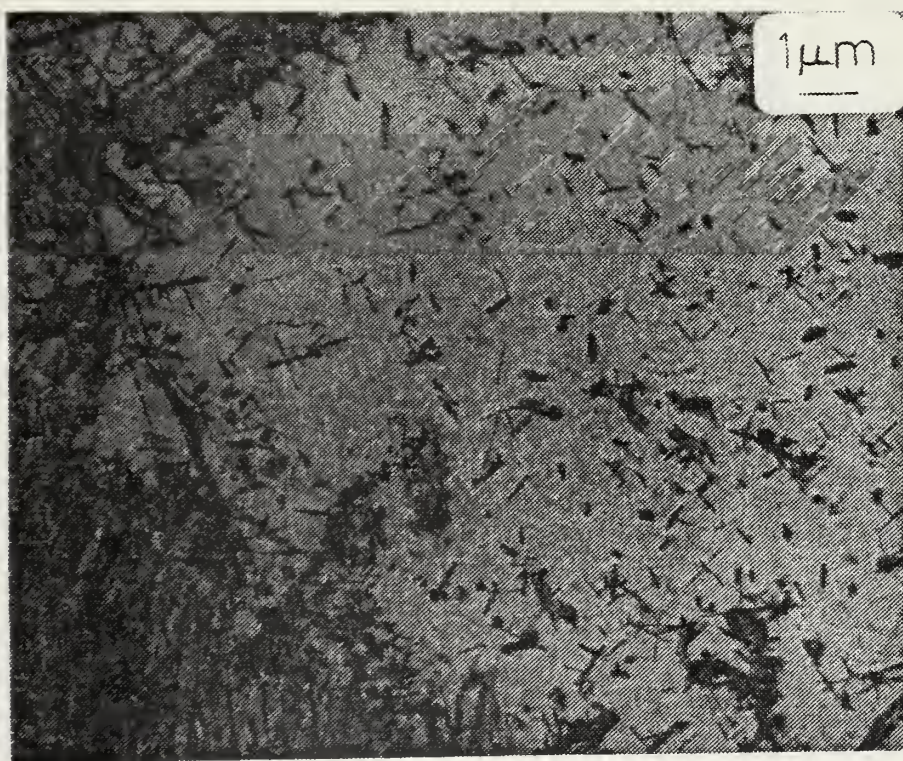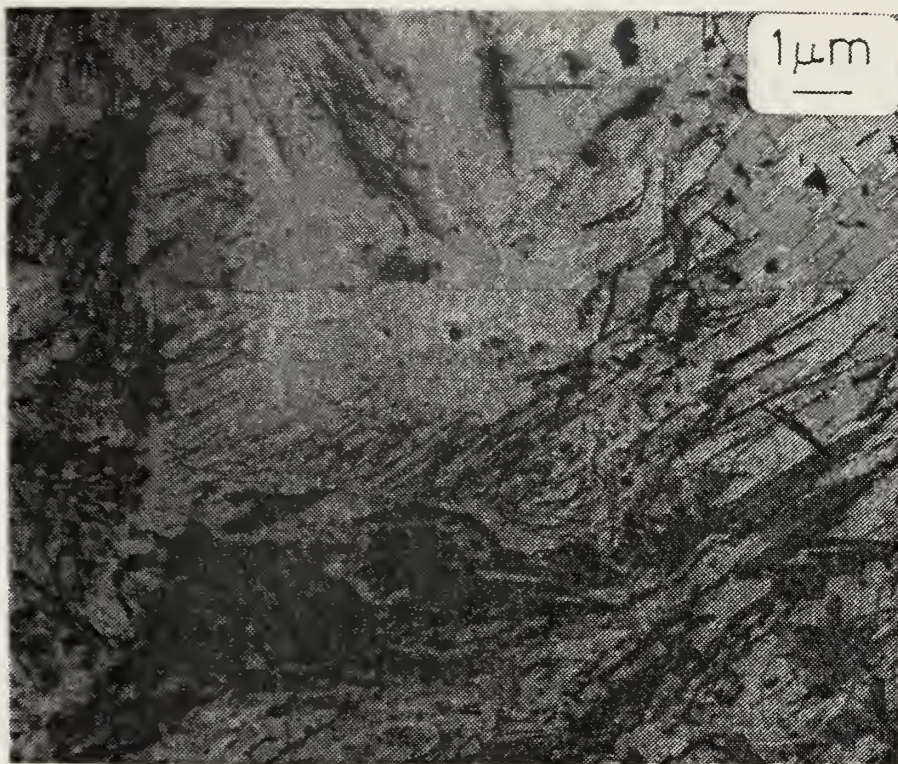
Figure 24.   MIL65 - TEM Photo of Carbon Extraction Replica

79
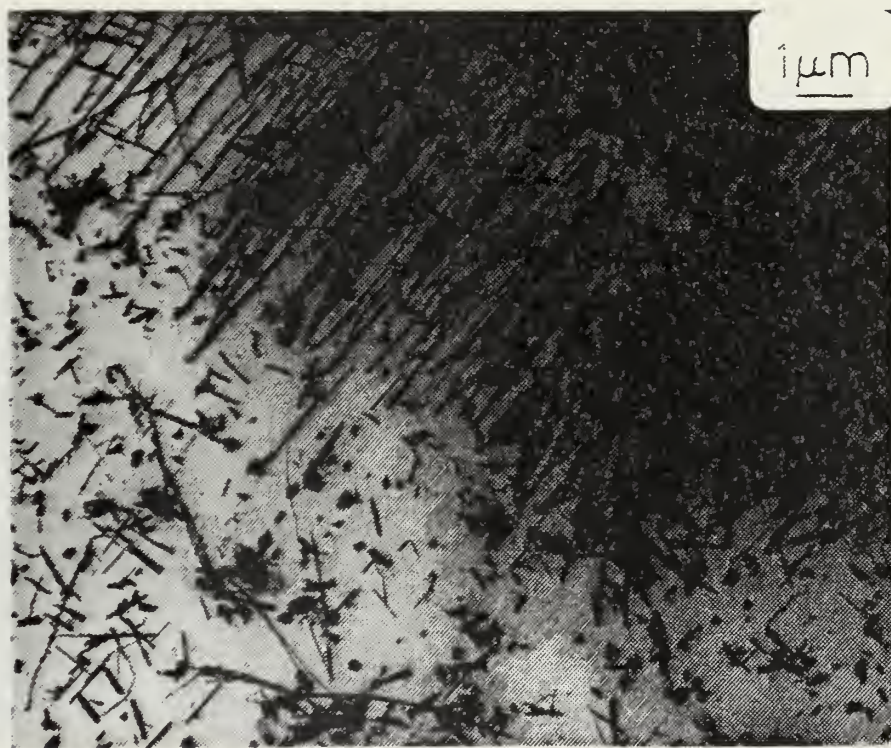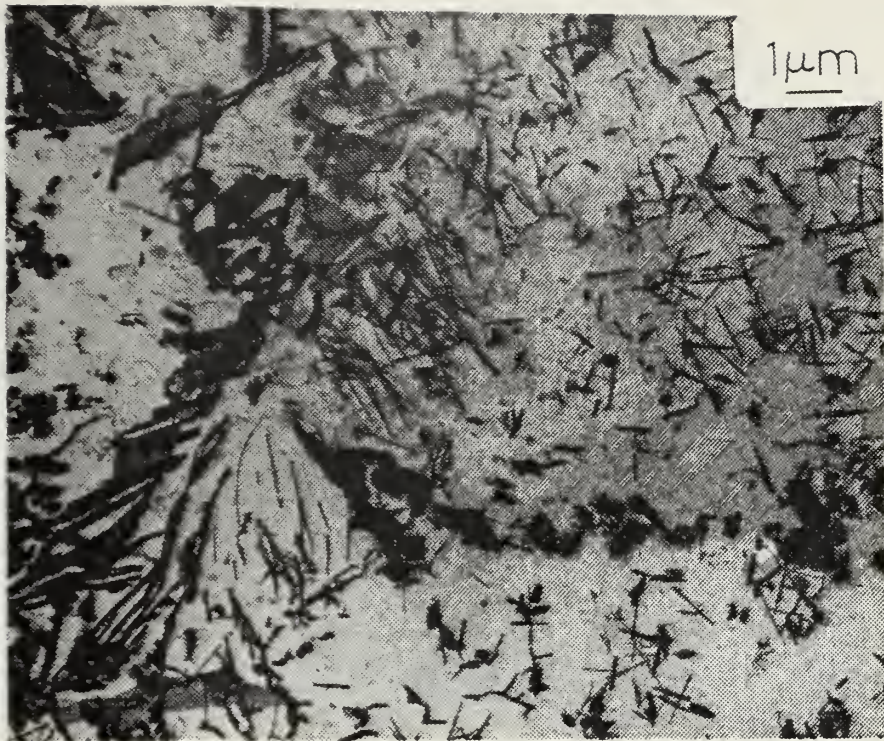
Figure 25.   MIL36 - TEM Photo of Carbon Extraction Replica

80
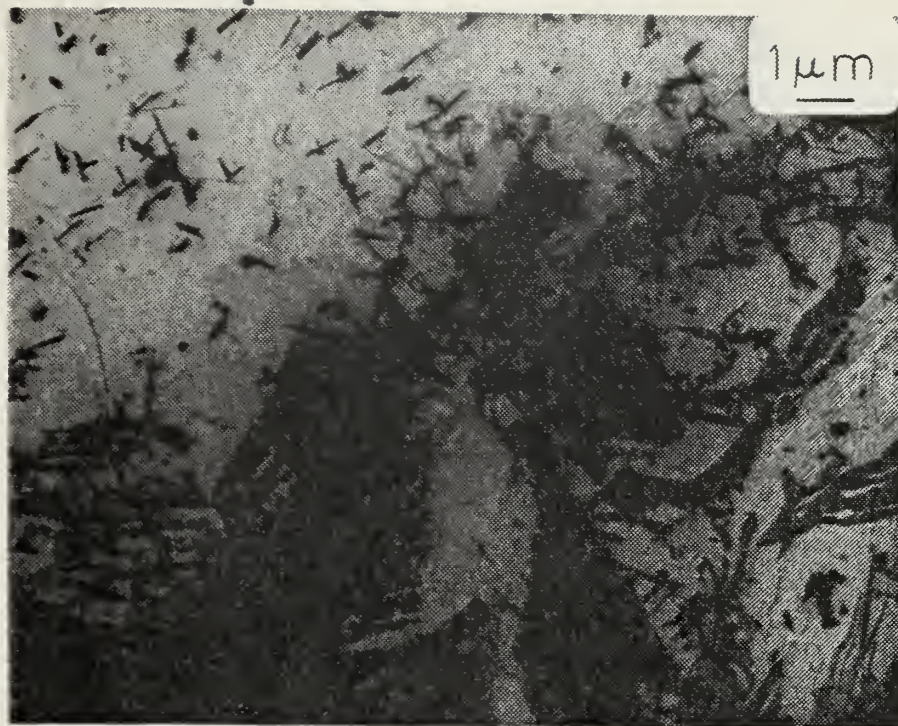
Figure 26. MIL10 - TEM Photo of Carbon Extraction Replica

81
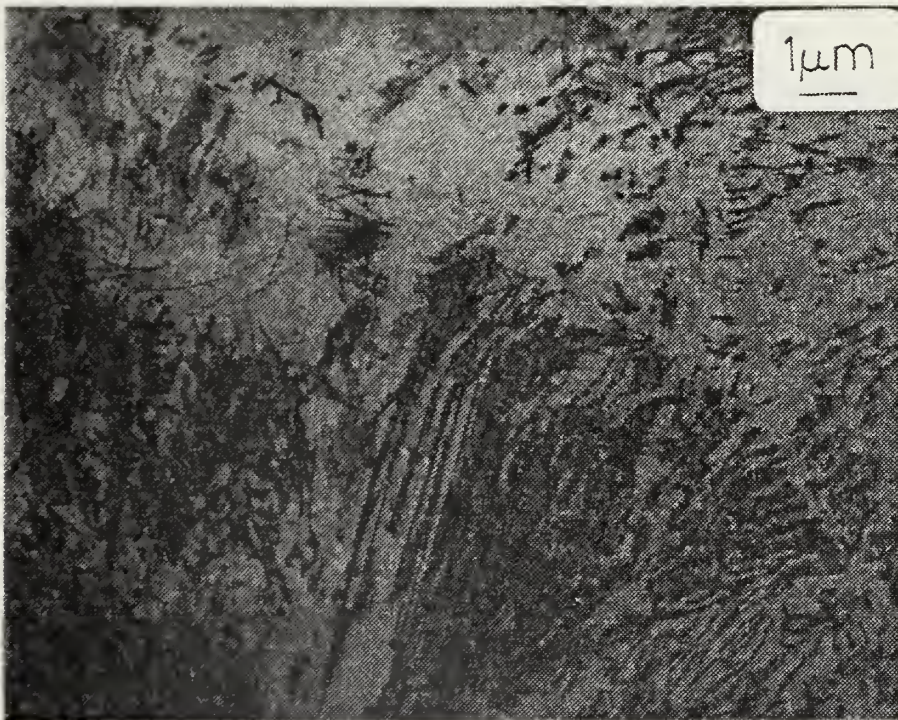
Figure 27.   MIL20 - TEM Photo of Carbon Extraction Replica

82

Figure 28. MIL34 - TEM Photo of Carbon Extraction Replica

83

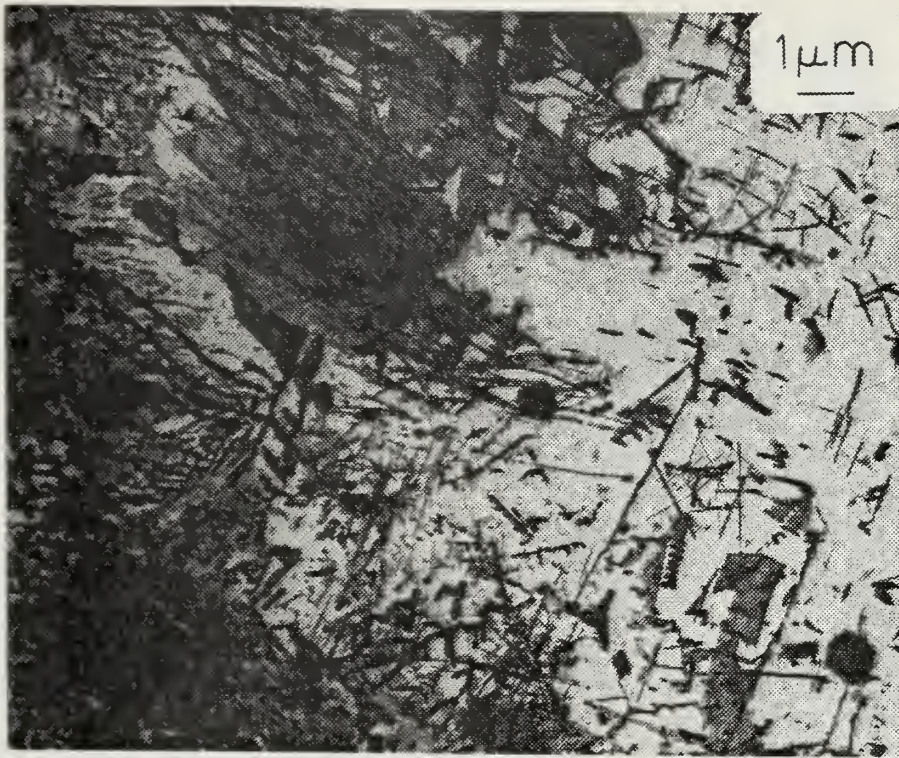Figure 29.   ITL127 - TEM Photo of Carbon Extraction Replica

84
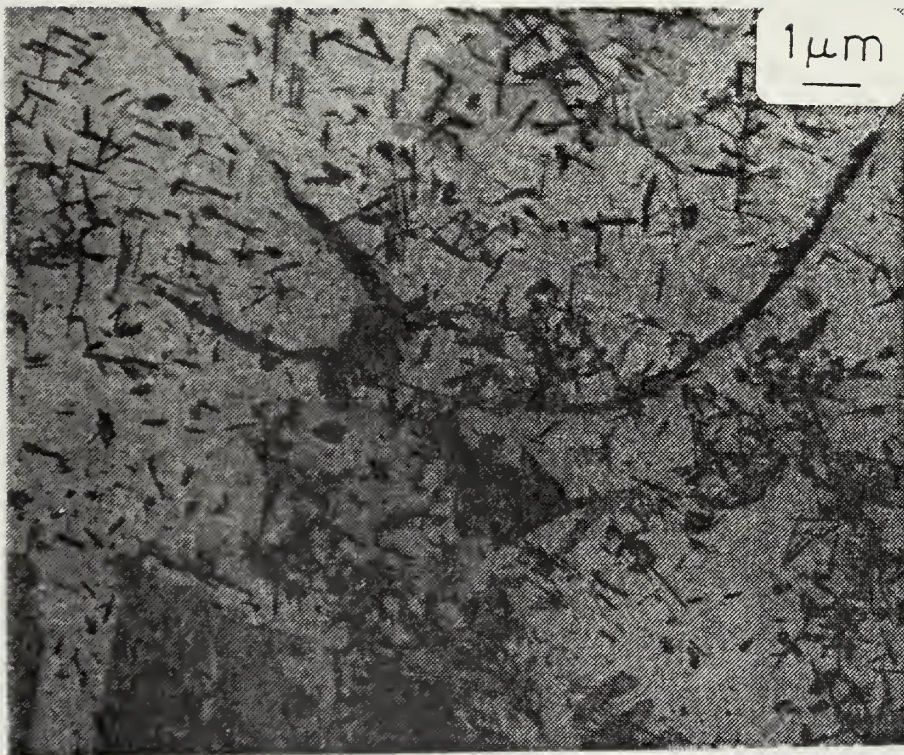
Figure 30.   MIL45 - TEM Photo of Carbon Extraction Replica

85

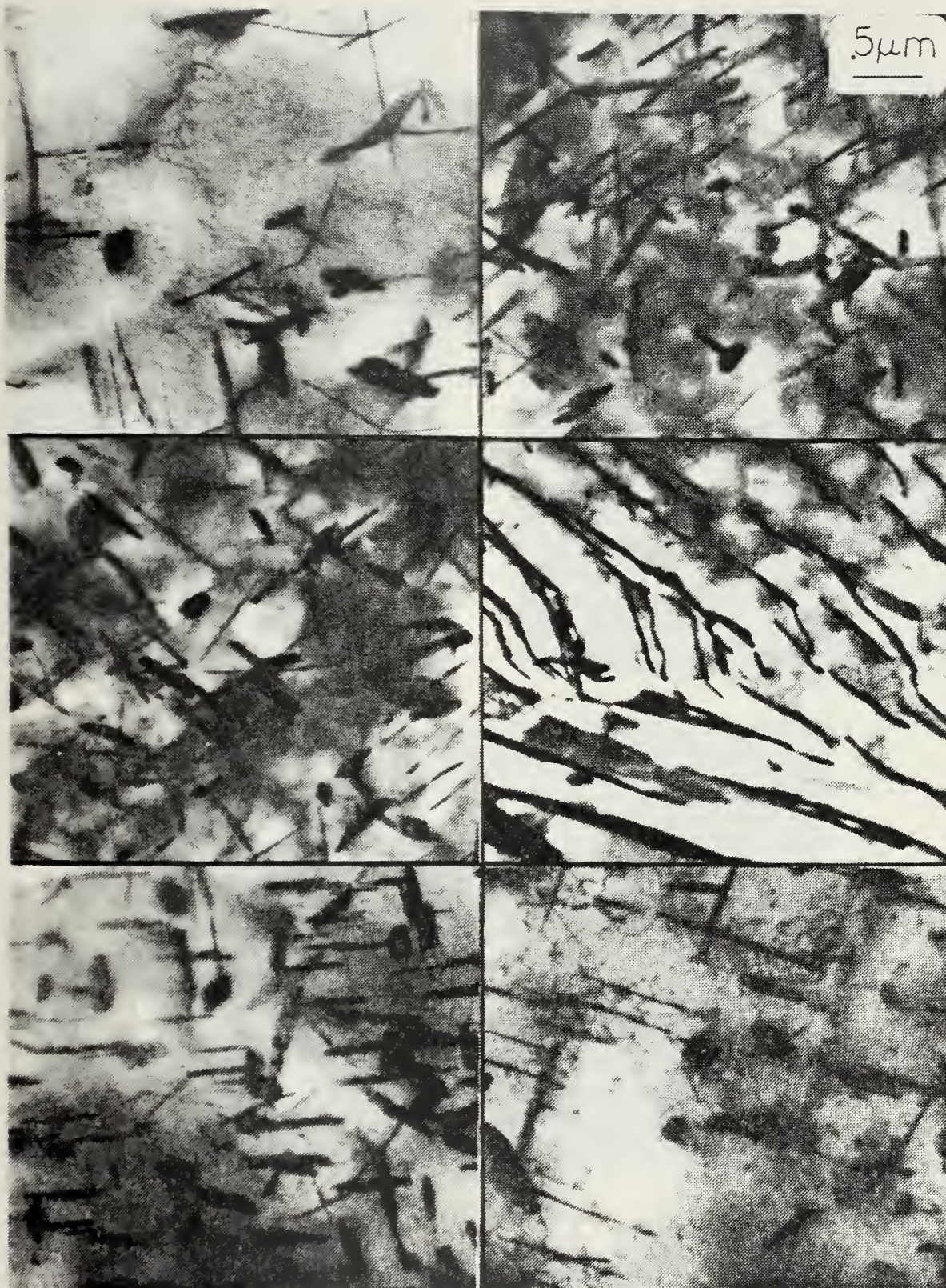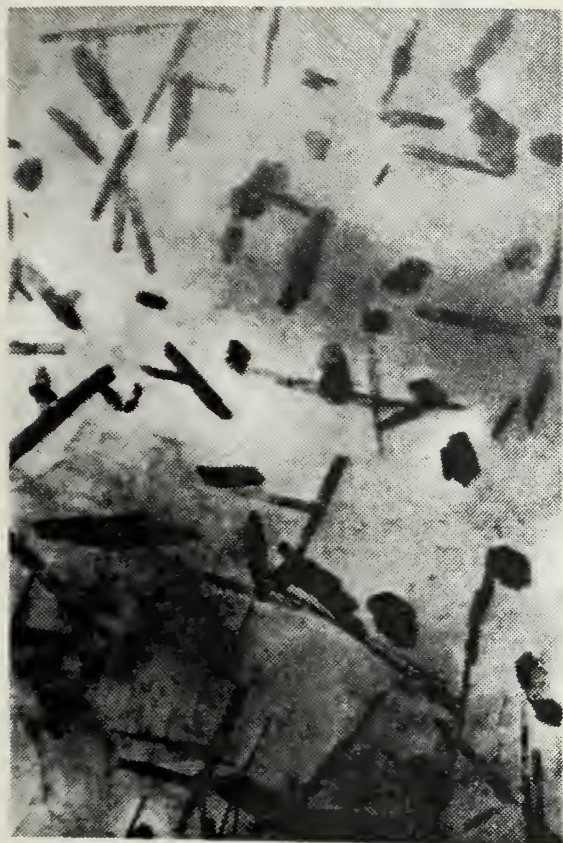Figure 31.   As Heat Treated Material - TEM Photo of Thin Foil
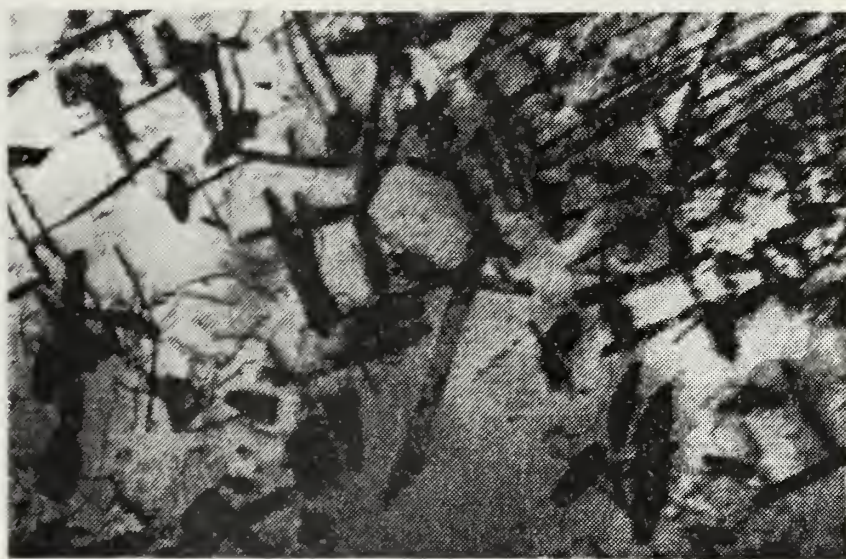
86

Figure 32.   MIL44 - TEM Photo of Thin Foil
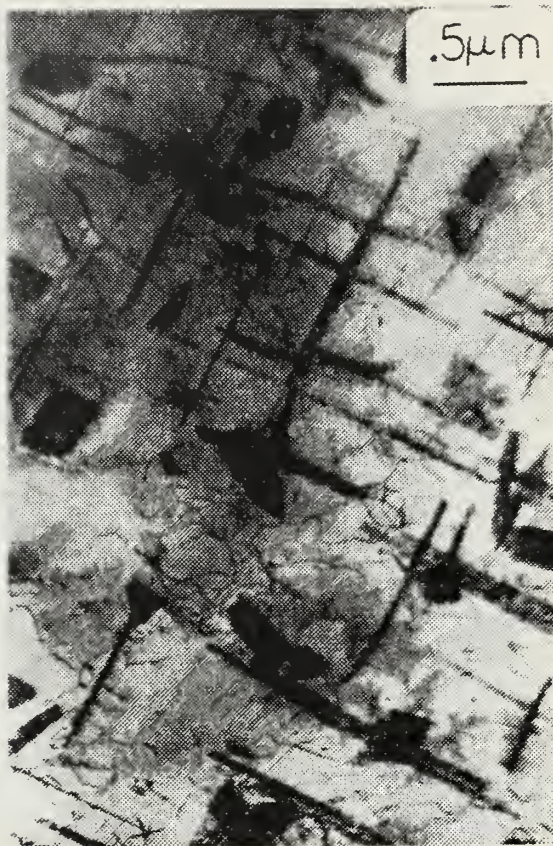
87

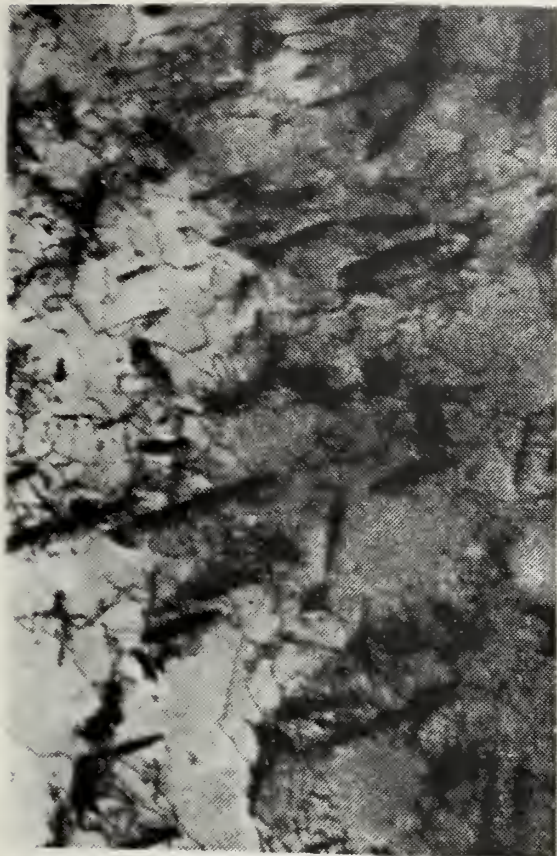Figure 33. MIL36 - TEM Photo of Thin Foil

88

.5μm

Figure 34. MIL27 - TEM Photo of Thin Foil

89

.5μm

Figure 35.   MIL65 - TEM Photo of Thin Foil

90

Figure 36. MIL18 - TEM Photo of Thin Foil

91
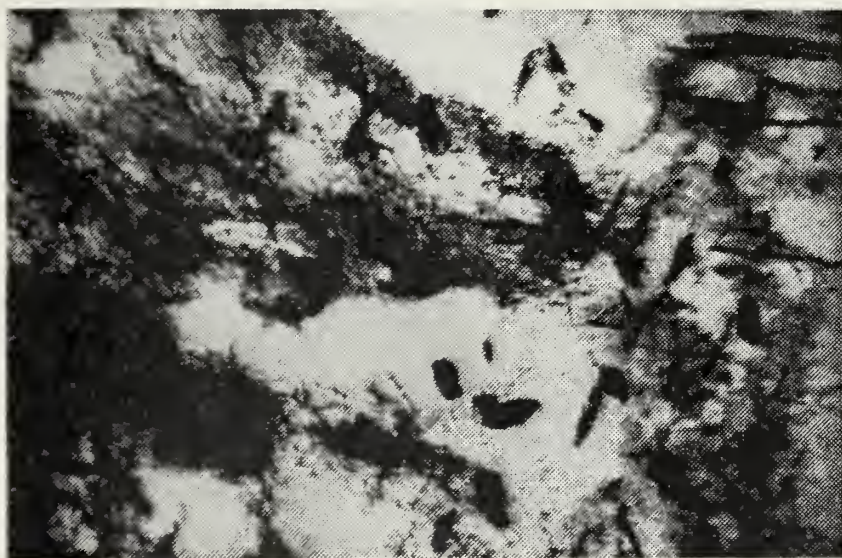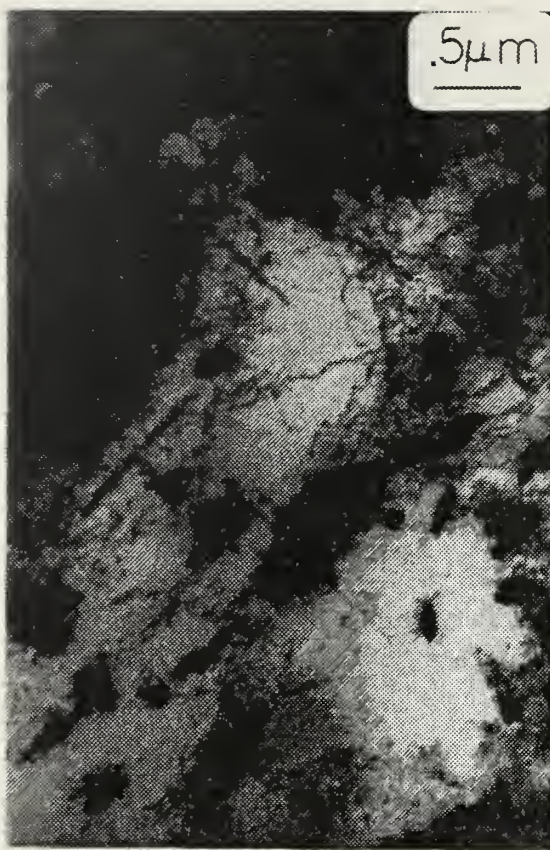
Figure 37. MIL24 - TEM Photo of Thin Foil

92
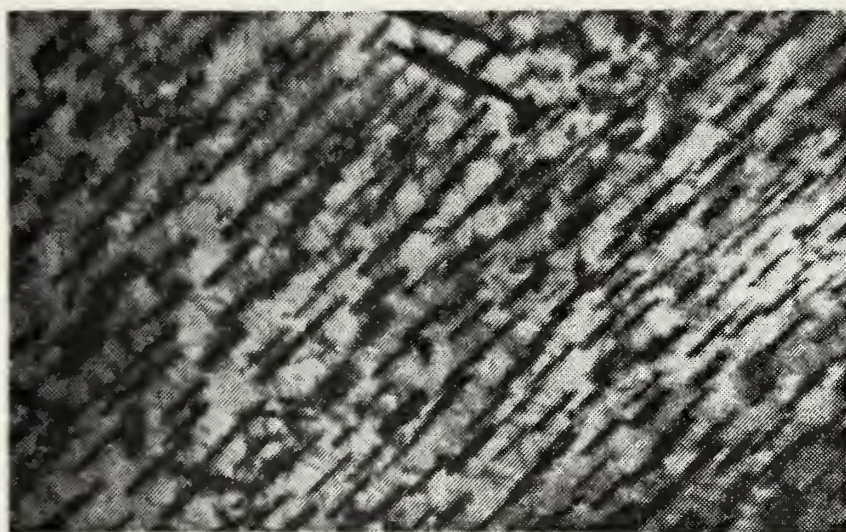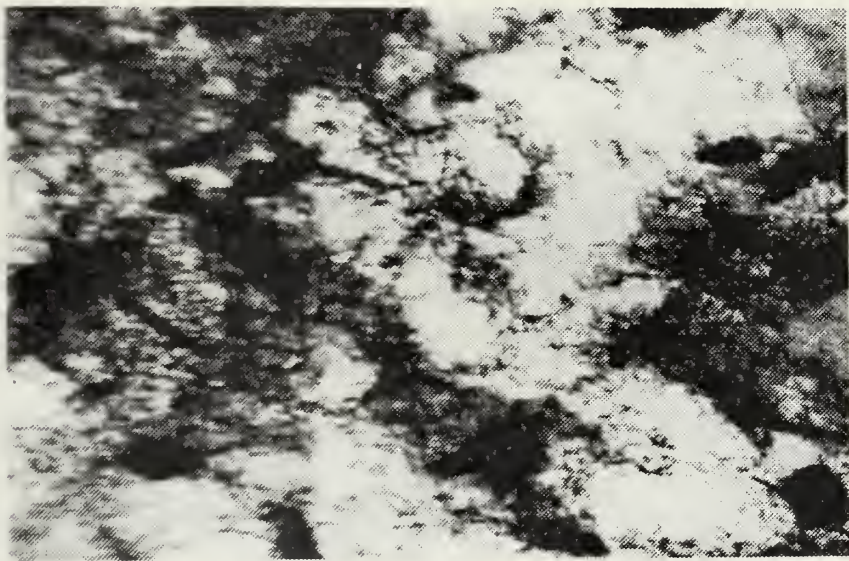
Figure 38.   MIL35 - TEM Photo of Thin Foil

93

.5μm
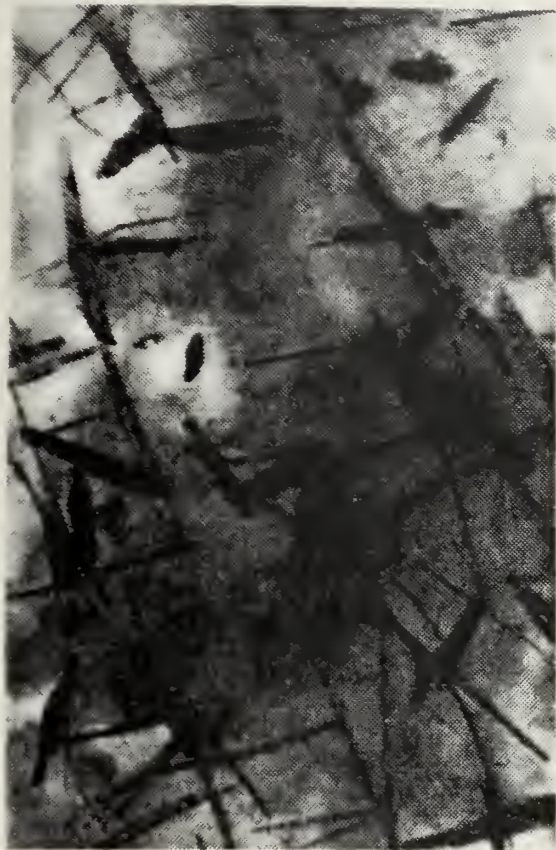
Figure 39.   MIL10 - TEM Photo of Thin Foil

94
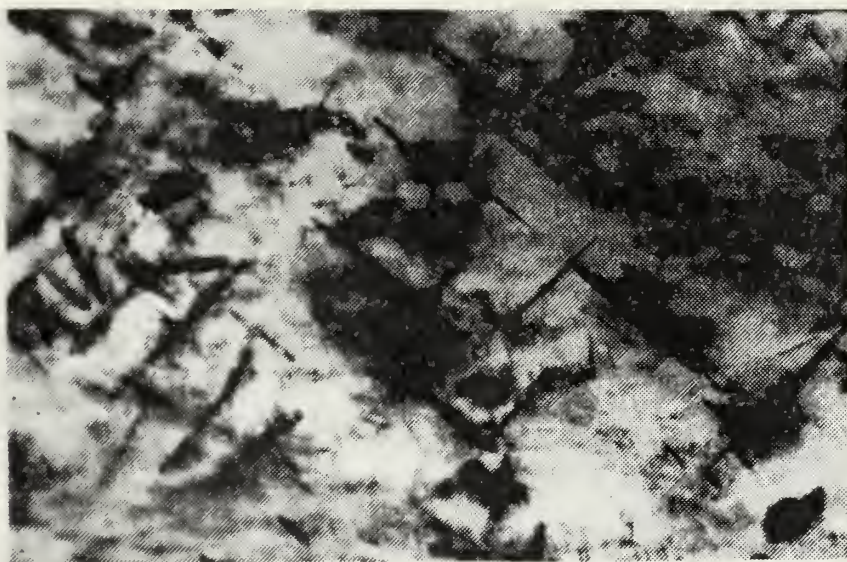
Figure 40. MIL34 - TEM Photo of Thin Foil

95
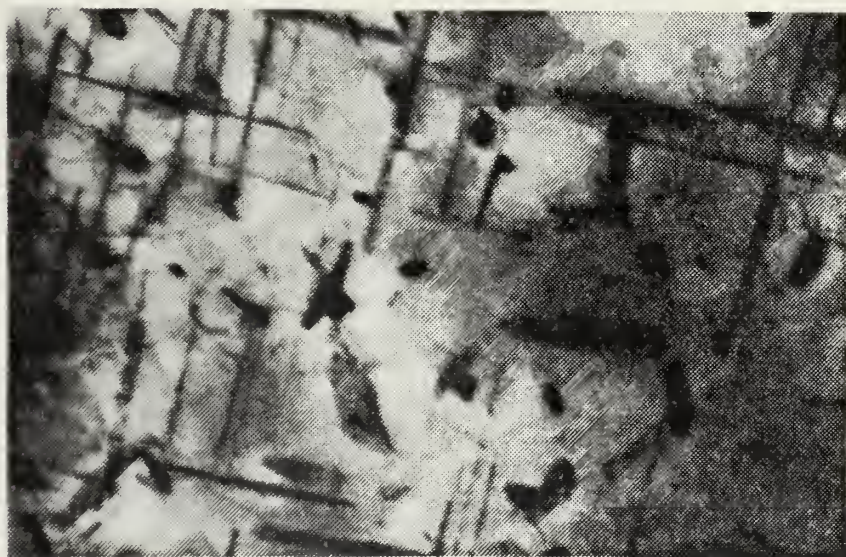
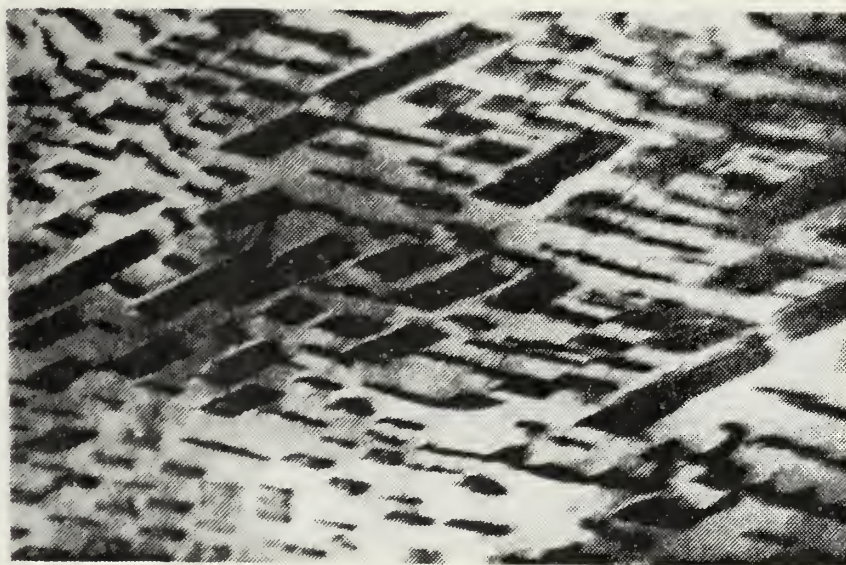Figure 41.   MIL20 - TEM Photo of Thin Foil

96
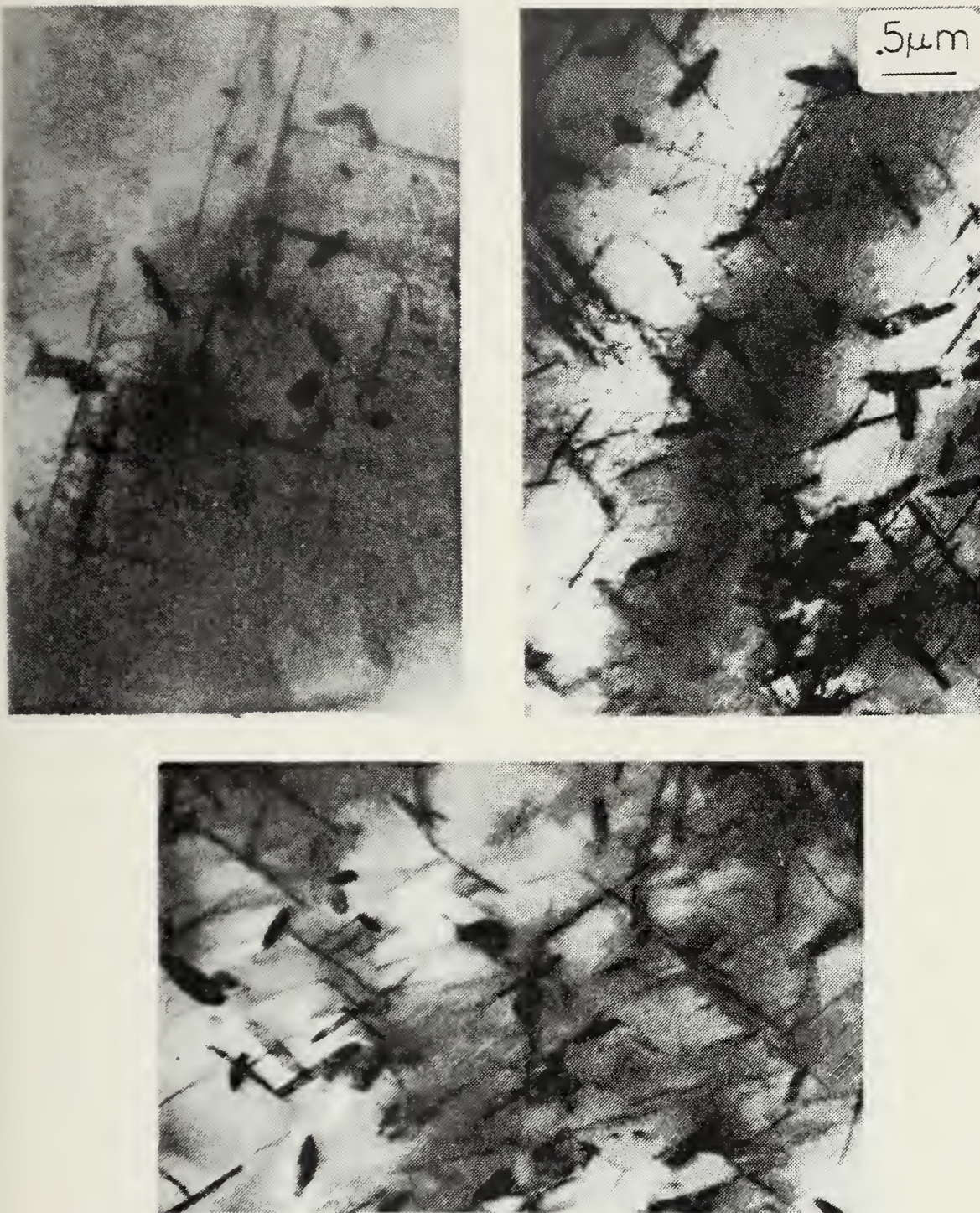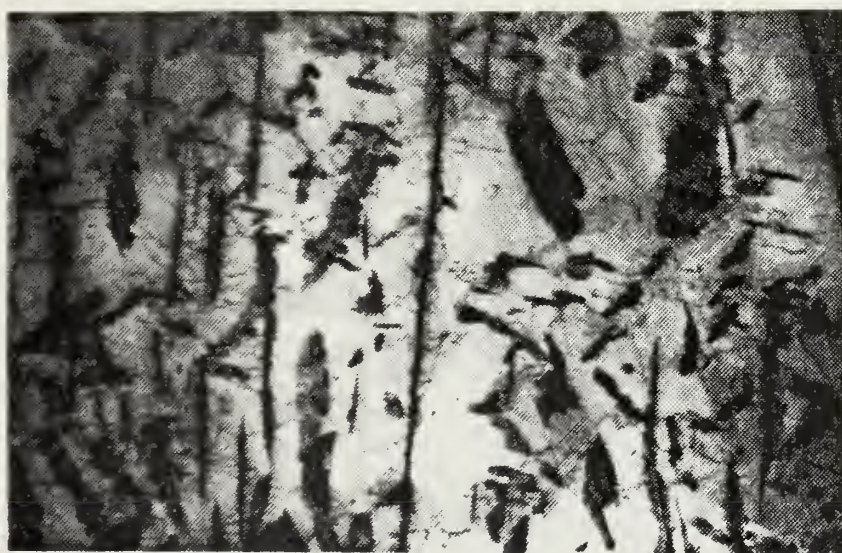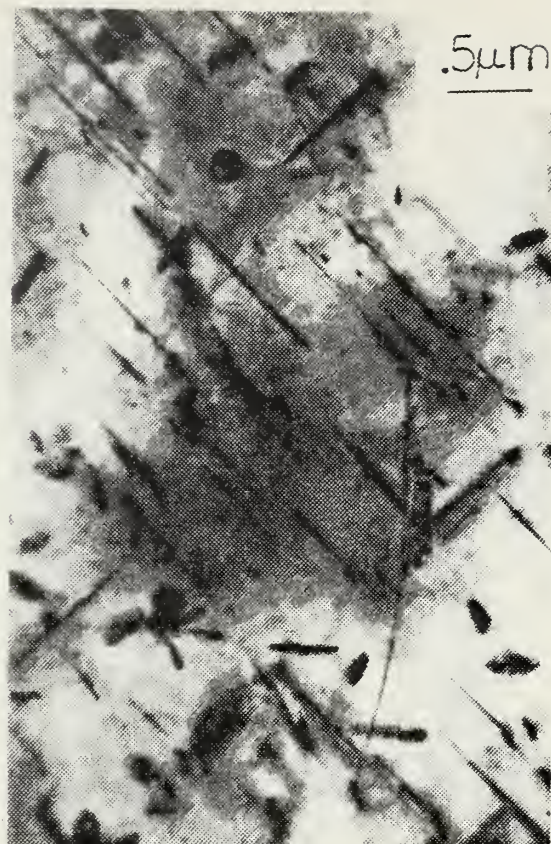
Figure 42.   ITL127 - TEM Photo of Thin Foil

97
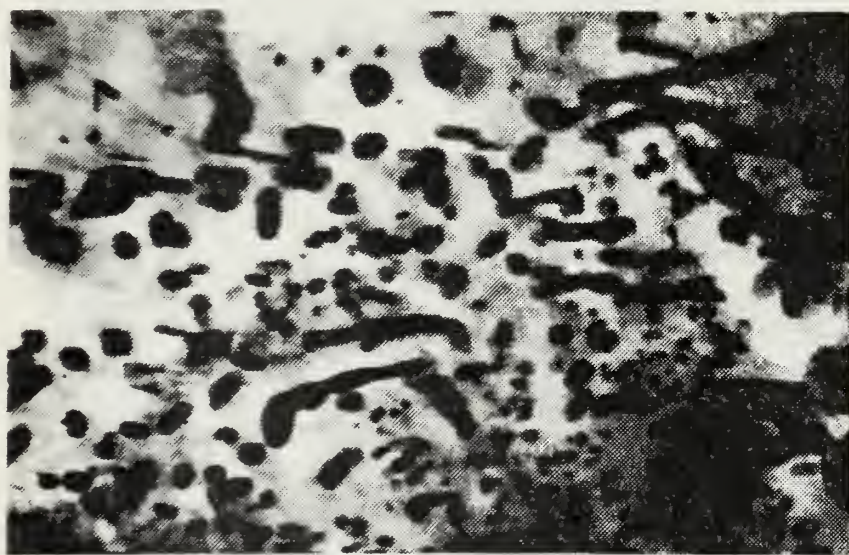
Figure 43. MIL45 - TEM Photo of Thin Foil

98
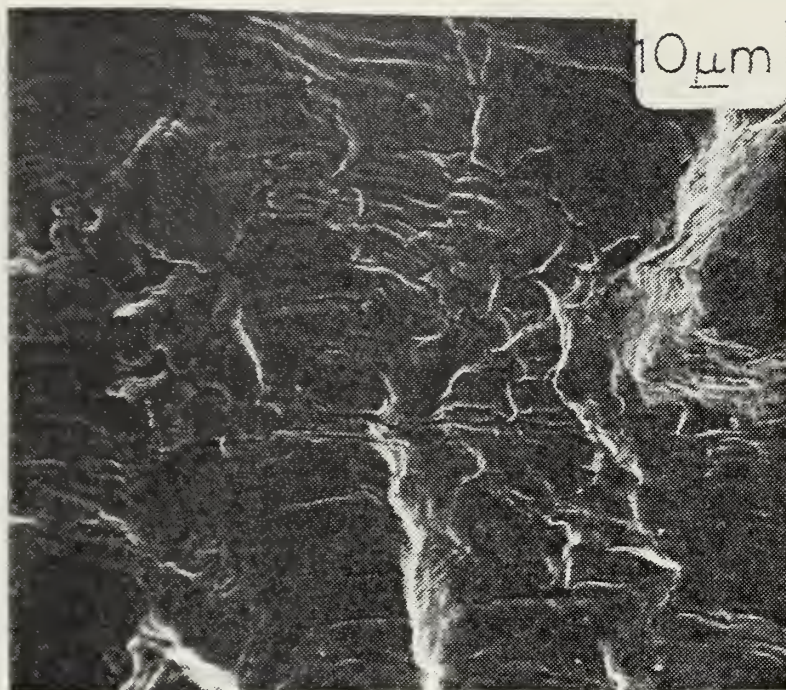
Figure 44.   MIL44 - SEM Fractograph
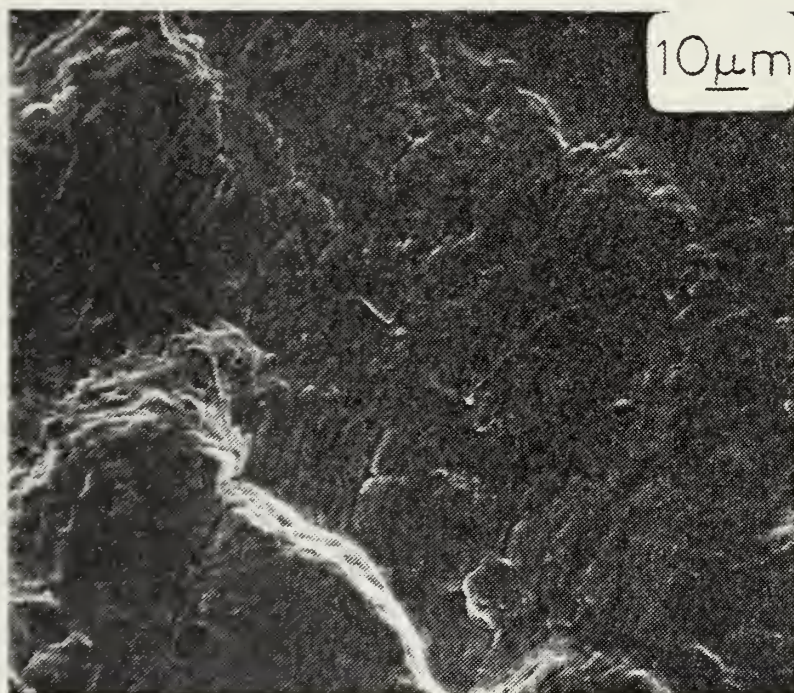
Figure 45.   MIL10 - SEM Fractograph
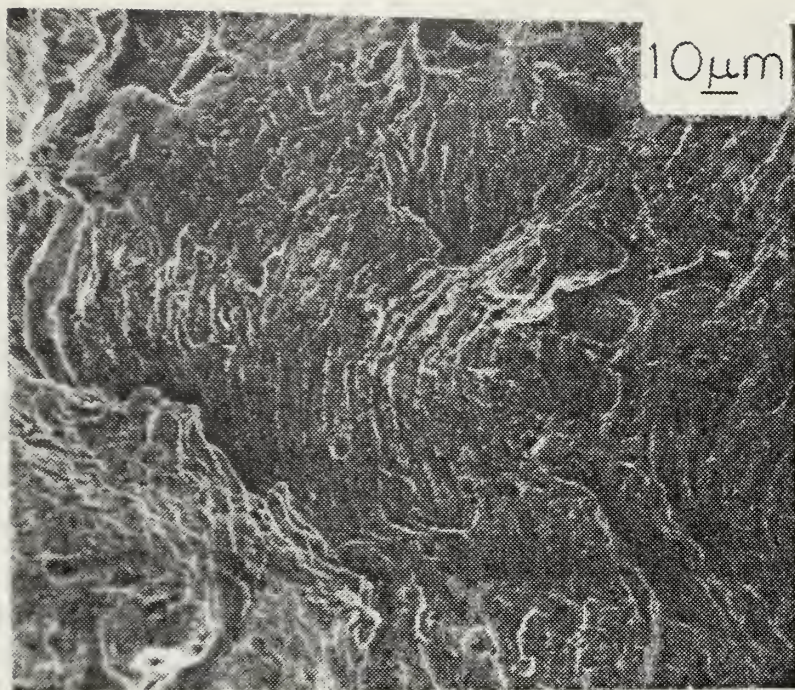
Figure 46.   MIL27 - SEM Fractograph
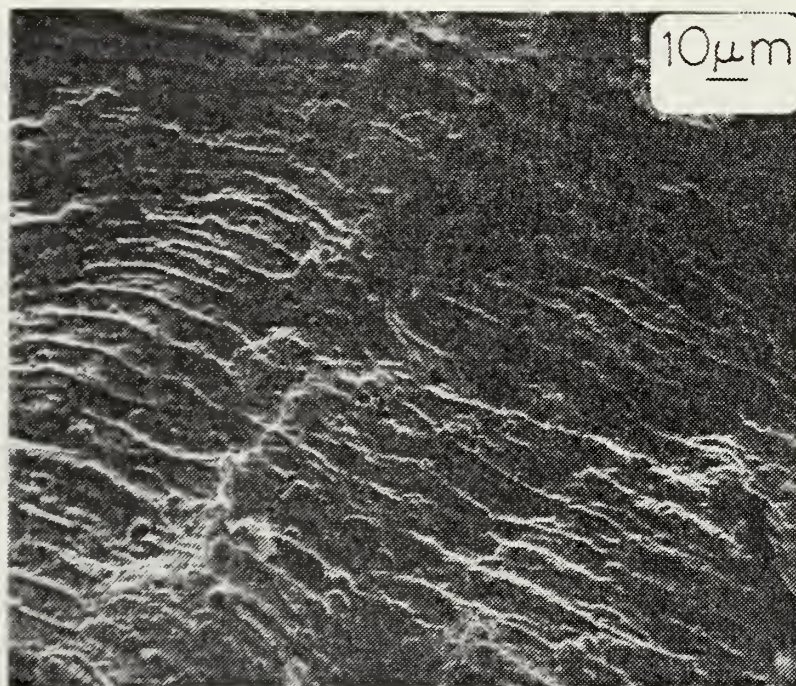
Figure 47.   MIL20 - SEM Fractograph

100
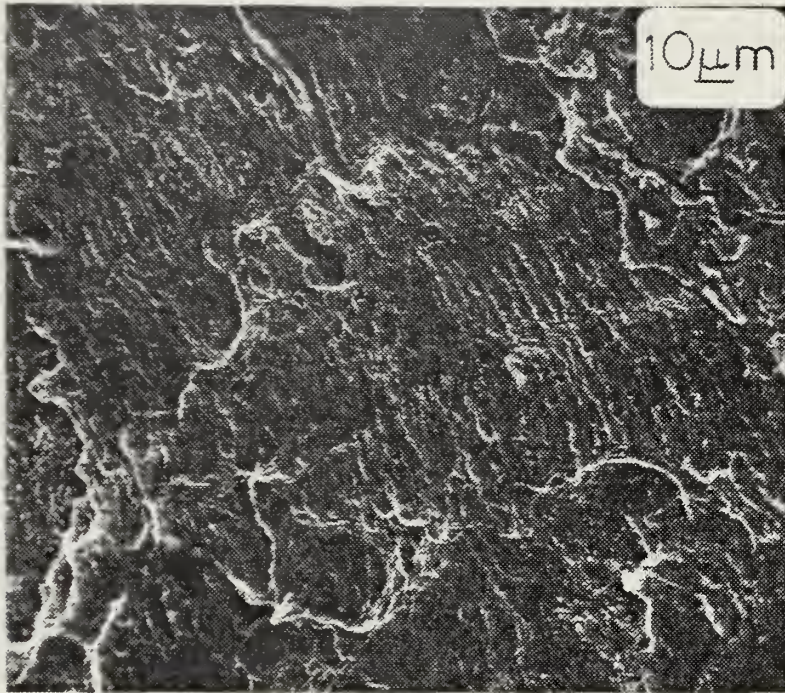
Figure 48.   MIL36 - SEM Fractograph
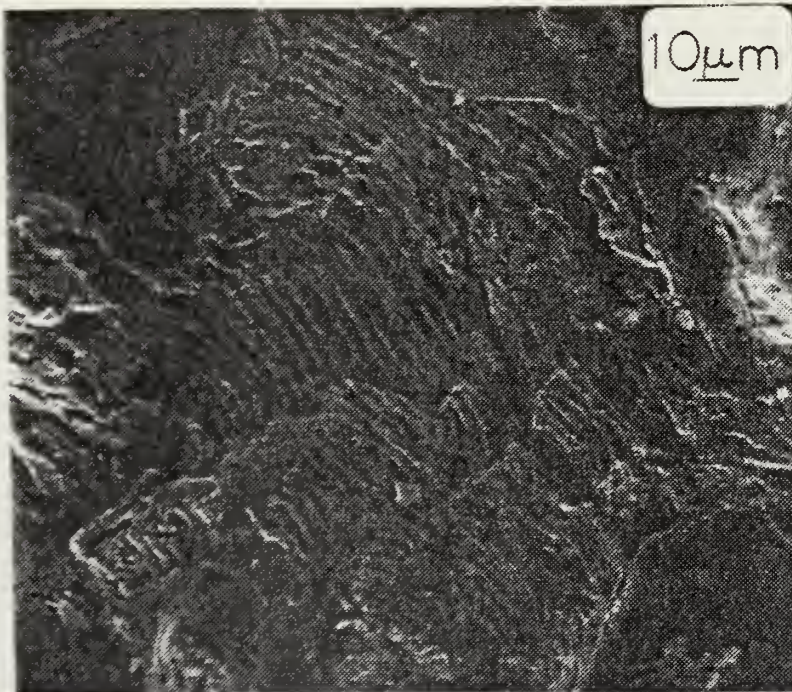
Figure 49.   MIL35 - SEM Fractograph

101
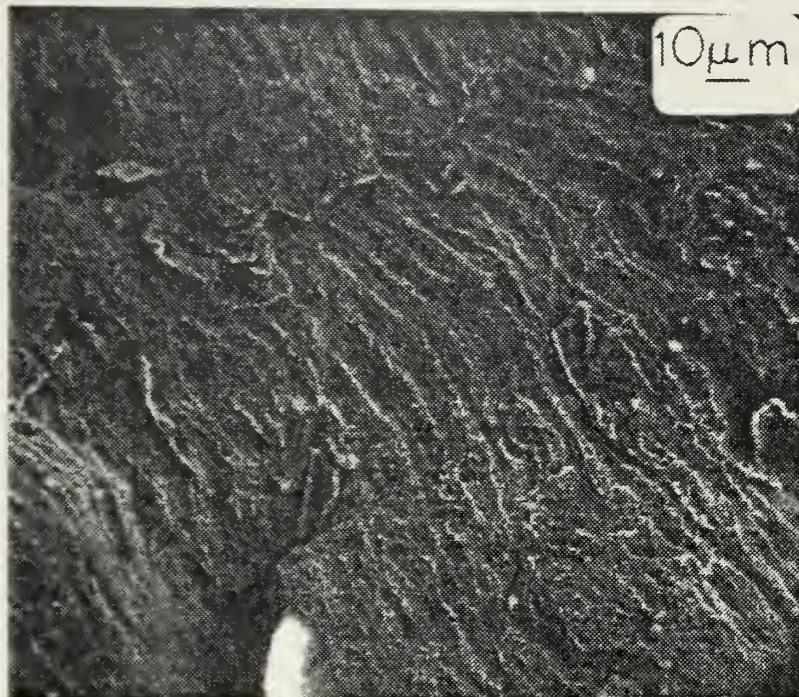
Figure 50. MIL65 - SEM Fractograph
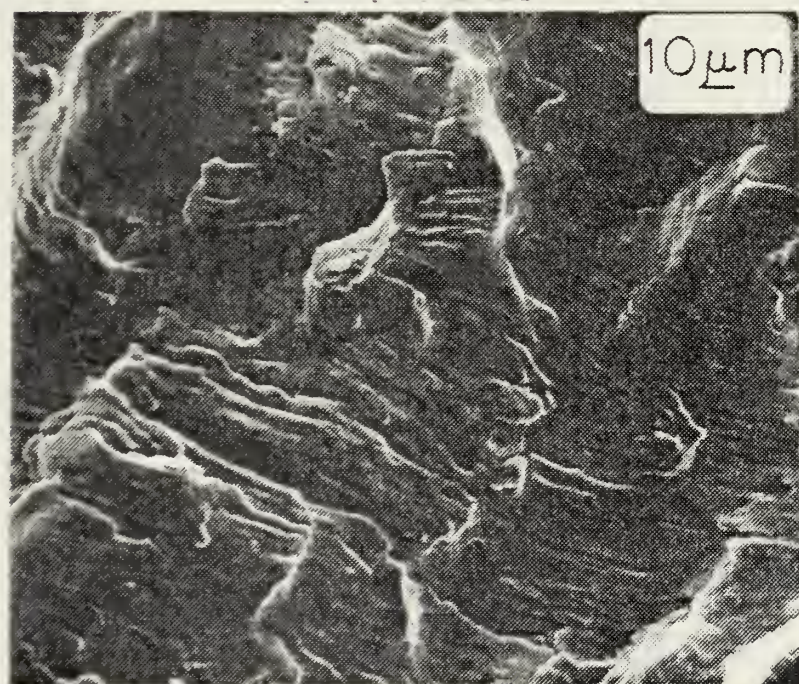
Figure 51. MIL18 - SEM Fractograph
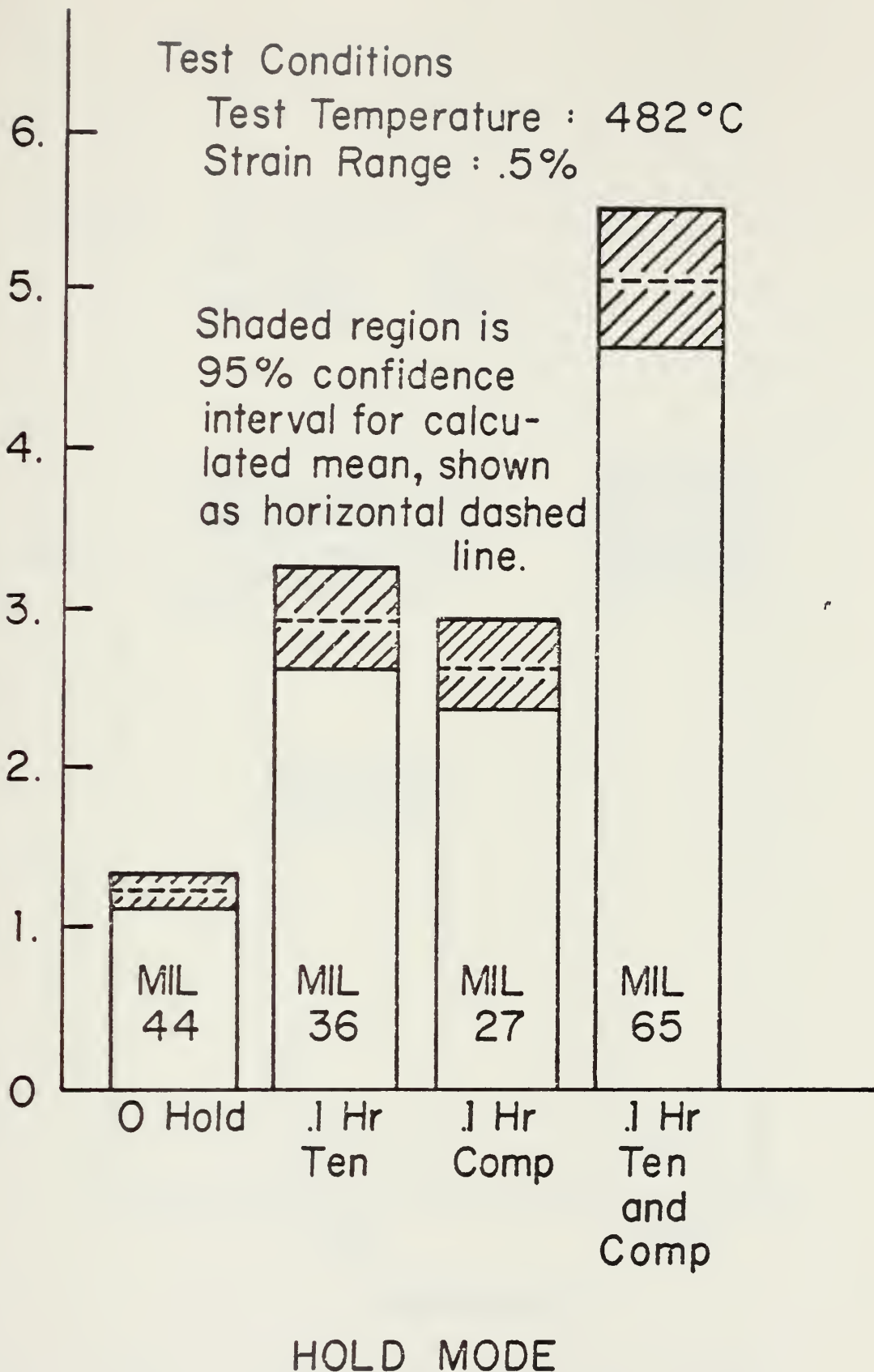
Figure 52. Effects of Hold Periods on Striation Spacing

103
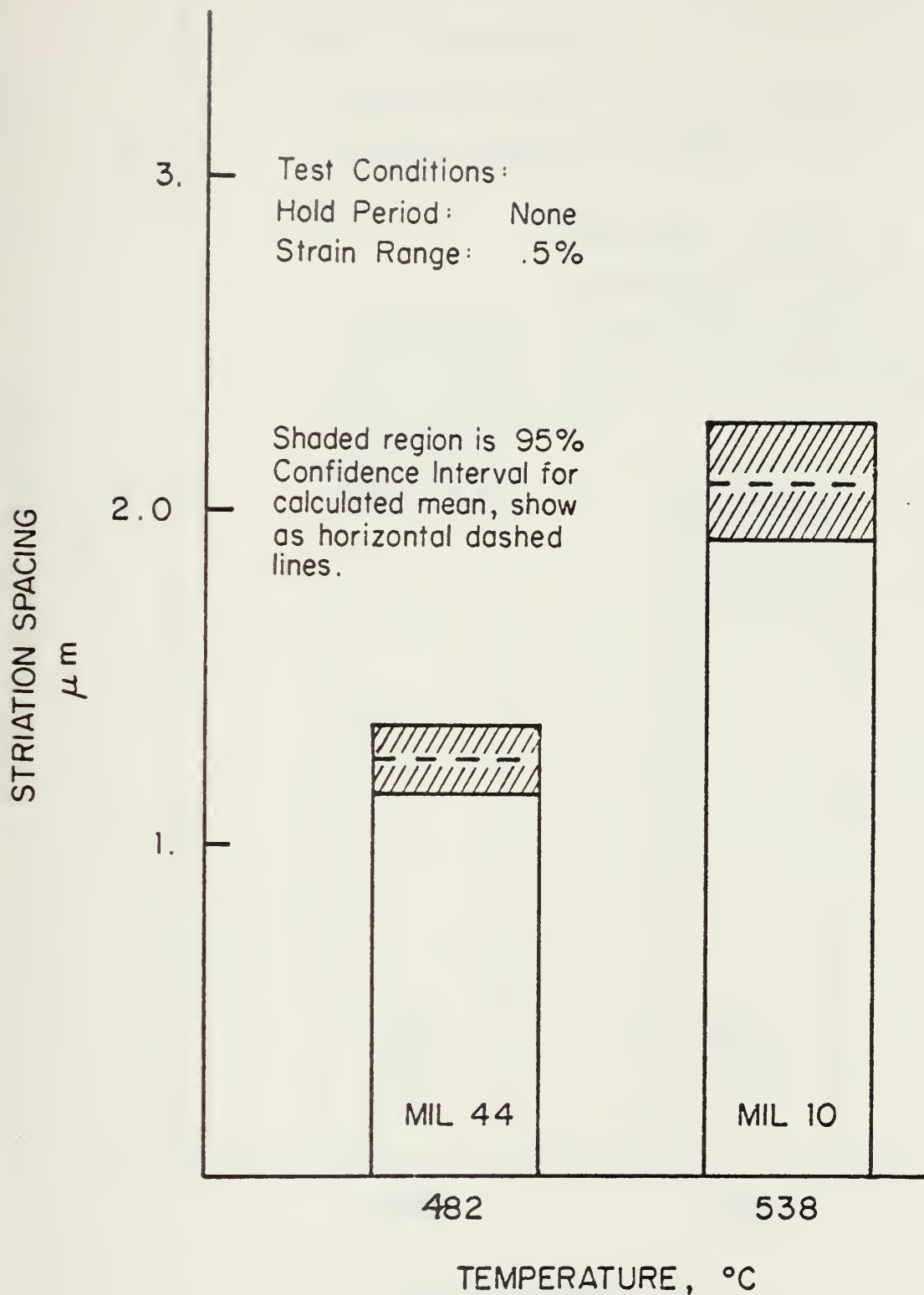
Figure 53. Effects of Temperature on Striation Spacing - Continuously Cycled

104
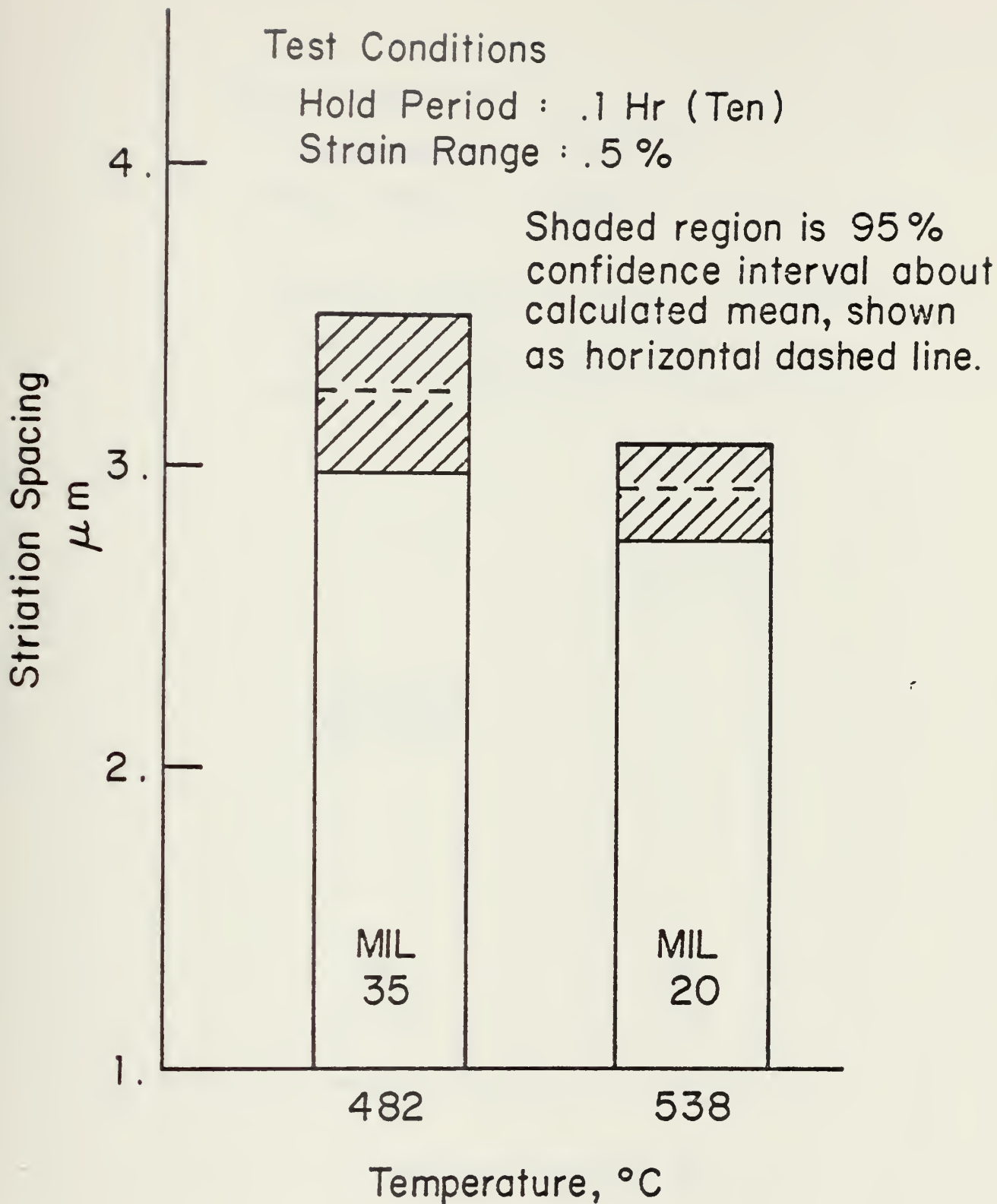
Figure 54. Effects of Temperature on Striation Spacing - 0.1 hr. Tension Hold
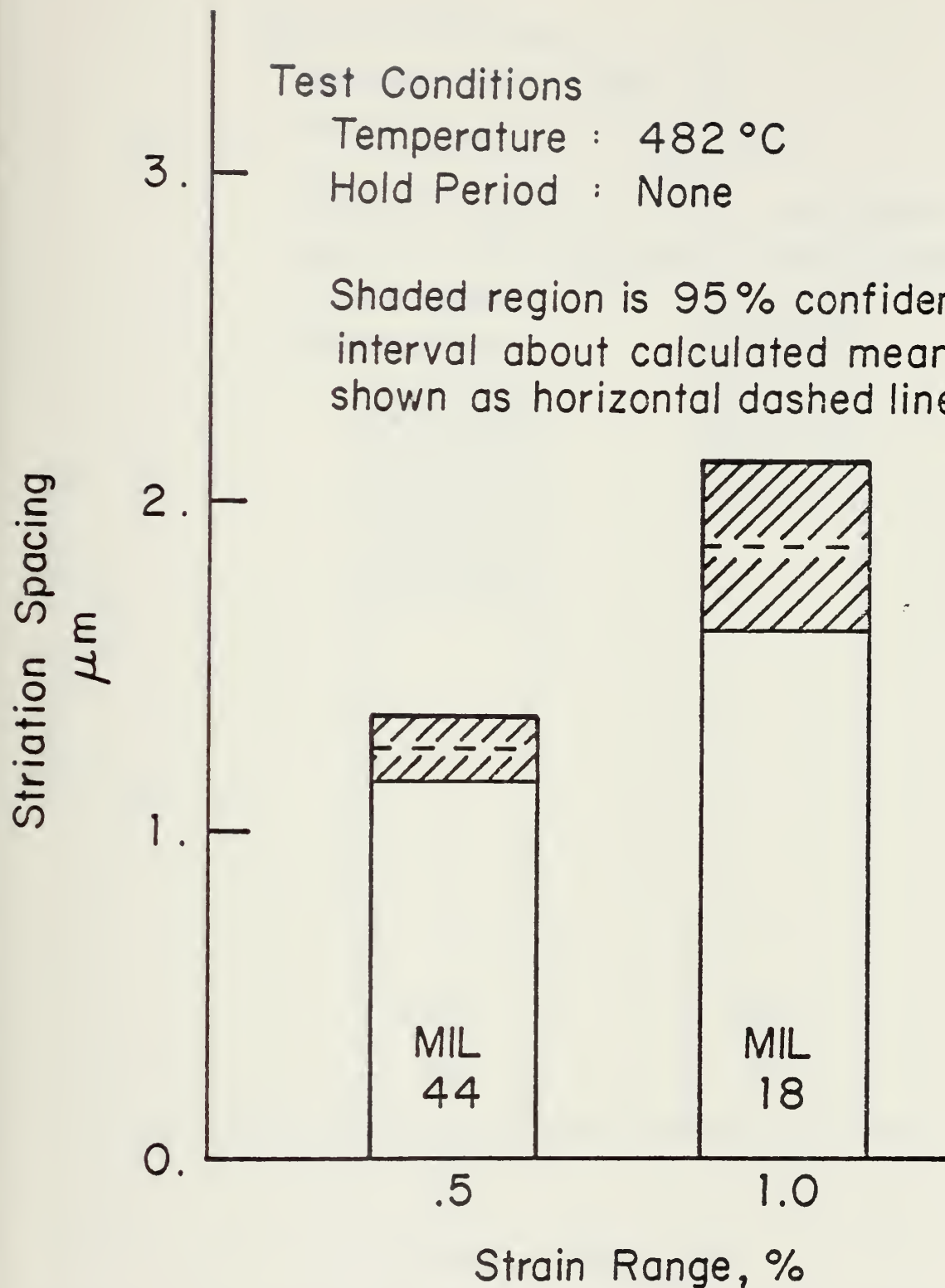
Figure 55. Effects of Strain Range on Striation Spacing -
Continuously Cycled
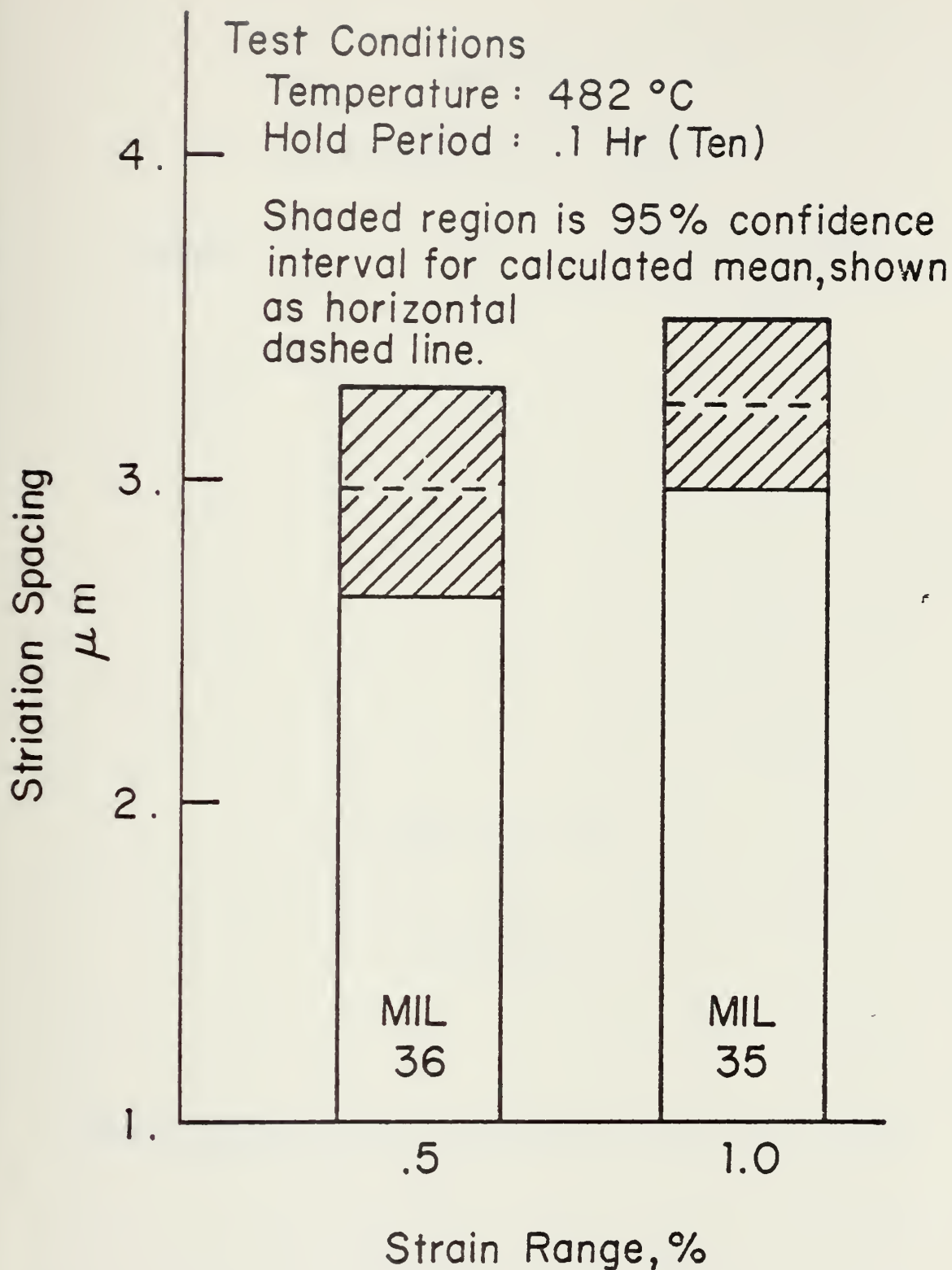
Figure 56. Effects of Strain Range on Striation Spacing - 0.1 hr. Tension Hold

TABLE I

ASTM GRAIN SIZE 5 ($\approx$ 55μm)

ELEMENT	WEIGHT PERCENT
C	0.12
Mn	1.35
Si	0.27
Cr	2.3
Mo	0.96
Ni	0.20
S	0.022
P	0.009
N	0.0135

COMPOSITION DATA

for

HEAT 3P5601

CHEMICAL COMPOSITION OF BABCOCK AND WILCOX HEAT 3P5601

TABLE II

SPEC#	TEMP	TOTAL STRAIN RANGE	HOLD TIME	CYCLES TO FAILURE	TIME TO FAILURE	PLASTIC STRAIN RANGE	SATURATED STRESS AMPL.	OPTICAL	CARBON REPL.	THIN FOIL	SEM
MIL44	482°C	.5%	0	51656	48.6hrs.	.253%	222MPa	•	•	•	•
MIL27	482°C	.5%	.1hr C	6111	615	.285%	216MPa	•	•	•	•
MIL36	482°C	.5%	.1hr T	20147	2029	.291%	209MPa	•	•	•	•
MIL65	482°C	.5%	.1hr T+C	3420	680	.309%	209MPa	•	•	•	•
MIL18	482°C	1.0%	0	3721	.6	.720%	259MPa	•	•	•	•
MIL24	482°C	1.0%	.1hr C	1924	195	.750%	264MPa	•	•	•	NMF
MIL35	482°C	1.0%	.1hr T	2059	209	.770%	252MPa	•	•	•	NMF
MIL10	538°C	.5%	0	16036	11.1	.280%	196MPa	•	•	•	•
MIL34	538°C	1.0	.1hr C	1577	160	.810%	213MPa	•	•	•	NMF
MIL20	538°C	1.0	.1hr T	1499	152	.810%	206MPa	•	•	•	•
MIL45	538°C	.3	.1hr C	13131	1319	.135%	162MPa	•	•	•	
ITL127	538°C	.5	.1hr T+C	1954	392	.314%	202MPa	•	•	•	

SPECIMENS EXAMINED AND PERTINENT TEST DATA

TABLE III

STRIATION SPACING DATA

SPEC. DESIG.	MAXIMUM SPACING			MINIMUM SPACING			
	[1]No. of Readings	MEAN (μm)	σ (μm)	[1]No. of Readings	MEAN (μm)	σ (μm)	95% CONF. INT. (μm)
MIL44	10	3.7	.5	6	1.3	.1	1.1 → 1.4
MIL27	9	4.3	.4	10	2.7	.4	2.4 → 2.9
MIL36	25	3.7	.8	14	3.0	.5	2.7 → 3.3
MIL65	5	7.6	.7	24	5.1	1.0	4.7 → 5.5
MIL18	5	6.2	.9	23	1.9	.6	1.6 → 2.1
MIL35	11	4.7	.4	14	3.3	.4	3.0 → 3.5
MIL10	4	3.7	.3	8	2.1	.2	1.9 → 2.3
MIL20	10	7.0	.6	17	2.9	.3	2.8 → 3.1

Note 1. One "reading" refers to one striation spacing value from a single line intercept measurement. Refer to text for details.

110

APPENDIX A

INTRODUCTION

One of the more time consuming aspects of completing a thesis in the materials science area is the development of an adequate faculty in the various laboratory techniques intrinsic to a careful metallurgical study. The purpose of this appendix is to set forth in as explicit a form as possible certain of the more uncommon specimen preparation procedures utilized by the author during the course of this research. While the steps detailed may directly relate only to the subject alloy system, it is hoped that the general ideas and especially the warnings of potential pitfalls will find more widespread application. Successful uses for each technique on other alloys will be identified.

A. FRACTURE SURFACE CLEANING BY A CELLULOSE ACETATE REPLICA PROCESS

    1.   General Application

Fracture surface studies using scanning electron microscopy technique.

    2.   Equipment/Materials Required

Acetate replicating tape, acetone, cotton swabs.

    3.   Procedure

        a)   Cut a small (approximately 1/2" x 1") piece of heavy cellulose acetate replicating tape from the roll.

b) Saturate a cotton swab with acetone and apply to only one side of the tape. Continually flood the tape surface with acetone until it begins to soften and cloud slightly.

c) Using a thumb or finger work the wet side of the tape thoroughly into the surface to be cleaned. It is permissible to use the stick end of the swab to push the softened tape into small features which cannot be reached otherwise. Do not use anything harder than the stick however, as surface damage may result.

d) Set aside and let dry completely. This usually takes at least twenty minutes.

e) Carefully pull the tape free of the surface, ensuring that all the tape is removed.

f) Repeat steps a) through e) until no visible oxides or contaminants are pulled off with the replica.

g) Ultrasonically clean the specimen in acetone for 10-20 minutes. This will soften and remove any traces of the tape left in the surface.

4. Discussion

A general rule of thumb with fracture surfaces is the less done to them to expose the requisite detail the better. Each cleaning method leaves its imprint on the surface and this is especially true with any form of chemical cleaning. Accordingly, less drastic methods should be employed before replica stripping is attempted. Further, acetone attacks some alloys, so ensure the material being examined is not susceptible

to this before this technique is tried. Replica cleaning has
been used successfully on many low alloy steels at the Naval
Postgraduate School.

B. FRACTURE SURFACE CLEANING BY AN ACID CLEANING TECHNIQUE

1. General Application

Fractography of heavily oxidized ferritic steel sur-
faces using scanning electron microscopy.

2. Equipment/Materials Required

Concentrated HCl, distilled water, hexamethylene te-
tramine, ultrasonic cleaner.

3. Procedure

a) Into 50 cc of distilled water slowly pour 50 cc
concentrated HCl. Add 0.2 gm hexamethylene tetramine and
stir until completely dissolved.

b) Place approximately one inch of the solution in
a small beaker and ultrasonically clean the specimen for
approximately 10 seconds in the solution at room temperature.

c) Rinse the specimen thoroughly in ethanol and
visually inspect the surface. An adequately cleaned steel
surface will have a grayish cast.

d) If the surface is still badly contaminated repeat
steps a) through c) until satisfactory results are obtained.
Cleaning times greater than 30 seconds are unusual and will
probably damage the specimen.

e. Replica clean the surface in accordance with the
previously described technique.

4. Discussion

This is a last resort technique and should only be used if all else fails. Note that a fairly concentrated acid solution is called for and even though the hexamethylene tetramine serves as an organic inhibitor, the solution is still very reactive. The caveats proffered in the replica cleaning discussion cannot be overstated. Excessive use of this technique will definitely eradicate much surface detail. This inhibited HCl cleaning method has been used successfully on several low alloy steels. Figure A1 and A2 show typical results on a high temperature fatigue specimen. All fracture surfaces examined in this study except those of the continuously cycled specimens were cleaned using this technique. For further information on cleaning techniques see the SEM/TEM Fractography Handbook, published by Battelle Columbus Laboratories, Columbus, Ohio in December 1975.

C. THIN FOIL SPECIMEN PREPARATION TECHNIQUE

1. General Application

Microstructural studies using transmission electron microscopy.

2. Equipment/Materials Required

Low speed diamond saw, wet sandpaper units (belt grinder and flat pads), micrometer, acetone, methethyl ketone, small brass block (1" x 2" x 1/2"), double stick tape, electro-thinning apparatus (Fig. A3) consisting of power unit, pump/jet assembly,

tank, Fishcione specimen holder, low power microscope and light source, electrolyte, alcohol, small tweezers, specimen punch.

3. Procedure

a) Using the low speed diamond saw, cut a wafer of the material to be examined about .015-.020 inch thick. It is fairly important that the faces of the wafer be as nearly parallel as possible.

b) Clean the wafer thoroughly to remove all traces of cutting oil/saw coolant, taking extreme care not to bend the wafer.

c) Mount the wafer on the brass block using double stick tape. Ensure that the block surface and wafer surface are absolutely dry and try not to touch the tape with your fingers. Press firmly to obtain good adhesion. Mounting the specimen on the block permits the use of the belt sander to reduce the wafer thickness more quickly. It also facilitates the use of the static wet papers.

d) Using the wet belt sander (240 grit) and static papers (240, 320, 400 and 600 grits) reduce the wafer thickness to between .005-.007 inch.

e) There are two ways to check the thickness. The first is as follows: Measure the thickness of the wafer before mounting, noting the value. Mount the wafer and measure the total thickness of the block and wafer. Determine what the total reduction should be by calculating difference between the original wafer thickness and the desired value. It is

then simply a matter of periodically checking the total thickness of the block and wafer until the necessary reduction is obtained. The second method is to remove the specimen from the block and measure it directly several times during the process, but this increases the chances of bending the wafer.

f) Removing the wafer from the block is accomplished by soaking the assembly in acetone with a small amount of methy ethyl ketone added. This is a very slow process, sometimes taking as long as two hours, and there are certain precautions to be observed.

(a) Ensure the wafer material is not attacked by the chemicals.

(b) Do not attempt to pry the specimen up away from the block. This will induce gross plastic deformation which will invalidate any microstructural features observed. The proper way to separate the wafer from the block is to slide it off by pressing down on the surface of the wafer and attempting to slide it off. Do not try to force it. If it will not slide off easily put it back in the acetone.

g) Once the wafer is free, wash it thoroughly in acetone to remove any mastic residue. Again, the importance of not bending the specimen cannot be over emphasized.

h) Use the 600 grit wet paper and reduce the wafer thickness to .003-.004 inch. It is best to do this without the aid of the block and double stick tape by simply using finger pressure to draw the specimen across the abrasive.

i) Cut out 3 mm discs using the Fullam TEM specimen punch, using a sharp, distinct blow to the plunger to minimize the plastic deformation at the center of the disc. An alternate method is to use an electrodischarge machining unit, which should be used for all high hardness materials.

j) Lightly sand each side of the 3 mm discs with 600 grit paper to remove the burrs around the edges. This will greatly improve the seal obtained in the Fischione holder and will also prolong the life of the holder.

k) Wash the discs in alcohol and blow dry using a hand held dryer.

l) The electro thinning apparatus used by this researcher is a modified Buehler Electromet and is shown in Figure A3. Figure A4 is a close up of the Fischione specimen holder showing a 3 mm disc for scale purposes.

m) Set up the apparatus as shown in Figure A5, and fill the tank with about 500 ml of electrolyte. Note that this will leave the jet nozzle above the surface of the electrolyte so that polishing is done without the specimen being completely submerged.

n) The Fishione holder must be completely dry inside. Place the specimen in the female end of the holder against the platinum electrode and screw the male plug in place ensuring that:

(a) The specimen stays in place, and

(b) The plug is brought snugly in contact, but
not over-tightened as this causes excessive wear of the mating
surfaces.

o) Fit the holder to the clamp, connect the power
lead to the holder and connect the ground lead to the spring
electrode on the jet.

p) The specimen holder should be positioned such
that the specimen surface is nearly perpendicular to the jet
and about 3/8" from the jet tip. The female side of the
holder should face the jet.

q) Energize the power supply and dial in the desired
voltage then turn on the pump and adjust the pump speed to
obtain a vigorous jet of fluid against the specimen. Run at
this speed until approximately one third of the specimen thick-
ness is polished away, then reduce the pump speed to the lowest
possible value while still maintaining the same stable current
reading. Run at this speed unitl approximately half of the
sample thickness has been removed.

r) Turn off the main power switch on the Electromet,
securing both the pump and the power supply for the electro-
chemical cell. Disconnect the power lead from the holder,
unclamp the holder and rinse the PVC portion of the holder and
the specimen thoroughly.

s) Unscrew the male plug from the holder, extract the
specimen, rinse it in alcohol again and blow dry it. Thoroughly
dry the specimen holder.

t) Place the specimen in the holder again, this time with the unpolished side against the platinum electrode.

u) Reassemble the holder, clamp it in position, align it in front of the jet and connect the power lead.

v) Carefully align and focus the light source and low power microscope to permit viewing of the polished side of the specimen.

w) Begin electropolishing the specimen again at the high jet speed for about half the amount of time run at this speed on the first side, then reduce speed as before (step q). Continue polishing until penetration is observed through the microscope then immediately turn off the main power switch.

x) Penetration is best observed as a small spurt of electrolyte through the hold formed, or as a small darkened area on the surface. It is imperative that both the pump and cell voltage be turned off immediately. The purpose of this procedure is to develop a thin (on the order of $1000\overset{\circ}{A}$) area around the hole of uniform thickness which can be penetrated by the TEM's electron beam. If the pump is left on, the fragile area will be deformed. Leaving the cell voltage on gives accelerated attack at the edges of the hole, rapidly destroying them. It should be apparent that this phase of the process is largely an art born of many hours of practice.

y) Unclamp the holder and rinse gently as before. Remove the specimen from the holder, rinse in alcohol and blow dry. Place the foil in a small vial and place the vial into

a dessicator until you are ready to place it in the TEM and examine it.

4. Discussion

This procedure requires a large measure of patience. Each step requires some trial and error to find the best specific technique for each different alloy.

For 2 1/4 Cr - 1 Mo steel the author has had the best results using a 5% perchloric/95% glacial acetic acid (by volume) electrolyte, preconditioned by electro-polishing a small disc (about 3/8" diameter) of the material in a simple electro chemical cell at 70 VDC until the electrolyte turns a very light golden green color. Using this solution in the Electromet at 70 VDC gives current readings of between 12 ma (fresh) to 35 ma (old) and results in a very smooth polish. When the current readings exceed 35 ma, discard the electrolyte and make a fresh batch.

A word of caution is appropriate. Perchloric is a strong oxider and the dry powder may be explosive. When mixing the electrolyte, ensure the outside of the perchloric bottle is wiped clean.

The pump speeds and polishing times used by this researcher on 2 1/4 Cr - 1 Mo steels were:

First side: 35-45 seconds with a jet speed setting
               of "3 1/3 - 4", then 20-40 seconds at
               just slightly below "3".

Second side: 20-30 seconds at "3 1/2 - 4", then just below "3" until penetration.

Additionally, the specimen holder was always rinsed in glacial acetic acid prior to the alcohol rinse.

If you are having trouble getting small diameter penetrations one technique is to use a cotton swab and put a small drop of acetic acid on the polished side of the specimen in step w). The surface tension of the liquid adds some strength to the foil.

There are several other techniques which can be used if you are having difficulty getting usable foils. Very often the specimen holder will leak, causing the back side of the specimen to etch as the other side (the one facing the jet) is polished. This problem can be alleviated by polishing one side for 10-15 seconds, stopping the procedure and then polishing the other side for the same short period. Alternating this way will minimize the etching effects and help give a smoother, more even surface.

Another technique which will help develop a better thin area is to bulk thin the specimen by energizing the Electromet unit and immersing the specimen holder into the electrolyte. This will evely reduce both sides of the specimen simultaneously. The polishing occurs fairly quickly so care must be taken that you don't achieve penetration during this process. The bulk thinning process can also be used to initially

reduce the wafer thickness prior to clamping the specimen in front of the jet for final thinning.

The procedures and polishing conditions described here have been used successfully on 2 1/4 Cr - 1 Mo and 52100 steels.

D. CARBON EXTRACTION REPLICA TECHNIQUE

1. General Application

Carbide distribution studies using TEM. (Primarily for ferritic steels.)

2. Equipment/Materials Required

Metallographic mounting equipment and materials, Fullam evaporator with carbon electrodes and holder (Fig. A6), 20% HNO_3 in ethanol, specimen grids, fine tweezers, large forceps (preferably stainless steel), two small (approximately 3" dia. by 1 1/2" deep) glass bowls, small sharp scribe or hobby knife, plastic specimen vials.

3. Procedure

a) The methods oulined here apply specifically to 2 1/4 Cr - 1 Mo steel and are an adaptation of the techniques developed for 52100 steel by LT C. W. Schultz (MS Thesis). The only modifications made were fine adjustments to the carbon deposition conditions due to the very different carbide morphologies of the two materials.

b) Mount the specimen and polish as you would for optical metallographic examination.

c) Lightly etch the surface as would be appropriate for moderately high magnification optical microscopy (400-800X).

122

d) Start up the evaporator in accordance with the operator's manual. The warmup times specified are absolute minimums and should not be curtailed.

e) Place the specimen to be coated in the chamber. Care should be taken to ensure the specimen is centered under the arc (i.e. center the specimen under the point of contact of the electrodes).

f) Evacuate the chamber following the manufacturer's written procedure. Filling the cold trap with liquid nitrogen prior to unisolating the diffusion pump from the chamber will greatly speed the process.

g) Connect the power leads to the electrodes, first ensuring that the "Filament" switch on the power panel is turned off.

h) Set the desired potential which, for 2 1/4 Cr - 1 Mo steel, is about 50-55 volts.

i) Energize the "Filament" switch and observe that a bright, even arc appears immediately. Keep the arc on for 3-4 seconds (again for 2 1/4 Cr - 1 Mo steel) then turn off the switch.

j) Allow the unit to cool for about thirty seconds, then break vacuum according to the instructions for the evaporator and remove the specimen.

k) Scribe a grid pattern across the surface of about 1/16 inch spacing.

1) Fill a small bowl with 20% HNO_3 in ethanol and a second bowl with distilled water. Squirt a few ml. of ethanol into the water to lower the surface tension.

m) The nitric acid will diffuse through the carbon layer dissolving the metal underneath and leaving the carbides untouched and attached to the deposited carbon layer. As the attack progresses small bubbles will form under the carbon layer and begin to coalesce.

n) When fairly large bubbles exist (covering about one grid square) remove the specimen from the acid gently and carefully palce in the distilled water.

o) The replicas may not float off immediately and often require in excess of thirty minutes to loosen.

p) As the replicas float off, catch them on small copper specimen grids using the fine tweezers. Self locking tweezers are the best for this purpose. Dip the grid into the water some distance from the replica to be picked up and try to move the grid just next to the replica keeping it just submerged and at about a 70° angle with the water surface. Use a scooping motion to retrieve the replica.

q) Place the replica on a wet paper towel, keeping the tweezers as nearly parallel to the paper as possible. This will minimize the tendancy of the capillary action between the tweezer points to draw the specimen up away from the paper.

r) After the replica has dried seal it in a small plastic specimen vial.

4. Discussion

There are several aspects of this procedure which cannot be explicitly detailed. The phrase "lightly etch" is open to interpretation. This researcher has general used 6-8 seconds with 2% nital with fairly reproduceable results. The time and voltage for carbon deposition will require some modification if different materials are to be examined. Retrieving the replicas takes practice.

One final word of caution is appropriate. Carbon extraction replicas may not always lift all carbides in the surface. Replicas should be compared with thin foils of the same material if possible to determine the validity of the carbide structures observed. Figures A7 and A8 are TEM micrographs of a thin foil and a carbon replica respectively of the as heat treated material examined in this work. Note that while the similarities are easily discerned, the carbide distributions differ markedly.
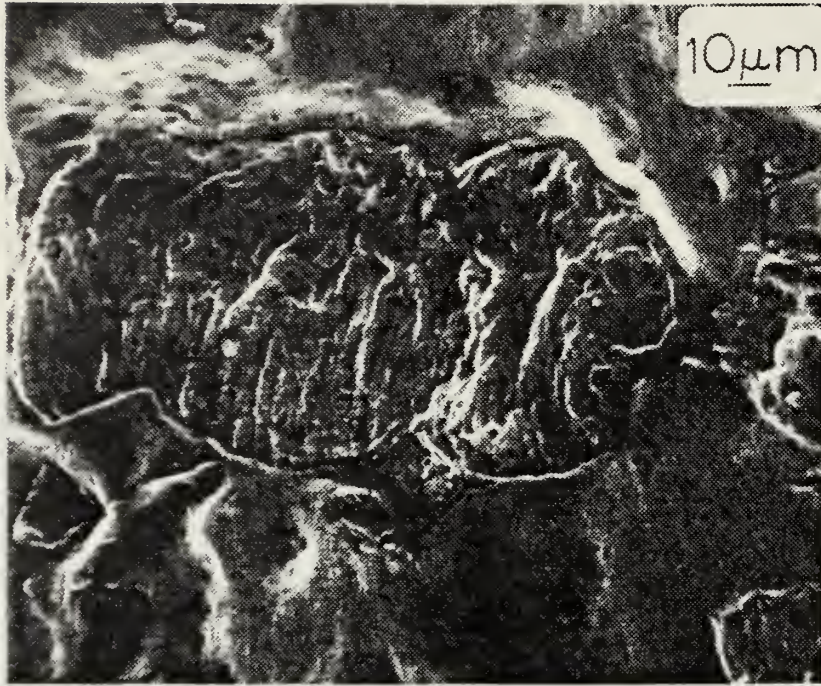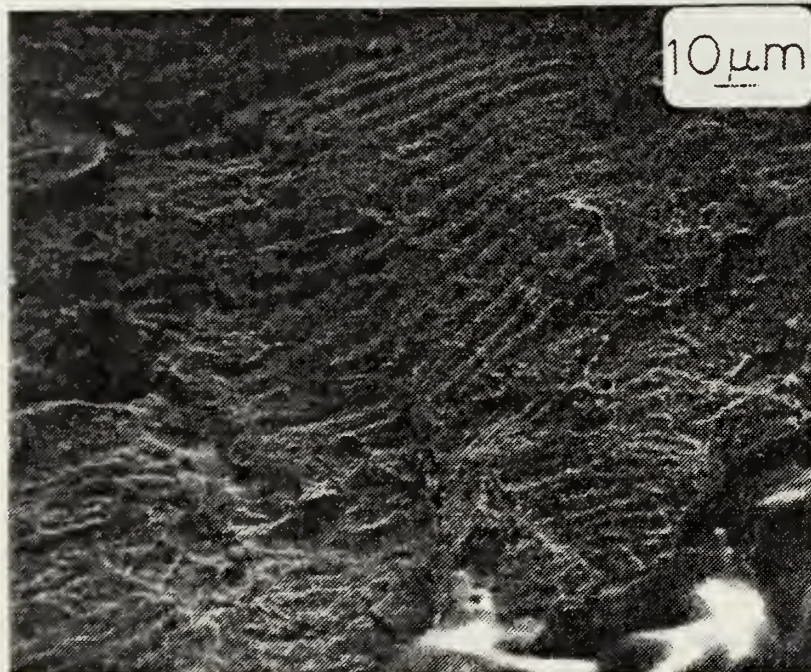
Figure A-1.   Fracture Surface Before Cleaning
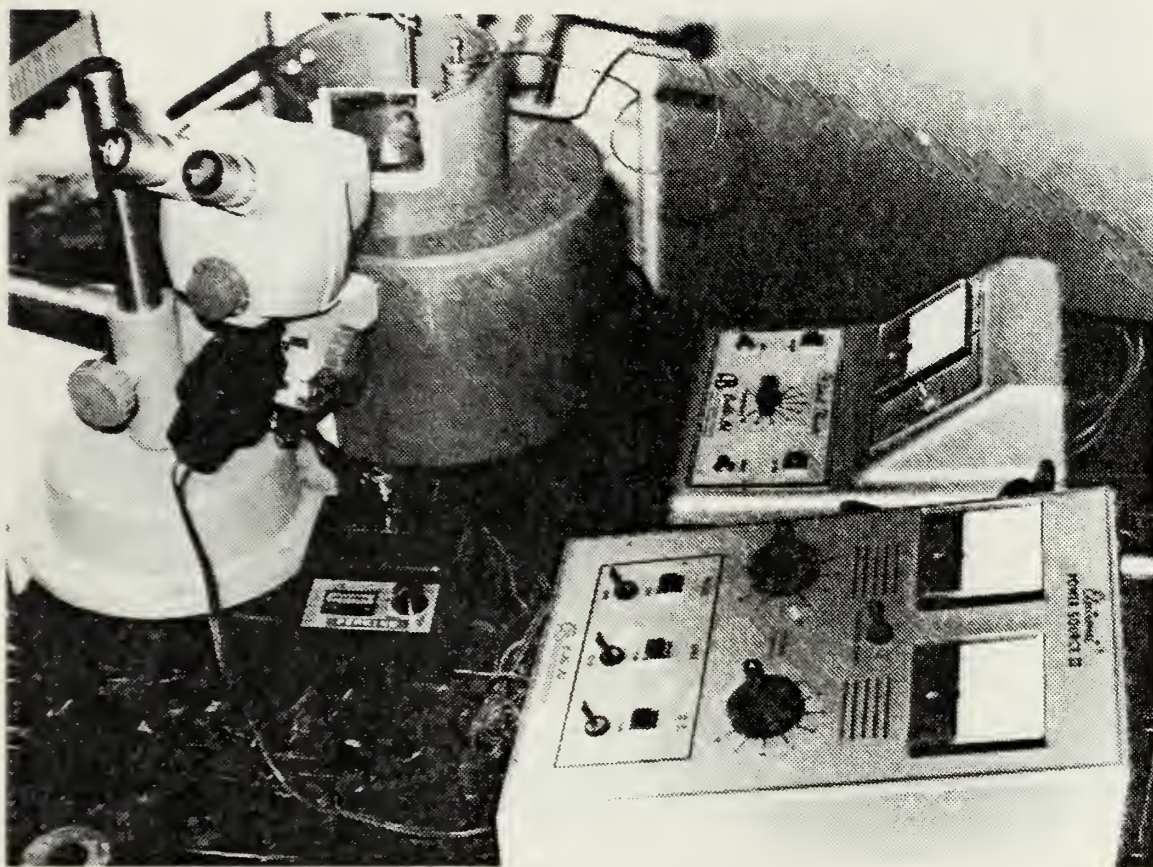

Figure A-2.   Fracture Surface After Cleaning

126

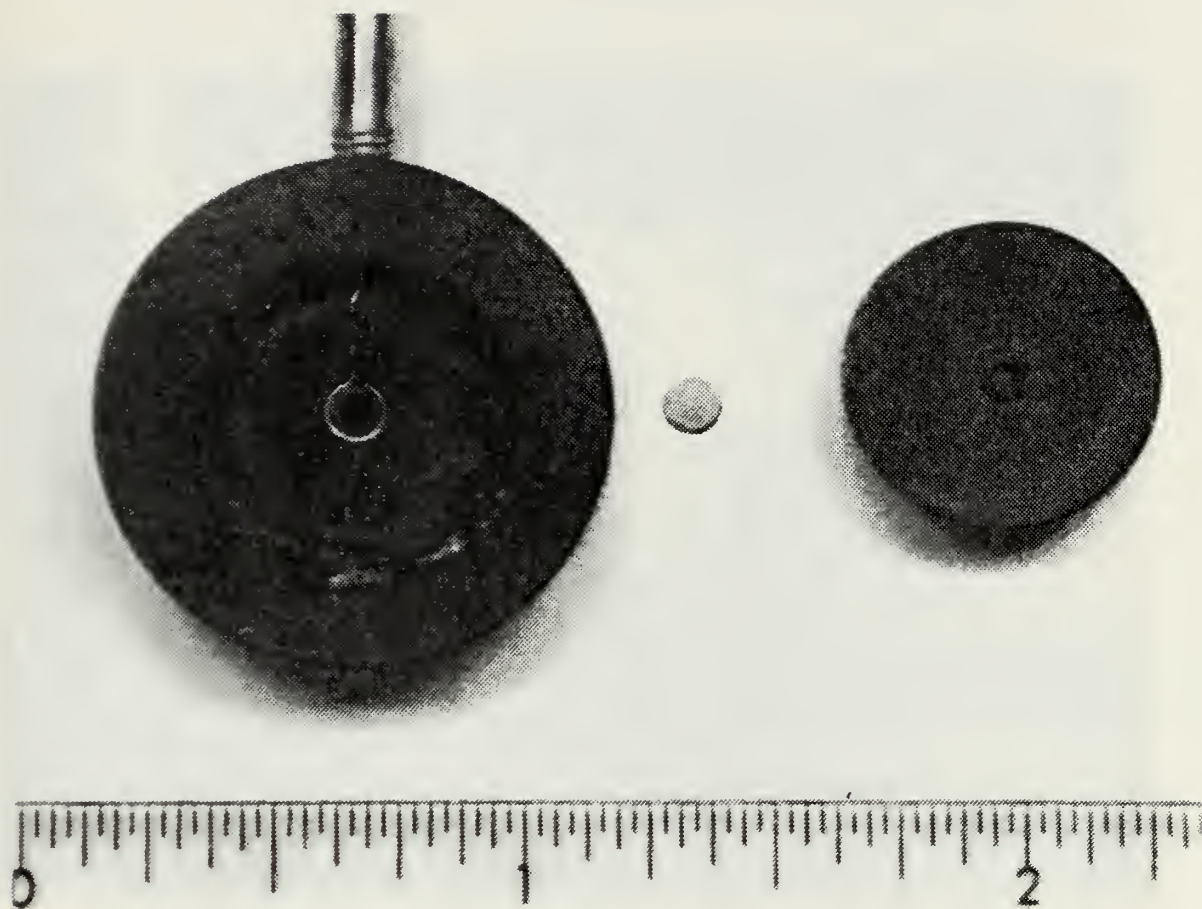Figure A-3. Electropolishing Apparatus
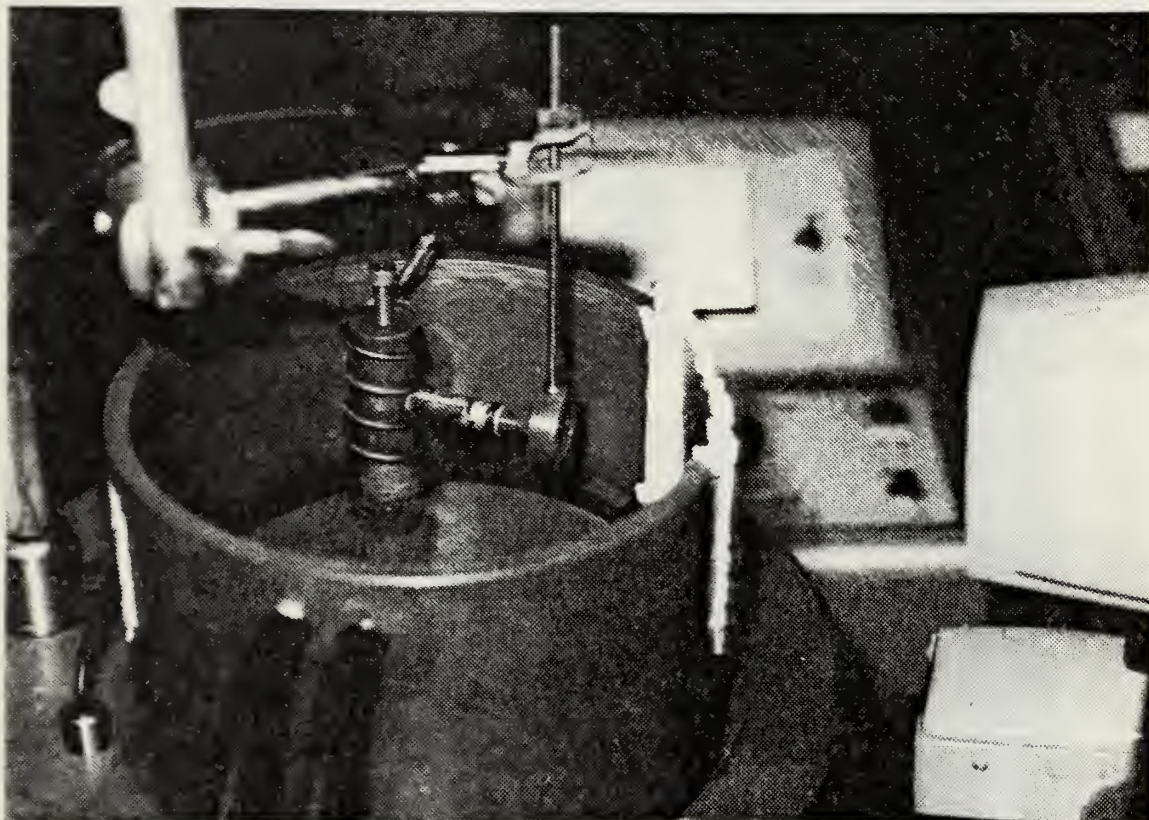
Figure A-4. Specimen Holder and Specimen

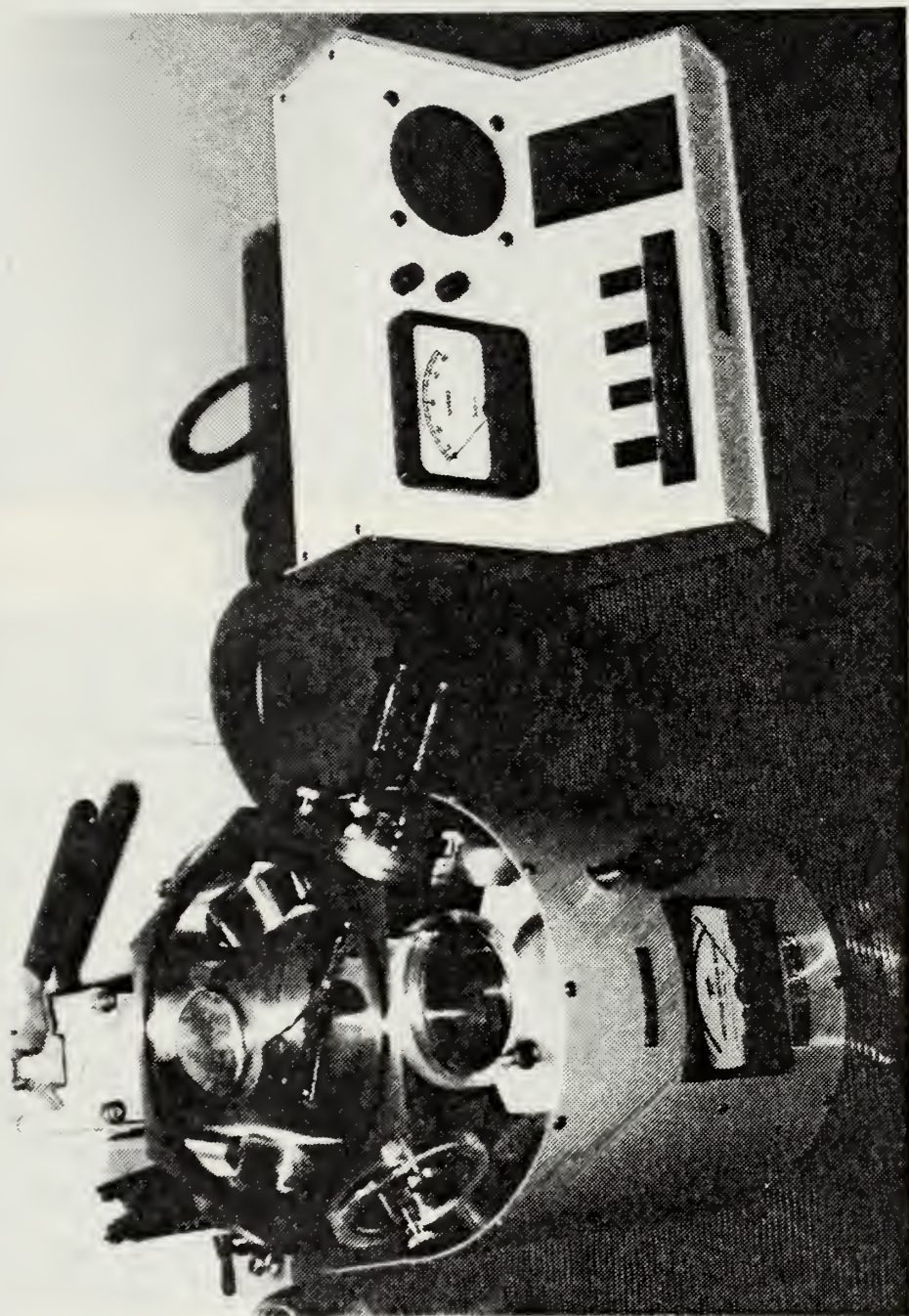Figure A-5. Detail of Electropolishing Apparatus
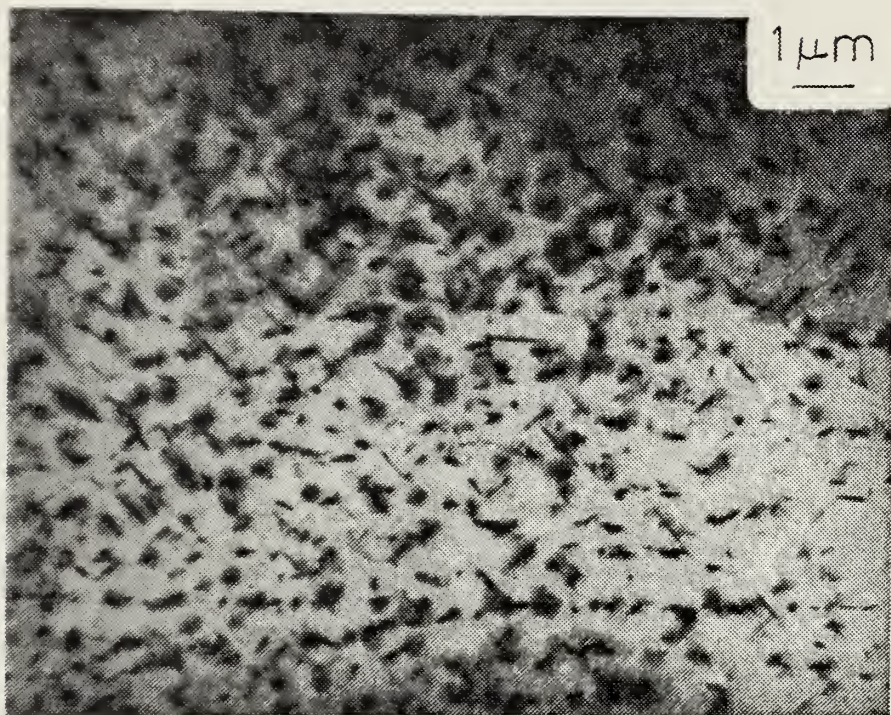
FIGURE A-6. Evaporator Unit

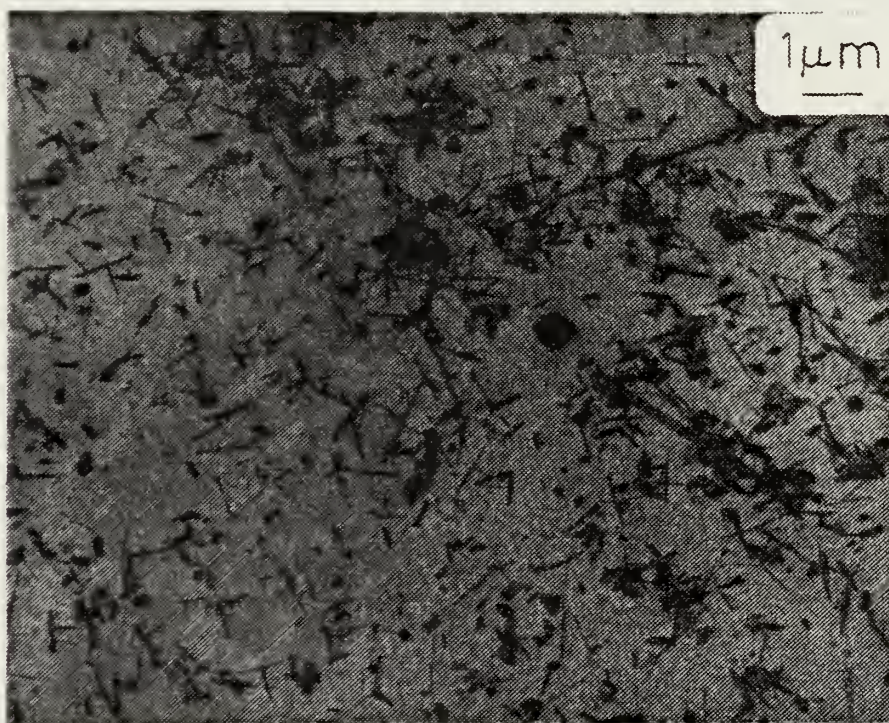Figure A-7. Thin Foil of Proeutectoid Ferrite

Figure A-8. Carbon Extraction Replica of Proeutectoid Ferrite

131

LIST OF REFERENCES

1. J. S. Armijo, J. L. Krankota, C. N. Spalaris, K. M. Horst, F. E. Tippets, "Materials Selection and Expected Performance in Near Term LMFBR Steam Generators," Proceedings of a Symposium, BNES, London, 1974.

2. R. G. Baker, J. Nutting, "The Tempering of 2 1/4 Cr - 1 Mo Steel After Quenching and Normalizing," Journal of the Iron and Steel Institute (JISI), Vol. 194, p. 257, July 1959.

3. J. D. Baird, A. Jamieson, "Effects of Manganese and Nitrogen on the Tensile Properties of Iron in the Range 20-600°C," JISI, Vol. 204, p. 793, August 1966.

4. R. E. Reed-Hill, Physical Metallurgy Principles, 2nd Ed. p. 347, Van Norstrand, 1973.

5. J. D. Baird, A. Jamieson, "High Temperature Tensile Properties of Some Synthesized Iron Alloys Containing Molybdenum and Chromium," JISI, Vol. 210, p. 841, November 1972.

6. J. D. Baird, A. Jamieson, "Creep Strength of Some Synthesized Iron Alloys Containing Manganese, Molybdenum and Chromium," JISI, Vol. 210, p.847, November 1972.

7. J. E. Bynum, F. V. Ellis, B. W. Roberts, "Creep and Tensile Properties and Constituitive Equations for a 2 1/4 Cr - 1 Mo Steel," Structural Materials for Service at Elevated Temperatures in Nuclear Power Generation, p. 146, ASME, 1975.

8. C. E. Jaske, B. N. Leis, C. E. Pugh, "Monotonic and Cyclic Stress Strain Response of Annealed 2 1/4 Cr - 1 Mo Steel," Structural Materials for Service at Elevated Temperatures in Nuclear Power Generation, p. 191, ASME, 1975.

9. M. K. Booker, C. R. Brinkman, V. K. Sikka, "Correlation and Extrapolation of Creep Data for Four Elevated Temperature Structural Materials," Structural Materials for Service of Elevated Temperatures in Nuclear Power Generation, p. 108, ASME, 1975.

10. R. L. Klueh, J. M. Leitnaker, "An Analysis of the Decarburization and Aging Processes in 2 1/4 Cr - 1 Mo Steel," Metallurgical Transactions, Vol. 6A, p. 2089, November 1975. (Oak Ridge National Laboratories Report TM4799)

11. R. L. Klueh, "Heat Treatment Effects on the Tensile Properties of Annealed 2 1/4 Cr - 1 Mo Steel," ORNL Report 5144, May 1976.

12. R. L. Klueh, "Heat Treatment Effects on Creep and Rupture Behavior of Annealed 2 1/4 Cr - 1 Mo Steel," Met. Trans. Vol. 9A, p. 1591, November 1978. (ORNL Report 5219)

13. R. W. Hertzberg, Deformation and Fracture Mechanics of Engineering Materials, p. 131, Wiley, 1976.

14. W. B. Jones, J. A. Van Den Avyle, "Sbustructure and Strengthening Mechanisms in 2 1/4 Cr - 1 Mo Steel," Met. Trans., Vol. 11A, p. 1275, August 1979.

15. J. R. Ellis, M. T. Jakub, C. E. Jaske, D. A. Utah, "Elevated Temperature Fatigue and Creep-Fatigue Properties of an Annealed 2 1/4 Cr - 1 Mo Steel," Structural Materials for Service at elevated Temperatures in Nuclear Power Generation, p. 213, ASME, 1975.

16. C. R. Brinkman, J. P. Strizak, M. K. Booker, C. E. Jaske, "Time Dependent Strain Controlled Fatigue Behavior of Annealed 2 1/4 Cr - 1 Mo Steel for Use in Nuclear Steam Generator Design," Journal of Nuclear Materials, Vol. 62, p. 181, November 1976.

17. K. D. Challenger, A. K. Miller, C. R. Brinkman, "An Explanation for the Effects of Hold Periods on the Elevated Temperature Fatigue Behavior of 2 1/4 Cr - 1 Mo Steel," Trans. of ASME, Journal of Eng. Mat. and Tech., p. 7, January 1981.

18. R. W. Hertzberg, Deformation and Fracture Mechanics of Engineering Materials, p. 465, Wiley, 1976.

19. H. L. Marcus, "Environmental Effects II: Fatigue Crack Growth in Metals and Alloys," Fatigue and Microstructure, p. 365, ASME, 1978.

20. W. L. Morris, "The Early Stage of Fatigue Crack Propagation in AL2048," Met. Trans., Vol. 8A, p. 589, April 1977.

21. J. D. Frandsen, N. E. Paton, H. L. Marcus, "The Influence of Gaseous Environments on Fatigue Crack Growth in a Nickel Copper Alloy," Met. Trans., Vol. 5A, p. 1655, July 1974.

22. J. W. Swanson, H. L. Marcus, "Oxygen Transport During Fatigue Crack Growth," Met. Trans., Vol. 9A, p. 291, February 1978.

23. J. Atawani, K. Katagiri, H. Nakai, "Dislocation Structures Around Propagating Fatigue Cracks in Iron," Met. Trans., Vol. 9A, p. 111, January 1978.

24. C. H. Wells, "High Temperature Fatigue," Fatigue and Microstructure, p. 307, ASM, 1978.

25. H. H. Smith, P. Shahinian, M. R. Achter, "Fatigue Crack Growth Rates in Type 316 Stainless Steel at Elevated Temperature as a Function of Oxygen Pressure," Trans. of Metallurgical Soc. of AIME, Vol. 245, p. 947, May 1969.

26. H. D. Solomon, L. F. Coffin, Jr., "Effects of Frequency and Environment of Fatigue Crack Growth in A286 at 1100°F," Fatigue at Elevated Temperatures, STP 520, p. 112, ASTM 1976.

27. L. A. Jmaes, R. L. Knecht, "Fatigue Crack Propagation Behavior of Type 304 Stainless Steel in Liquid Sodium," Met. Trans., Vol. 6A, p. 109, January 1975.

28 Priddle, Walker, Wiltshire, "The Effects of Helium, Sodium, and Other Environments on the Fatigue Crack Propagation Characteristics of a Stainless Steel," Proceedings of a Conference on The Influence of Environment on Fatigue, held in London by the Institution of Mechanical Engineers, p. 137, May 1977.

29. H. G. Edmunds, D. J. White, "Observations of the Effect of Creep Relaxation on High Strain Fatigue," Journal of Mech. Eng. Sci., Vol 8, p. 310, March 1966.

30. D. J. White, "Effect of Environment and Hold Time on the High Strain Fatigue Endurance of 1/2 Percent Molybdenum Steel," Proc. Instn. Mech. Eng., Vol. 184, p. 223, 1969-70.

31. W. R. Corwin, C. R. Brinkman, "Effects of Steam and Helium Environments on the Elevated Temperature Subcritical Crack Growth of 2 1/4 Cr - 1 Mo Steel," Proceedings of 2nd International Conference on Mechanical Behavior of Materials, p. 1498, ASM, 1976.

32. C. A. Zapffe, C. O. Worden, "Fractographic Registrations of Fatigue," _Trans. of ASM_, Vol. 43, p. 958, 1951.

33. P. J. E. Forsyth, D. A. Ryder, "Some Results Derived from the Microscopic Examination of Crack Surfaces," _Aircraft Engineering_, Vol. 32, p. 96, April 1960.

34. P. J. E. Forsyth, D. A. Ryder, "Some Results of the Examination of Aluminum Alloy Specimen Fracture Surfaces," _Metallurgica_, Vol 63, p. 117, March 1961.

35. M. R. Spiegel, _Schaum's Outline Series: Theory and Problems of Probability and Statistics_, p. 195, McGraw-Hill, 1975.

36. J. T. McGrath, W. J. Bratina, "Dislocation Structures in Fatigued Iron-Carbon Alloys," _Pholosophical Magazine_, Vol. 12, p. 1293, 1965.

37. C. E. Jaske, B. N. Leis, "Final Report on Cyclic Stress Strain of 2 1/4 Cr - 1 Mo Steel," ORNL Subcontract 4004-1 prepared by Battelle (Columbus) Laboratories, October 1974.

38. H. Abdel-Raouf, P. P. Benham, A. Plumtree, "Mechanical Behaviour and Substructure of Strain-Cycled Iron," _Canadian Metallurgical Quarterly_. Vol. 10, p. 87, June 1971.

39. F. V. Lawrence, Jr., R. C. Jones, "The Formation of Cell Structures in Fatigued Iron Crystals," _Met. Trans._, Vol. 1, p. 367, February 1970.

40. J. E. Pratt, "Dislocation Substructure in Strain-Cycled Copper as Influenced by Temperature," _Acta. Met_, Vol. 15, p. 319, February 1967.

41. J. L. Lytton, K. H. Westmacott, L. C. Potter, "The Relation Between Flow Stress and Dislocation Structure During Recovery of High Purity Aluminum," _Trans. of Met. Soc. of AIME_, Vol. 223, p. 1757, September 1965.

42. J. D. Embury, A. S. Keh, R. M. Fisher, "Substructural Strengthening in Materials Subject to Large Plastic Strains," _Trans. of Met. Soc. of AIME_, Vol. 236, p. 1253, September 1966.

43. L. Anand, J. Gurland, "The Relationship Between the Size of Cementite Particles and the Subgrain Size in Quenched and Tempered Steels," _Met. Trans._, Vol. 6A, p. 928, April 1975.

44. D. Kalish, B. G. LeFevre, "Subgrain Strengthening of
     Aluminum Conductor Wires," <u>Met. Trans.</u>, Vol. 6A, p. 1319,
     July 1975.

45. J. T. Barnaby, E. Smith, "The Deformation of an Austenitic
     Steel Containing a Distribution of Coarse Precipitates,"
     <u>Acta Met.</u>, Vol. 12, p. 1353, December 1964.

INITIAL DISTRIBUTION LIST

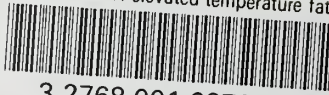|		No. Copies
1.	Defense Technical Information Center Cameron Station Alexandria, Virginia 22314	2
2.	Library, Code 0142 Naval Postgraduate School Monterey, California 93940	2
3.	Department Chairman, Code 69 Department of Mechanical Engineering Naval Postgraduate School Monterey, California 93940	1
4.	Prof. K. D. Challenger, Code 69Ch Department of Mechanical Engineering Naval Postgraduate School Monterey, California 93940	5
5.	Prof. T. McNelley, Code 69Mc Department of Mechanical Engineering Naval Postgraduate School Monterey, California 93940	1
6.	LCDR Pierre G. Vining 3508 King Drive Dunkirk, Maryland 20754	3